The Characterization of Drilling Process of Woven Composites Using Machinability Maps Approach

By

Sanjay Rawat

Department of Mechanical Engineering
McGill University, Montreal
August 2006

A Thesis Submitted to the Faculty of Graduate Studies and Research in Partial Fulfillment of the Requirement for the Degree of
Master of Engineering

Your file Votre référence
ISBN: 978-0-494-28617-3
Our file Notre référence
ISBN: 978-0-494-28617-3

Abstract

Woven carbon fiber composites are being extensively used in aerospace, automotive and civil applications, owing to their high specific strength, higher fracture toughness, and drapeability as compared to unidirectional composites. The processing phase of composite manufacturing has a high added value to the processed laminate, so any damage during machining has a significant economical impact. However, the characteristic attributes like non-homogeneous structure, anisotropy and high abrasiveness of fibers coupled with non-optimized cutting parameters and tool wear can result in damage to the laminate. This experimental research involves quantifying the effect of processing parameters i.e. spindle speed, feed, and tool wear on hole quality during the drilling of a quasi-isotropic woven graphite fiber epoxy laminate. Drilling tests were conducted for wide range of spindle speeds (1,500 rpm to 15,000 rpm) and feed rates (20 μm/rev to 800 μm/rev) with a 5 mm diameter standard point tungsten carbide twist drill. This investigation extended the drilling approach to evaluate the benefits of high speed (12,000 rpm and 15,000 rpm) and high feed (600 – 800 μm/rev) regimes, which were not explored or reported in the open literature. Dependence of damage mechanisms; namely, delamination, fiber pull out, thermal damage, surface roughness deterioration, hole circularity and hole diameter errors, on cutting conditions was established. A strong correlation between different types of damages and cutting forces and temperature was also identified. High speed drilling approach produced contrasting results as spindle speed of 15,000 rpm was found to reduce delamination damage and improve surface roughness but increase the hole circularity and diameter errors. Machinability maps were designed to illustrate the affect of cutting parameters on delamination damage, hole circularity, hole diameter error and hole surface roughness. The application of machinability maps as an aid for process engineers to avoid damage and optimize the process is demonstrated. Finally, it was concluded that the process could be controlled and delamination be eliminated by increasing the spindle speed up to 15,000 rpm and feed rate up to 100 μm/rev. It results a higher productivity if a compromise on hole circularity and diameter tolerances is accepted. Having established the benefits of high speed and low feed drilling, tool wear was evaluated at 12,000 rpm and 15,000 rpm and optimal feed rate of 100 μm/rev. Chipping, abrasion and adhesion of carbon were found to be the main wear mechanisms. Abrasion at the flank face of the drills was identified to be the main wear process that controls the deterioration of the drill at high speeds. The three wear regimes i.e. primary, secondary, and tertiary, were found to strongly influence the thrust force, delamination damage, hole circularity, diameter error and hole surface roughness. Finally, the tool wear analysis revealed that a tool change strategy could be devised by monitoring the thrust force, rather than measuring the progression of flank wear.

Résumé

Les matériaux composites tissés de fibres de carbone sont intensivement employés dans les applications de l'industrie de l'aérospatiale, de l'automobile et autres, dû à leur faible densité, à leur résistance élevée à la traction, et à leur capacité de dépose ou de drapage par rapport aux composites à fibres uni-directionels. La phase de fabrication des matériaux composites incombe une grande valeur ajoutée au stratifié. Par conséquent, n'importe quel défaut pendant l'usinage a un impact économique significatif. Cependant, les caractéristiques des matériaux composites telles que la structure non homogène, l'anisotropie et l'abrasivitée élevée des fibres, couplées aux paramètres non-optimisés de coupe et à l'usure de l'outil peuvent entraîner des endommagements au stratifié. Cette recherche expérimentale s'intéresse à la mesure des effets des paramètres de coupe tels que la vitesse de rotation de la broche, la vitesse d'avance ainsi que l'usure de l'outil sur la qualité des trous pendant le perçage d'un stratifié quasi-isotrope, tissé de fibres de graphite et imprégné de résines époxydes. Des essais de perçage ont été effectués pour des plages assez larges de vitesse de rotation (1.500 à 15.000 tours/mn) et de vitesse d'avance (20 à 800 microns/tour) avec un foret en carbure de tungstène de 5 millimètres de diamètre et une géométrie de pointe standard. Cette recherche a étendu l'approche du perçage pour évaluer les avantages des régimes à grande vitesse de rotation (12.000 et 15.000 tours/mn) et à grande vitesse d'avance (600 à 800 microns/tour), qui n'ont pas été explorés ou cités par des études antérieures. L'influence des conditions de coupe sur certains mécanismes d'endommagement a été établie. Ces mécanismes sont: le délaminage, l'arrachement des fibres, les endommagements thermiques, la détérioration de l'état de surface, et les erreurs de circularité et du diamètre du trou. Une forte corrélation a été identifiée entre les different types d'endommagements d'une part, et les forces et la température du perçage d'autre part. L'approche du perçage à grande vitesse a produit des résultats contrastants. En effet, pendant que la vitesse de rotation de 15.000 tours/mn a permis de réduire les endommagements du délaminage et d'améliorer la rugosité de l'état de surface, elle a engendré une augmentation des erreurs de circularité et de diamètre de trou. Des chartes d'usinabilité ont été conçues pour illustrer l'influence des paramètres du perçage sur les endommagements du délaminage, de l'erreur de circularité de trou, de l'erreur de diamètre de trou et de la rugosité de l'état de surface. L'utilisation de ces chartes comme un outil d'aide aux ingénieurs des méthodes pour éviter les endommagements et pour optimiser le processus du perçage a été démontrée. Finalement, il a été conclu que le processus du perçage pourrait être contrôlé et que le délaminage pourrait être éliminé en augmentant la vitesse de rotation jusqu'à 15.000 tours/mn et la vitesse d'avance jusqu'à 100 microns/tour. Il en résulte une meilleure productivité si un compromis sur les tolérances de circularité et de diamètre du trou est accepté. Après avoir établi les avantages du perçage à grande vitesse de rotation et faible vitesse d'avance, l'usure de l'outil a été évaluée à des vitesses de rotation de 12.000 tours/mn et de 15.000 tours/mn et à une vitesse optimale d'avance de 100 microns/tour. L'ébrèchement, l'abrasion et l'adhésion du carbone étaient les mécanismes d'usure principaux. L'abrasion sur la face de dépouille du foret a été identifiée comme le mécanisme principal entraînant la détérioration de l'outil à des vitesses élevées de rotation. Les trois régimes du frottement, à savoir le régime primaire, secondaire, et tertiaire, se sont avérés pour influencer fortement la force d'avance, les endommagements de délaminage, les erreurs de la circularité et du diamètre du trou, et la rugosité de l'état de surface. En conclusion, l'analyse de l'usure de l'outil a indiqué qu'une stratégie de changement de l'outil pourrait être conçue en surveillant la force d'avance, plutôt que de mesurer la progression de l'usure sur la face de dépouille du foret.

Acknowledgements

I would like to express my gratitude to my principal supervisor Prof. Helmi Attia and co-supervisor Prof. Larry Lessard for their invaluable guidance in the accomplishment of this research work. An additional gratefulness is extended to Dr. Nejah Tounsi and Mr. Raul Vargas for their contributions in the experimental setup and instrumentation. I also would like to thank Prof. Helmi Attia for his critical review, continuous technical and financial support, and for the opportunity to access the equipment used for the machining tests performed during the course of this research at the Aerospace Manufacturing Technology Centre (AMTC), National Research Council Canada (NRC). I would also like to thank Prof. Pascal Hubert for his support in arranging material from Structures and Materials Laboratory of National Research Council Canada. I am grateful to Mr. Danen Challen for his technical help and support in the performance of the machining tests. As well, my deep appreciation is extended to all the members of Advanced Material Removal Group at AMTC - NRC who helped me during the experimental phase, and to Mrs. Helen Campbell at McGill University for her help with SEM images.

Lastly, I would like to express my sincere thanks to my parents, my family members, and my friends for their many contributions in helping me to complete my Master's degree.

Table of Contents

List of Figures

List of Tables

Chapter 1

Introduction

1.1 General

Composites materials consist of two or more constituents, mainly the reinforcements and the base material. They have become very popular primarily because of their high specific strength and stiffness as compared to conventional materials. The composite materials not only find extensive use in high technology areas like aerospace, defence and automotive, but also in civil construction and sports. Furthermore, by deliberately designing the constituent materials, their ratios and orientation of each ply in the laminate, one can tailor the material properties to match specific needs.

Ever since its inception in 1970's, the technology in the area of composite material design and manufacturing has matured to a level that today the aerospace sector has become one of the largest users of composites. For example Boeing, the commercial aircrafts manufacturer is using 50% of composite material, for majority of the primary structure (including the fuselage and wings), on its new 787 aircraft. Owing to the large volumes being used, the machining processes like milling, drilling, trimming, etc., are of equal importance as the composite manufacturing techniques like autoclave moulding, resin transfer moulding etc. The machining of composites, specifically drilling is used extensively for producing bolted joint and riveting during the structural assembly. Any defect arising in the structure during machining demands rework, or in worst case renders it as scrap, and thus can have tremendous economical impact. So the machining of composites, which demands high performance and precision, is an important process in the whole production cycle. Hence, this research is primarily focussed on drilling of woven graphite epoxy composites at conventional and high speeds. The following sections give a basic understanding about composite material constituents, manufacturing techniques, major machining methods used in composites, drill geometry, drilling mechanics, composite structural mechanics, and finally the machinability aspects of composite drilling.

1.2 Reinforcements

The commonly used composite materials are composed of a reinforcing material embedded in a base material. The reinforcing material provides the key structural properties like high specific strength and modulus. The reinforcements can be in the form of fibers, particulates or flakes depending on the material used and the manufacturing process. The most frequently used reinforcements are the fibrous ones made out of glass, graphite, aramid and boron. The fibers can be further processed as chopped strand mat, unidirectional tape or woven into cloth. Graphite being one of the most common reinforcements for aerospace applications is used in this research work. Moreover, Graphite in the form of woven cloth is preferred and is gaining popularity over unidirectional tapes, but it has not been researched to large extent.

1.3 Matrix

The base material, often called the matrix, holds the fibers in place and constitutes the body of the composite. It serves two other main functions:

i. Under an applied load it deforms and distributes the stress to the high-modulus fibrous constituent.
ii. It protects the fibers from abrasion by external environment and abrasive action of contacting bodies.

In order to successfully perform these tasks, an ideal matrix material should possess the following properties:

i. It should initially be a low viscosity liquid and should readily convert to a tough solid on curing.
ii. It must wet the fibers and form a strong interface.
iii. It should possess high shear strength.
iv. It should be tough enough to protect the reinforcements from external damage.

Plastics, metals and ceramics have been used as matrix materials. One of the most common matrix materials for structural composites is the epoxy resin. Table 1.1 lists some of the most common types of fiber reinforced composites used and their modulus properties, in which E_x, E_y, ν_x and E_s represent the longitudinal Young's modulus, transverse Young's modulus, longitudinal Poisson's ratio and longitudinal shear modulus, respectively. Table 1.2 highlights the physical and thermal properties of graphite, glass and aramid fiber based epoxy composites. In this research, Graphite fiber epoxy woven prepreg is used to manufacture the laminate.

Table 1.1: Common Types of Fiber Composites Used in Industry with their Mechanical Properties [1]

Type	Carbon Fiber Reinforced Plastic	Glass Fiber Reinforced Plastic	Kevlar Fiber Reinforced Plastic	Carbon Fiber Reinforced Thermoplastic	Carbon Cloth Reinforced Plastic
Fiber	T300	E-glass	Kev 49	AS4	T300- 7mil
Matrix	N5208	Epoxy	Epoxy	PEEK	F934
Engineering Constants, GPa or dimensionless					
E_x	181.00	38.60	76.00	134.00	66.00
E_y	10.30	8.27	5.50	8.90	66.00
ν_x	0.28	0.26	0.34	0.28	0.04
E_s	7.17	4.14	2.30	5.10	4.10

Table 1.2: Common Types of Fiber Composites Used in Industry with their Thermal Properties [2]

Material	Density (kg/m3)	Specific Heat (J/kg.K)	Thermal Conductivity (W/m.K)
Graphite Fiber Epoxy	1550	950	25
Glass Fiber Epoxy	1900	1000	0.60
Aramid Fiber Epoxy	1350	1300	0.13

1.4 Composite Architecture

Composite materials can have different types of fiber architecture; e.g. unidirectional, woven, chopped and cross ply. Composites are most commonly available in the form of prepreg. Prepreg comprises of fiber yarns pre-impregnated with resin. Unidirectional prepreg has the fibers laid in one direction while the woven have fibers in the form of weave like woven cloth. Unidirectional fibers are strong in the longitudinal direction but are weaker in the transverse direction. Most of the in-plane load in the longitudinal direction is taken up by the fibers. So the unidirectional prepregs are highly suitable for directional loading conditions.

A woven fabric contains fibers oriented in at least two axes, in order to provide good all-around strength and stiffness. A sheet of woven fabric once cured can take flexural and tensile loads on multiple axes, and even exhibits good stiffness properties along off axis. They also lend great toughness and durability to a composite structure. The real benefits of woven materials, however, come from their behaviour in less than ideal circumstances, such as when punctured or exposed to bearing loads. A carbon strand is strongest when straight, and therefore loses some of its theoretical strength when it is bent around other fibers to produce a weave, but if a strand is broken or punctured in a weave, the surrounding fibers, because of this bend, behaves as if unbroken. Therefore, if a hole is punched in a weave, strands punctured in one place, will behave at full strength within a very short distance (typically one to two weave widths) from the damage. With a unidirectional fabric, however, a fiber puncture compromises the strength for the entire length of the fiber, relying on the resin to distribute loading across the broken fibers. This results in lower toughness and impact strength as compared to woven material. Owing to these specific characteristics, woven fabric has been the norm for the outermost covering of any carbon fiber component [3].

Owing to the beneficial characteristics of woven fabrics and their increased use, a quasi-isotropic laminate made of woven prepreg has been investigated in this research work. The detailed design of this laminate will be addressed in chapter 3 of this thesis.

1.5 Composite Laminate Lay-up

A universal notation is used to facilitate the description of a composite material, which is as follows:

$[(\theta_1)_i / (\theta_2)_j / (\theta_3)_k / \ldots\ldots]_s$

Here 'θ_1' represents the first ply angle i.e. the lowermost ply, 'i' represents the number of such plies and 's' represents symmetry of the laminate across the mean plane. Examples of ply sequence in fully expanded form are as below:

$[0_2 / 90]_s = [0 / 0 / 90 / 90 / 0 / 0]$

$[(0_2 / +30)_2 / +45]_s = [0 / 0 / +30 / -30 / 0 / 0 / +30 / -30 / +45 / -45]_s$

1.6 Composite Manufacturing

Theoretical mechanics and material characterization are the pioneering research areas of composite materials. With gradual maturity in these areas, interests in other aspects are growing. In fact, large-scale substitution of fiber-reinforced plastics for metallic materials in areas ranging from aerospace to sports has attracted immense focus on manufacturing of composites. Till today most of the composite processing is done by hand layup method, wherein the prepreg plies are cut to desired orientation and made to lay on the tool, vacuum bagged and then cured inside a high-pressure autoclave to get the desired degree of cure. In the last 10 years, invention of fast curing resins has helped develop new techniques of composite processing, e.g., resin transfer molding, vacuum assisted resin transfer moulding, compression molding etc.[4]. Recently, new computer numerical controlled fiber winding machines have been developed to ensure that parts manufactured have high geometrical tolerance and lower variability. Apart from processing where there has been tremendous improvement and development, the other area, which is still in development stage, is the machining of composites.

Machining of composites is an essential post-processing step in composite part manufacturing. Though a number of small, medium and large size components can be made near net shape, still machining is indispensable for different stages of production especially in assembly. Lack of proper machining technology and processing knowledge can results in poor assembly tolerance and long-term deterioration of structural performance. In broad terms, the machining processes involved in composites are the same as those for metals, i.e. turning, drilling, milling, trimming, sawing etc. The toolings, processing conditions and process control strategies, however, are very much different. As composite materials are highly anisotropic, locally inhomogeneous and are mostly prepared in laminate form before they undergo the machining process, metal cutting techniques and conditions have to be critically evaluated and modified to avoid damage to the composite part. The current research in this thesis has been carried out with similar objective in mind.

1.7 Post Processing (Machining Processes) for Composites

All traditional machining processes remove material in the form of chips to produce surfaces. The basic cutting mechanics of metals is essentially based on shearing the material continuously along a shear plane [5]. Unlike metals, cutting of composites is governed by a fracture phenomenon. Composites, being anisotropic and elasto-plastic, behave and respond differently to conventional machining processes. Due to their abrasive nature and load fluctuation during the cutting process, owing to softer matrix and harder reinforcements, the life of cutting tools is greatly reduced. For example, in glass epoxy composite, the tool encounters a low temperature soft epoxy matrix and brittle glass fibers while in the case of Kevlar epoxy the fibers have to be preloaded in tension and then cut with shearing action. Hence owing to heterogeneity, abrasiveness and heat sensitivity the machining of composites is quite a complex science to postulate.

1.7.1 Major Machining Operations on Composite

Wide varieties of machining methods are currently being used/ proposed for composite materials [3,6, 7, 8, 9]. These operations can be classified as:

i. Conventional
ii. Non-Conventional
iii. Combined/Hybrid Methods

A broad comparison of the methods listed in Table 1.3 has been illustrated in Table 1.4 in terms of the machined part quality, tool wear and machining time [7, 8,10]. The classification in Table 1.3 is, however, dependent on the type of composite material, i.e., glass, graphite, aramid fibers etc., matrix material, i.e., thermosets, thermoplastics etc. as well as the tool used for machining. Of all the operations listed in Table 1.3, drilling and milling are the most frequently practiced machining processes mainly because of the need of desired shape / contour and for component assembly in mechanical structures. Thus in this research work specifically drilling of woven composites has been investigated.

Table 1.3: Main Machining Processes Used for Material Removal in Composite [3, 6, 7, 8, 9]

Conventional	Non Conventional	Combined Methods
Drilling	Ultrasonic Machining	Vibration Assisted Drilling
Turning	Liquid Abrasive Jet Machining	Chemical-Electrical Discharge Machining
Milling	Electrical Discharge Machining	Mechanical-Electrical Discharge Machining
Trimming	Laser Beam Cutting	Thermally assisted Turning
Sawing and Sanding	Electrochemical Machining	

Table 1.4: Comparison of Material Removal Processes for Composites [7, 8, 10]

Method	Product Quality	Tool Wear	Machining Time
Conventional	Moderate/ Low	High	Least
Non Conventional	High	Negligible	High
Combined Methods	Intermediate	Low	Moderate

1.8 Drilling Analysis

To understand the mechanics of drilling it is imperative to have understanding about the tool first. Over the years a number of tool geometries and materials have been investigated by various researchers. Some of the drill geometries specifically developed for composite drilling namely Brad and Spur drill, candle stick drill, spade drill, number of custom made drills etc. have been researched and investigated to give best hole quality [2, 3, 7, 10]. Most of these innovative geometries have not been commercialized so far. So still till date the most common tool used for drilling of composites in industry is a conical point twist drill with two flutes, as shown in Figure 1.1. In terms of tool materials, high speed steel (HSS), tungsten carbide (WC), diamond coated HSS and WC, coated carbides etc. have been investigated for their toughness, wear resistance and service life during drilling of glass, graphite and aramid composites [2, 3, 7, 10]. For this research, however, WC standard point drill was chosen owing to its preference in industry due to better resistance against abrasion and longer life as compared to HSS [7].

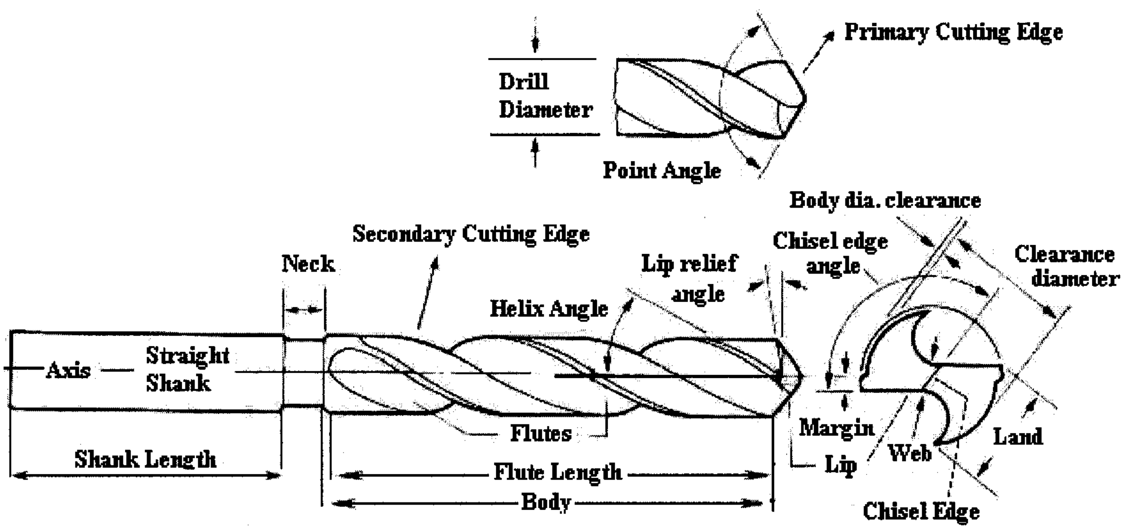

Figure 1.1: Conical Point Twist Drill with Two Flutes [5]

1.8.1 Drill Nomenclature

The conical point WC twist drill has three distinct types of cutting surfaces: chisel edge, two primary (main) cutting edges and two secondary (marginal) cutting edges. The main features of the point are: point angle, lip-relief angle, chisel-edge angle and helix angle. The machining action of chisel edge is more like extrusion than cutting, particularly at the center of the edge. The chisel edge makes a significant contribution to the total thrust force at full engagement of the drill. On the other hand, major cutting is performed by the two primary cutting edges. The main geometry parameters of the standard twist drill, as shown in Figure 1.1, are explained below:

Lips/Primary Cutting Edges: The cutting edges of a two-flute drill extending from the chisel edge to the periphery.

Chisel Edge: The edge at the end of the web that connects the cutting lips.

Chisel Edge Angle: The angle included between the chisel edge and the cutting lip, as viewed from the end of the drill.

Flutes: Helical or straight grooves cut or formed in the body of the drill to provide cutting lips, to permit removal of chips, and to allow cutting fluid to reach the cutting lips.

Land: The peripheral portion of the body between adjacent flutes.

Helix Angle (δ): The angle made by the leading edge of the land with a plane containing the axis of the drill. This angle can be calculated as per equation (1.1), where "*L*" is the pitch length of helix and "*R*" is the drill radius.

$$\delta = \tan^{-1}\left(\frac{2\Pi R}{L}\right) \tag{1.1}$$

Lip Relief: The axial relief on the drill point.

Lip Relief Angle: The axial relief angle at the outer corner of the lip; it is measured by the projection into a plane tangent to the periphery at the outer corner of the lip.

Margin: The cylindrical portion of the land that is not cut away to provide clearance.

Web: The central portion of the drill body having a thickness "*w*" that joins the lands.

Peripheral Rake Angle (α_s): The angle between the leading edge of the land and an axial plane at the drill point. This angle can be calculated as per equation (1.2), where "*w*" is the web thickness and "*R*" is the drill radius.

$$\alpha_s = \sin^{-1}\left(\frac{w}{2R}\right) \tag{1.2}$$

Normal Rake Angle: Figure 1.2 illustrates the concept of normal rake angle for a primary cutting edge of a tool having an inclination angle "*i*". The normal rake angle is defined as the angle measured from a normal to the finished surface (i.e, oz as shown in Figure 1.2) in a plane perpendicular to the cutting edge, i.e., oz'. The geometry of the drill tip is such that the normal rake angle and the velocity of the cutting edge vary with distance from the centre of the drill.

Point Angle: The angle included between the cutting lips projected upon a plane parallel to the drill axis and parallel to the two cutting lips.

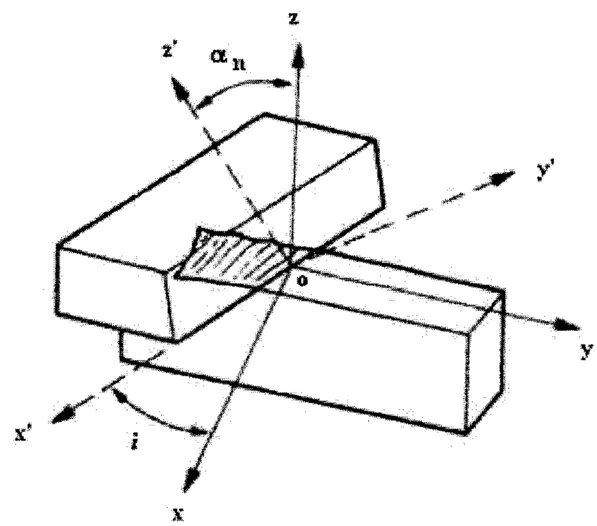

Figure 1.2: Sketch of Inclined Cutting Edge showing the Normal Rake Angle and Reference Axis [5]

1.8.2 Drilling Mechanics

The cutting action in a conventional two-flute twist drill takes place at the chisel edge and the two primary cutting edges. The chisel edge extrudes the material at the hole center while the two primary cutting edges perform cutting. For a drill with web thickness equal to 18% of its diameter (a typical value for conventional twist drills), the cutting edges remove almost 97% of the material [5]. The secondary cutting edge helps in locating the drill in the cavity created by the two primary cutting edges and remove any leftover uncut material. The main processing parameters involved in the drilling are explained below:

Feed (f): The rate at which the drill advances into the material, generally measured in distance moved per flute per revolution. Normally for a standard twist drill it is referred as feed per rev.

Speed (V): The cutting speed is usually measured at the periphery of the drill in meters per minute. The spindle speed (N) is measured in revolution per minute (rpm).

Thrust Force (F_z): The axial thrust force required to drill.

Torque (T_z): The twisting moment required to drill at the periphery of cutting edge.

The thrust force at the chisel edge is larger than that of the cutting edges, but the torque is much smaller than that of the cutting edges because the chisel edge is located at the center of the drill. Figure 1.3 shows the distribution of cutting force and the thrust force on the chisel edge, primary cutting edges and the secondary cutting edges. The total thrust force (F_Z) on the drill is basically a sum of thrust force on the chisel edge (F_{ac}), thrust force on the primary cutting edges (F_a), and the thrust force on the secondary cutting edges (F_a'). The total cutting force (F_c) is sum of the cutting force at chisel edge (F_{tc}) and the primary cutting edges (F_{tr}, which is the resultant of the tangential force, i.e., F_t and radial force, i.e., F_r acting at a distance 'r' from drill center). The radial force components F_r' at the two secondary cutting edges in a standard two flute twist drill are 180° apart and hence cancel each other.

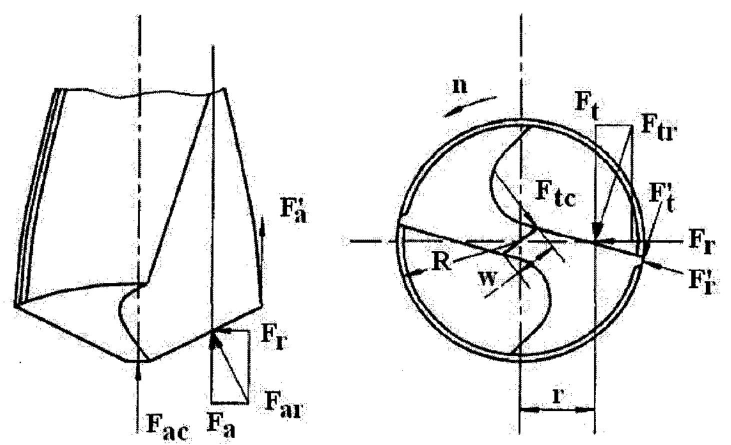

Figure 1.3: Thrust and Cutting Force Distribution on a Twist Drill [11]

In Figure 1.4, the conical point twist drill has been simplified to explain the cutting process. The straight line CD is a simplified chisel edge; the real chisel edge is slightly convex and has an obtuse center point. The straight lines BC and DE are simplifications of the cutting edges while the real cutting edges are twisted, the projection of these parts for the real drill are generally convex and the angles at points B, C, D and E are more obtuse. The point length 'P' is defined as the distance between the lines BE and the line CD, and the conical part is defined as the conic portion between the drill tip and the horizontal plane containing the line BE. Figure 1.5 shows the simplified two-dimensional drill and its relative position with respect to the top surface and the bottom surface of the workpiece. In general, there are two transient phases in the drilling process. The first phase ranges from air cutting to full engagement of drill point at the top surface and the second phase encompasses full drilling to air cutting at the bottom surface. The transient phases can be geometrically regarded as the stages of drilling in which the cutting edges, *i.e.* the straight lines BC and DE of Figure 1.4 completely intersect the top surface or the bottom surface as shown in Figure 1.5.

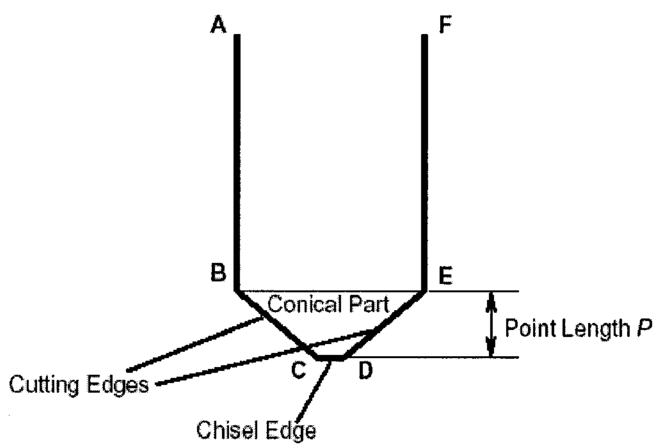

Figure 1.4: Simplified Two Dimensional Representation of Two Flute Drill [12]

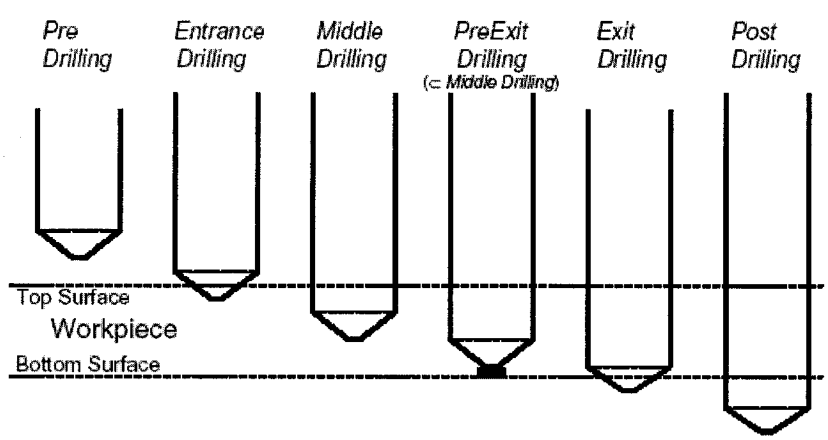

Figure 1.5: Simplified drill and the Drilling Phases [12]

In a normal drilling process with standard two-flute drill, the workpiece thickness is at most thirty times the point length. Hence, these two transient phases account for a negligible percentage of the total process. But since most of the laminated composites are thin structures, these transient phases are not negligible anymore and become very important. When thin laminated composites are drilled, the stiffness of the remaining laminate progressively decreases as the drill advances deeper inside the thin laminate due to the material being removed. So, in thin composite drilling, the cutting forces during these transient phases directly influence the hole quality. In the cases of turning and milling, there also exists a corresponding transient period, i.e. when the edge touches the workpiece and begins cutting and when the edge leaves the workpiece. The duration of these phases is, however, negligible when compared to the total machining time. On the other hand, turning and milling can include sudden or gradual changes in the cutting conditions due to changes in radius, height or properties of the workpiece material. No corresponding changes exist for drilling, except when there is time-varying interference between the drill flutes and the drilled hole, or when there are changes in material properties as the case with stiffness of thin composite laminate. Figure 1.6 shows a typical thrust force and torque signals obtained at a feed rate of 0.03 mm/rev and spindle speed of 455 rpm during drilling of cross winding glass fiber polyester composite laminate using a carbide drill obtained in [13]. The transient phase from OA to OB represents the full entry of drill point while OC to OD represents the full exit of drill point. It is obvious that these phases contribute significantly to the whole drilling cycle. The fluctuations in both the force and torque signals as shown in Figure 1.6 reflect the composite material in-homogeneity and anisotropy.

A number of empirical models have been developed by researchers to relate the thrust force and torque with cutting parameters, tool geometry and workpiece material properties. The most used model for metal drilling is that of Shaw and Oxfords [14,15]. The empirical relations as described by equation (1.3) and (1.4), relate the drill thrust (F_z) and torque (T_z) with the cutting parameter mainly feed rate (f), drill geometry i.e. chisel edge length (c) and drill diameter (d) and the work piece material hardness (H_B):

$$\frac{F_z}{d^2 H_B} = k_1 \left(\frac{f^{1-a}}{d^{1+a}} \right) \left[\frac{1-\dfrac{c}{d}}{\left(1+\dfrac{c}{d}\right)^a} + k_2 \left(\frac{c}{d} \right)^{1-a} \right] + k_3 \left(\frac{c}{d} \right)^2 \tag{1.3}$$

$$\frac{T_z}{d^2 H_B} = k_4 \left(\frac{f^{1-a}}{d^{1+a}} \right) \left[\frac{1-\left(\dfrac{c}{d}\right)^2}{\left(1+\dfrac{c}{d}\right)^a} + k_5 \left(\frac{c}{d} \right)^{2-a} \right] \tag{1.4}$$

where, "k_1", "k_2", "k_3", "k_4" and "a" are constant for a given work material and drill to be evaluated from experimental data.

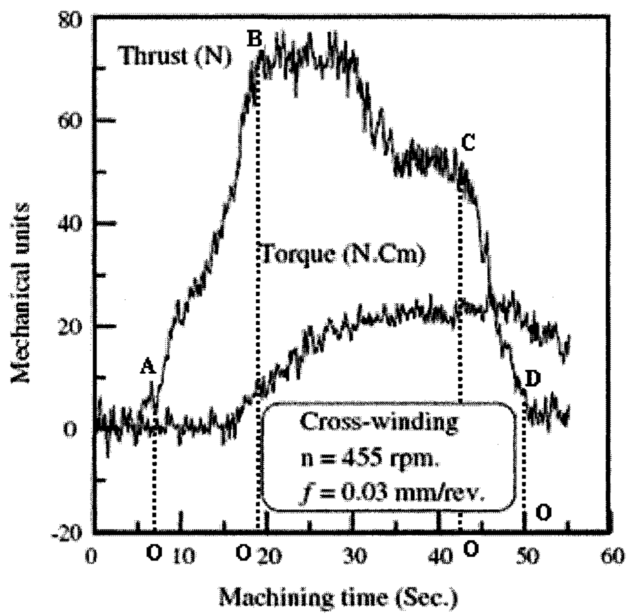

Figure 1.6: Thrust and Torque over Drilling Cycle of a Cross Winding Glass Fiber Polyester Composite at Spindle Speed 'n' = 455 rpm and Feed Rate 'f' = 0.03mm/rev. Time at OA, OB, OC and OD Represents the Start of Drilling, Full Entry of Drill Point, Start of Drill Exit and Full Exit of Drill Point [13]

For the standard twist drills used in this research, the value of "c/d" is constant, therefore the thrust force and torque can be further simplified as described by equation (1.5) and (1.6), respectively:

$$F_z = K_1 (fd)^{1-a} + K_2 d^2 \tag{1.5}$$

$$T_z = K_3 (f)^{1-a} d^{2-a} \tag{1.6}$$

where, "K_1", "K_2", "K_3" and "a" are constants.

Shaw's experimental tests on AISI 3245 steel at cutting speed of 6.1 m/min and range of feed rates provided nonlinear relations between the thrust force, torque or cutting force and feed rate by regression as illustrated by simplified equation (1.5a) and (1.6a), respectively:

$$F_z = K_1 (f)^{0.8} + K_2 \tag{1.5a}$$

$$F_c = K_3 (f)^{0.8} \tag{1.6a}$$

Shaw and Oxford derived another expression of the torque, taking into account the specific cutting energy 'u' of the work piece material. From the size-effect theory, the effective specific energy was found to be inversely proportional to the product of feed and drill diameter as described by equation (1.7) [5]:

$$u = \frac{8T_z}{fd^2} \propto (fd)^{-a} \tag{1.7}$$

Most of the empirical models developed for drilling of composites, which will be discussed in chapter 2, also use the Shaw and Oxford's model for relating thrust and cutting force to cutting parameters.

1.9 Structural Mechanics of Composites

Most composite materials for structural use are laminated. Due to their marked anisotropy and macroscopic heterogeneity, the mechanics used is different when compared to conventional materials such as metals. In the mechanics of composite laminates the first step is to develop the stress-strain law for a single ply oriented along its axis of material symmetry [16]. This is obtained from classical theory of elasticity which identifies four material constants (in plane stress): Young's moduli in the 1 and 2 directions, in-plane shear modulus, and the Poisson's ratio in the 1-2 direction. To determine these constants from constitutive properties, the mechanics of material approach is most widely employed for its good estimate and ease in computation.

Having obtained the governing relationship in the principal material directions, one is further interested to obtain the off axis responses of stress and strain, for solving a general problem, the geometrically natural directions do not necessarily coincide with the principal axes. The results show a complex behaviour, including coupling between shear and normal stresses and strains [16].

The third step is to combine the stress-strain laws for individual plies into a single stress-strain law for the laminate [16]. The basic assumption is that, when the plies are modeled into the laminate, a rigid bond of infinitesimal thickness is formed between the adjacent plies so that under plane stress conditions, the strains are uniform at all points on a line through the thickness. By equating the resultant forces of the whole structure, one obtains an in-plane laminate stiffness matrix which depicts the elastic constitutive relation for the laminate. The stiffness matrix can be calculated routinely given the single-ply moduli and the lay-up pattern.

1.10 Machinability of Composite Laminate

Machinability of a material is defined as the ease with which a material can be satisfactorily machined. Machinability is usually quantified in terms of machinability index. It is basically a comparison of machinability of a different material to a standard material as described by equation (1.8). For example, US material standards for 100 % machinability are SAE 1112 hot rolled steel. Machinability Index can be based on tool life, end of a specific wear regime, time to develop a standard land wear, surface finish, cutting force, power consumption etc. for example:

$$M_{20} = \frac{V_{20,1}}{V_{20,2}} \tag{1.8}$$

where, M_{20} is machinability index based on tool life, $V_{20,1}$ is cutting speed of metal investigated for 20 minutes tool life and $V_{20,2}$ is cutting speed of standard steel for 20 minutes tool life. In the case of fiber based composite materials, machinability is dependent more on producing a damage free hole with correct geometrical tolerances. The following section discusses the classification of hole quality and its importance in determining the machinability of fiber based composites.

1.10.1 Drilled Hole Quality Classification

The productivity of drilling process is dependent both on the number of holes drilled and the quality of the hole. In cases where the structural loading is critical and any damage to the structure can lead to failure during service, the in-process quality becomes extremely important. Therefore characterizing the hole quality is of utmost importance in case of laminated composites. In this research work, the quality of drilled holes is characterized in terms of damage i.e. surface delaminations at the entry of the drill (top side of laminate) and the exit surface damage (bottom side of laminate), surface roughness of hole, internal damage and the geometrical tolerance i.e. hole diameter error and hole circularity.

1.10.1.1 Surface Delamination

Delamination describes the separation of two laminated plies at their interface and is essentially debonding in case of laminates made out of prepreg [17]. During drilling of laminated composites delamination can occur at two instances. First, when the drill is trying to dig into the laminate, this is known as entry delamination (Peel Up) and, secondly, when the drill is exiting the laminate, this is known as exit delamination (Push Out). Figure 1.7 illustrates these two types of damage.

The entry and exit delaminations are attributed to high cutting and thrust forces, respectively. These forces when exceed the interlaminar shear strength of the laminate, which is essentially the shear strength of the matrix, result in the separation of the two plies at their matrix interface. Also, degree of cure has been found to affect damage with low cured laminates having higher damage [18]. These delaminations reduce the effective stiffness of the laminate and can act as regions for crack initiation leading to failure under certain loading conditions.

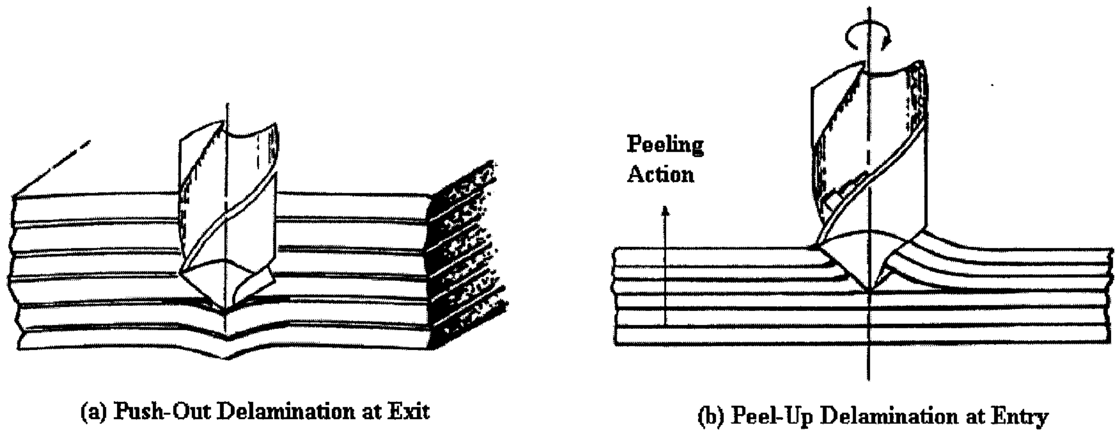

Figure 1.7: (a) Delamination at Exit, i.e., Push-out (b) Delamination at Entry, i.e., Peel-Up [19]

Figure 1.8 shows the scanning electron image (SEM) of entry delamination obtained during this research work of drilling a quasi-isotropic woven carbon fiber epoxy laminate with a 5mm standard point carbide drill at spindle speed of 15000 rpm and feed rate of 800 μm/rev.

The entry and exit delamination damage ($\phi_{d[entry,exit]}$) can been evaluated as the ratio of maximum diameter of the damage to the drilled hole diameter as described by equation (1.9) and shown in Figure 1.8. It shows the maximum diameter of the delaminated zone i.e. "$\phi_{maximum}$" and the diameter of hole i.e. "ϕ_{hole}" drilled at spindle speed of 15,000 rpm and feed rate 800 μm/rev.

$$\phi_{d[\text{entry,exit}]} = \frac{\phi_{\text{maximum}}}{\phi_{\text{hole}}} \tag{1.9}$$

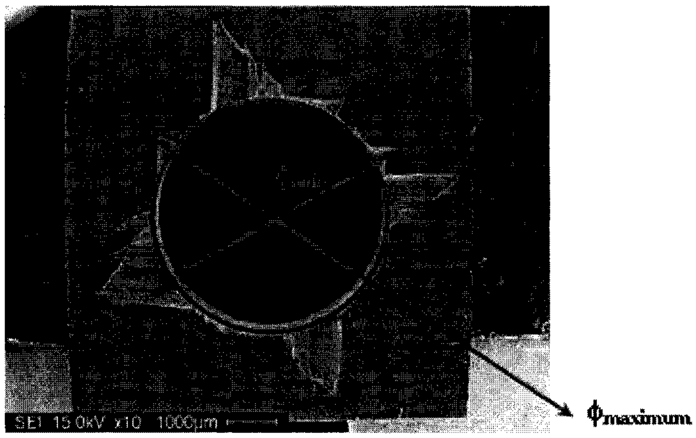

Figure 1.8: Delamination at Entry for Woven Carbon Fiber Epoxy Laminate at Spindle Speed = 15,000 rpm and Feed Rate = 800 µm/rev with a 5 mm Standard Carbide Drill.

Delamination damage can also be expressed in terms of percentage of the hole diameter as described by equation (1.10). This definition of percentage delamination damage has been used in this research work (see Figure 1.9).

$$R_d(\%) = \frac{\phi_{\max imum} - \phi_{hole}}{\phi_{\text{hole}}} \tag{1.10}$$

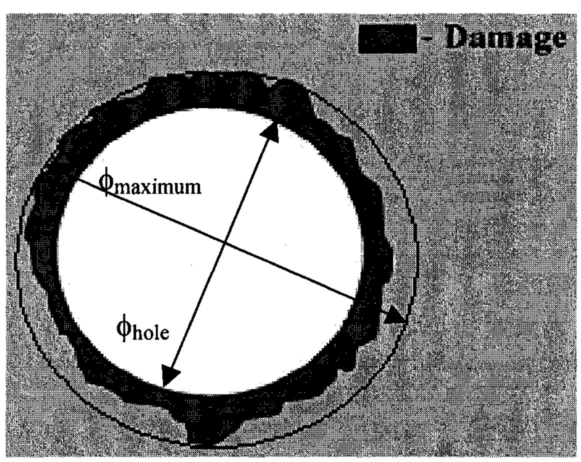

Figure 1.9: Schematic for the Measurement of Maximum Diameter of Damage and the Drilled Hole Diameter.

1.10.1.2 Internal Delaminations

Internal delaminations are the delamination damages observed at micro scale and thus are not visible to the naked eye. They are micro cracks, which develop at the ply interfaces in the matrix phase of the laminate. The reason for this micro-separation could be higher thrust force generated during drilling, voids in the laminate due to air entrapment or foreign bodies, local uncured regions resulting in lower strength as compared to bulk, etc. [6, 7, 9, 17]. These internal delaminations are critical to the life of the component as they can initiate crack propagation during fatigue loading and thus reduce the in-service life of the component. Figure 1.10 shows the internal delaminations observed in [20] during drilling of woven carbon fiber epoxy laminate at two different feed rate.

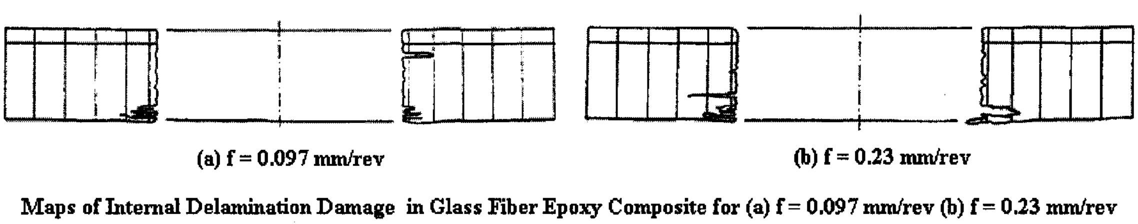

Figure 1.10: Maps for Internal Material Damage [20].

1.10.1.3 Fiber Pull Out

Fiber pull out occurs when the fiber instead of being cut are plucked from the base by the peripheral action of the cutting edges. This phenomenon of pull out creates a cavity in the matrix phase and thus disturbs the load path of the fibers. Figure 1.11 shows the SEM image of fiber pull out observed at spindle speed of 5,000 rpm and fed rate of 20 μm/rev during the course of this research work.

Fiber pull out can happen at higher cutting speeds when the interaction time between the cutting edges of the drill and laminate plies is very small. The effect of the cutting conditions on this type of damage will be discussed in detail in section 4.2.8. Also during continuous drilling, the tool wears and becomes blunt and thus further aggravates fiber pull out.

Figure 1.11: SEM Image Showing Fiber Pull Out Obtained at N = 5,000 rpm and f = 20 mm/rev During Drilling of Woven Graphite Epoxy Composite with a Standard Point Carbide Drill.

It is difficult to directly quantify the internal delamination damage and fiber pull out unless measurements are made at different drilled depths, after carefully splitting the specimen, which is time consuming and can induce errors. In this research the author has related the effect of internal delamination and fiber pull out on an easy measurable surface roughness parameter i.e. the valley void volume of the surface (S_v). The valley void volume of the unit sampling area is defined as a void volume at the valley zone from 80 to 100 % surface bearing area as described by equation (1.11):

$$S_v = \frac{V_r\left(h_{0.20}\right) - V_r\left(h_{0.10}\right)}{\left(M-1\right)\left(N-1\right)\delta x \delta y} \tag{1.11}$$

where, $V_r(h_{0.20})$, $V_r(h_{0.10})$, M, N and $\delta x \delta y$ represent the volume occupied at normalized surface height of 20 % of bearing area, volume occupied at normalized surface height of 10 % of bearing area, number of points measured per profile, number of profiles measured, and unit sampling area, respectively.

In tribology this value represents the fluid retention ability of a highly worn out surface. The higher this value the higher is the fluid retention capability and thus higher are the number of voids. So functionally, valley void volume of the surface can indirectly reflect the extent of internal delamination and fiber pull out in composites. The valley void volume of the surface (S_v) is easy to measure with a three dimensional scanning device like a 3-D surface profilometer.

1.10.1.4 Hole Circularity

Hole circularity is a geometrical defect. The circularity tolerance defines a pair of concentric circles that must contain the maximum and minimum radius points of a circle. It reflects directly the error in roundness of the hole [13]. The higher the circularity, the higher is the difference between the maximum and minimum radius of the hole, and thus larger the roundness or circularity error.

1.10.1.5 Hole diameter error

Hole diameter error is defined as the deviation from the desired hole diameter. It can be either over size or under size. Large error in hole diameter will result in misalignment of the structural components during assembly, while under sized holes will demand rework for diameter correction and thus will impact on productivity. The hole diameter error can be normalized to represent an absolute number for comparison. The normalised hole diameter error is expressed by equation (1.12):

$$\phi^{n}_{error} = \frac{\phi_{actual} - \phi_{desired}}{\phi_{desired}} \tag{1.12}$$

where, "ϕ_{actual}" is the actual mean diameter of the circle measured by taking 'n' number of measurements from the centre of the hole and "$\phi_{desired}$" is the required hole diameter. The hole diameter error "ϕ^{n}_{error}" can be measured using a standard coordinate measuring machine.

1.10.1.6 Hole Surface Roughness

Roughness consists of surface irregularities, which result from the various machining conditions. In drilling, roughness of the lateral surface of the hole is affected by the cutting parameters i.e. the cutting speed and feed. The average surface roughness (R_a) is one of the most commonly adopted means of defining surface finish in general engineering practice. It gives a good general description of the height variations in the surface. Figure 1.12 shows a roughness profile along the depth of a hole drilled at spindle speed of 12,000 rpm and feed rate of 600 μm/rev. To evaluate R_a, a mean line is first found that is parallel to the general surface direction and divides the surface in such a way that the sum of the areas formed above the line is equal to the sum of the areas formed below the line. Then the surface roughness is given by the sum of the absolute values 'z' of all the areas above and below the mean line divided by the sampling length '' as described by equation (1.13) [21]:

$$R_a = \frac{1}{l}\int_0^l |z(x)|dx \tag{1.13}$$

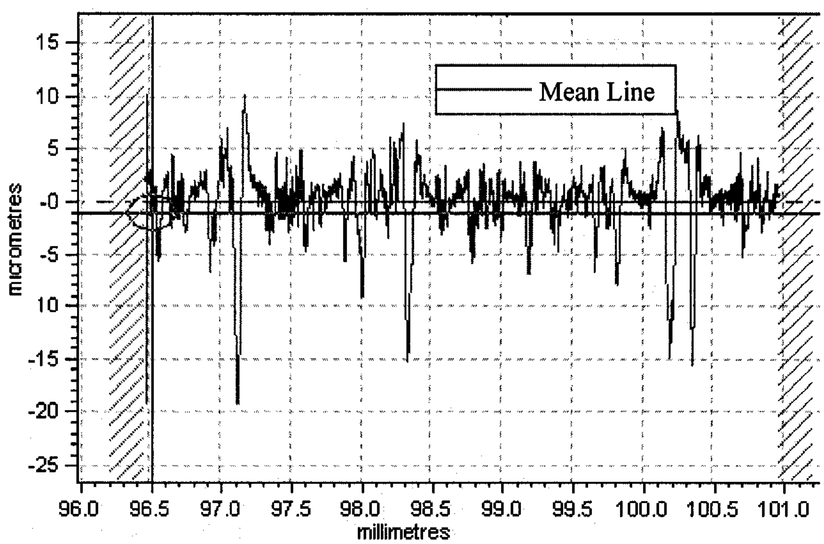

Figure 1.12: Surface Roughness Profile Measured Along the Depth for a Hole Drilled at N =12,000 rpm and f = 600 μm/rev in Woven Graphite Epoxy Composite with a Standard Point Carbide Drill. Average Surface Roughness Value (R_a) Measured was 2.3 μm.

The surface roughness indirectly affects the load bearing strength of the hole. A higher surface roughness will result in lower real contact area between the fastener and the hole surface thus resulting in higher stress, while better surface finish will increase the area of contact and thus the load bearing area. The surface roughness measurements can be easily carried out with a surface profilometer.

1.11 Thesis Outline

Chapter one of this research work provides a concise introduction to composite materials, its constituents, properties and architecture, methods of material removal, tool nomenclature, drilling mechanics, structural mechanics of composites and its machinability aspects. It is then followed by a preview of each chapter in this thesis.

Chapter two presents an in-depth literature review of the past research done in the area of drilling of composites. The review is followed by specific objectives to be achieved in this work.

Chapter three describes the experimental setup and the experimental matrix devised to carry out the different stages of research. It describes in detail the equipments and procedures used for each stage during the course of research.

Chapter four discusses the results obtained from the machinability assessment for the range of selected cutting parameters. The results are followed by critical reviews, explanations and finally the machinability maps.

Chapter five discusses the tool wear assessment and the impact of tool wear on part quality for the selected cutting parameters. The results are followed by in depth analysis.

Chapter six states the conclusion of the research work and recommendations for future work.

Chapter 2

Literature Review

2.1 Introduction

Machining of composites is a complex task owing to its heterogeneity, heat sensitivity and to the fact that reinforcements are extremely abrasive. The drilling of laminated composites results in a series of mini-fiber fractures, fiber pullouts, matrix cracking, delaminations and tool wear. Over the years there has been great deal of effort from the research community to address these issues. Research in drilling of composite laminates is focused on a number of areas: force and delamination modeling, machinability characterization of different composite types, tool life and wear characterization, tool geometry optimization, adaptive process control, non-conventional machining techniques etc. Most of these areas are, however, interrelated in composite machining. A major improvement in tool material or geometry is bound to impact the machinability characteristics and the damage mechanisms of the laminate.

In this chapter the author has specifically focused on the research done in the area of force and delamination modeling, effect of cutting variables on force, torque, delamination damage, hole quality and cutting temperature and characterization of tool wear during drilling of fiber based composites. Section 2.2 of this chapter highlights the work done in the area of force and delamination modeling. Section 2.3 discusses the work done in thrust force and torque analysis during composite drilling for different cutting conditions. Section 2.4 highlights the work done in the area of delamination damage analysis and techniques for its avoidance. Section 2.5 highlights the effect of cutting variables on hole quality i.e. hole diameter error, hole circularity and surface roughness. Section 2.6 discusses the research work done for identifying tool wear mechanisms and predicting tool life for different composites at different cutting conditions. Section 2.7

$$F^*_{Exit}(h) = \pi \sqrt{\frac{8G_{IC}Eh^3}{3(1-v^2)}} \tag{2.1}$$

$$F^*_{Entry}(h) = k_p \pi \sqrt{\frac{8G_{IC}E(H-h)^3}{3(1-\upsilon^2)}} \tag{2.2}$$

where, H is the total laminate thickness are shown in Figure 2.1.

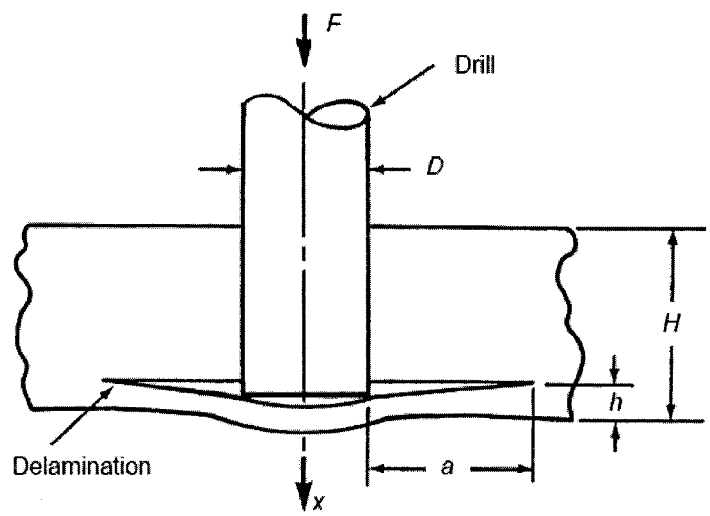

Figure 2.1: Ho-Cheng and Dharan's Circular Plate Model for Delamination Analysis [18]

This analytical model was, however, based on a number of assumptions, namely:

(a) Isotropy of each layer
(b) Use of linear elastic fracture mechanics
(c) Point loading on chisel and cutting edges
(d) Plane strain conditions

In reality, however, each layer is highly anisotropic, the cutting process involves elastic-plastic fracture mechanics, chisel and cutting edge involves uniformly distributed load. Moreover, the model considered the highest stiffness value (*E*) in the calculation of critical forces. This model hence predicted conservative forces and was mainly suitable for unidirectional composites.

highlights the work done in the area of cutting temperature measurement and its response to the change in cutting variables. Finally, the chapter is concluded with thesis objectives.

2.2 Force and Delamination Models

Most of the models developed in [18, 22, 23, 24, 25] focus on identifying the critical forces that cause delamination and provide strategy for either minimizing or avoiding them. A major concern that has received considerable attention in drilling holes in carbon fiber reinforced composite material is the delamination at the bottom surface (drill exit) of the laminate [18, 22, 23, 24, 25]. In [22, 23, 25] the authors found that there is a critical thrust force below, which no damage occurs. In [26], Dharan proposed fracture mechanics theory to predict the critical stress necessary for onset of fracture and the direction of crack propagation in laminated composites. These investigations have been elaborated in this section.

Shaw and Oxford [14, 15] were the pioneers in developing the empirical model for evaluation of thrust and torque during drilling of metals. Their force models, which have already been discussed in section (1.8.2), have also been extensively used in cutting force analysis in composite drilling.

Ho-Cheng and Dharan [18] were the first to develop a delamination model based on linear elastic fracture mechanics. Figure 3.1 shows the circular plate model used for delamination analysis by these authors. In their analytical approach, they defined the critical force that could lead to delamination at hole entry and exit. This critical force at the exit (F_{Exit}^{*}) and entry (F_{Entry}^{*}) at uncut depth (h) under the tool has been related to the material properties, namely energy release rate per unit area in mode 1 failure "G_{IC}", highest ply stiffness "E" and the Poisson's ratio "ν" of the laminate and the uncut laminate depth under the tool "h" in the form of equation (2.1) and (2.2):

In [22], Jain et. al. developed a variable feed rate strategy to avoid delamination using the basic knowledge developed by Ho-Cheng and Dharan [18]. They moved a step further and derived a model to predict critical thrust force (F_c^*) defined by equations (2.3) & (2.4). They established the relation for critical feed rate (f_c^*) at different ply levels for unidirectional fiber composites as given in equation (2.5).

$$F_C^* = 3\pi\left(\frac{b}{a}\right)\sqrt{2G_{IC}D_c^*} = 3\pi\sqrt[4]{\frac{D_{22}}{D_{11}}}\sqrt{2G_{IC}D_c^*} \tag{2.3}$$

$$D_c^* = 2D_{11} + \frac{2(D_{12}+2D_{66})}{3}\sqrt{\frac{D_{11}}{D_{22}}} \tag{2.4}$$

$$f_c^* = \left\{\frac{d^{1.2}}{1.91}\left[\frac{3\pi}{H_B(d)^2}\sqrt[4]{\frac{D_{22}}{D_{11}}}\sqrt{2G_{IC}D_c^*} - \frac{0.101}{d}\right]\right\}^{2.5} \tag{2.5}$$

where, "*a*" and "*b*" represent the half of delamination size along the fiber and transverse direction, "*D's*" represent the bending stiffnesses of the laminate, "*d*" represents the diameter of tool and "H_B" represents the hardness of the tool. Although Jain and Yang's Model [22] incorporated the directional behaviour of composite laminates (by use of on-axis and off-axis stiffnesses), it was still limited to unidirectional composites only.

Models developed by Ho-Cheng et. al. and Jain et. al. in [18, 22] were able to predict the critical thrust force and the feed rates, but they were not definitive about the delamination location. Tsao and Chen [23] addressed this issue and developed an analytical approach for the determination of location of onset of delamination based on a linear elastic fracture mechanics analysis. The critical thrust force (F_C^*) given by equation (2.6) was calculated from the predicted position of the onset of delamination given by equations (2.7 - 2.9):

$$F_C^* = 3\pi\left(\frac{E_{11}}{E_{22}}\right)^{0.5}\left(\frac{G_{IC}(h^*)^3}{6(1-\nu_{12}\nu_{21})}E_c^*\right)^{0.5} \tag{2.6}$$

$$h^{*} = (0.0000254)\, h_{ply} \left(h^{*}_{anisotropic}\right) \left(\frac{E_{22}}{E_{11}}\right)^{0.62208} \left(G_{IC} E^{*}_{c}\right) \tag{2.7}$$

$$h^{*}_{anisotropic} = \left\{ \frac{4\left(1-\nu_{12}\nu_{21}\right)}{3G_{IC}\pi} \left(\frac{E_{11}}{E_{22}}\right) 1/4 \left(E^{*}_{c}\right)^{-1} \right\}^{1/2} \tag{2.8}$$

$$E^{*}_{c} = 2E_{11} + \frac{2}{3}\left(\frac{E_{11}}{E_{22}}\right)^{0.5} \left(E_{22}\nu_{12} + 2G_{IC}\left(1-\nu_{12}\nu_{21}\right)\right) \tag{2.9}$$

where, "*h's*" represent the uncut depth under the tool, "E_{11}" and "E_{22}" represent the Young's modulus along longitudinal and transverse directions, "ν" represents the Poisson's ratio and "G_{IC}" represents the critical crack propagation energy in mode I failure. This model had a reasonable agreement with the experimental results obtained in drilling of T300/N5208 graphite epoxy composite with ¼ inch standard high-speed steel drill [22].

In [24], Zhang et. al analyzed multidirectional laminates and developed a general closed form mechanical model for predicting the critical thrust force causing delamination at different ply locations. Good correlation was observed between the model and experimental results. Their models aimed at optimizing the drilling parameters and use the same as a control strategy to avoid delamination for adaptive controlled drilling systems.

In [25], Lachaud et. al. proposed a critical thrust force model based on uniform distribution of load along the cutting edges and chisel edge in contrast to the point load used by Ho-Cheng & Dharan [18] and Jain &Yang [22]. The critical force (F_c^*) predicted by this model are described by equations (2.10) – (2.12):

$$F_C^* = 8\pi\left(\frac{G_{IC}D}{\left(\frac{1}{3}\right)-\frac{D^{'}}{8D}}\right)^{0.5} \tag{2.10}$$

$$D = \frac{1}{8}\left(3D_{11} + 2D_{12} + 4D_{66} + 3D_{22}\right) \tag{2.11}$$

$$D^{'} = \frac{D_{11} + D_{12}}{2} + \frac{D_{12} + D_{66}}{3} \tag{2.12}$$

where, "*D's*" represent the bending stiffnesses of the laminate and "G_{IC}" represents the critical crack propagation energy in mode I failure. This analytical model showed good agreement with experimental measurements of static punching for uniformly distributed contact between the tool and the laminate. Since this correlation was based on static punching test, it could be not capture the complete dynamics of actual drilling process, and hence was not referred by future researchers in their work.

In [30], Kapoor et. al. used mechanistic approach and developed a model to predict the thrust force and torque at the cutting edges and chisel edge. Using Shaw and Oxford [14, 15] approach, they developed analytical models relating force components to chip load based on the drill geometry and cutting mechanism for the chisel edge and cutting edges. They were able to establish a good correlation for the forces at cutting edge with experimental data. However, the chisel edge model failed to agree with the experimental data, suggesting that there were additional material removal mechanisms other than orthogonal cutting while drilling of fiber reinforced composite laminates.

Tsao and Ho-Cheng [31] studied in detail the effect of the chisel edge in the generation of thrust force as highlighted by previous researchers [22]. They established a process window for the chisel edge length, beyond which delamination was expected to occur. They also observed that the process window widened at lower feed rates, which corroborated with the fact that feed was one of the critical cutting parameter causing delamination.

2.3 Thrust Force and Torque

Cutting forces produced during drilling are very important in determining the final quality of the drilled hole. Estimation and evaluation of these forces has been the focus of research in composite drilling since long time.

In [29], Malhotra measured both the thrust force and torque during drilling of woven carbon epoxy laminate of 8 mm thickness with a HSS drill. The cutting conditions used were: (i) feed range: 0.06 - 0.19 mm/rev and (ii) rotational speed range: 500 – 1,250 rpm. He found that at constant speed of 1,250 rpm, the thrust force increased gradually with increase in feed from 0.06 to 0.19 mm/rev. Under similar cutting conditions, the torque was found minimum at feed rate of 0.10 mm/rev, after which it increased rapidly. At constant feed of 0.06 mm/rev, the thrust force did not show considerable change as the speed was increased from 500 to 1,250 rpm, but the torque reduced for the same change. It was therefore concluded that feed rate has a dominant role in increasing the thrust force.

Ho-Cheng and Puw [32] conducted drilling experiments on both thermosets (carbon epoxy with fiber volume fraction of 60%) and thermoplastics (carbon fiber + acrylonitrile butadiene styrene having a volume fraction of 10%) using 5mm diameter standard two-flute HSS twist drill. They used spindle speeds in the range of 125 to 4,000 rpm and feed rate in the range of 50 to 300 mm/min. The cutting speeds were in the range of 2.0 to 63.0 m/min. They found the thrust force to increase with the increase in feed rate as illustrated in Figure 2.2. This was attributed to the increase in feed rate, thus increasing the cutting area, which further increases the cutting effort, i.e., the thrust force.

In [33], Tsao et. al. conducted drilling tests on woven carbon fiber laminate using a 10 mm diameter twist drill of HSS. The laminate properties were: (i) stacking sequence of $[0/90]_{12s}$, (ii) thickness of 6 mm, (iii) fiber volume fraction of 55% , (iv) modulus of elasticity of 18.4 GPa, (v) energy release rate of 140J/m^2 and (vi) Poisson ratio of 0.3. The cutting conditions used were: (i) feed rate from 0.003 to 0.0133 mm/ rev, (ii) rotational speed from 900 to 1,000 rpm and (iii) cutting speed from 28.3 to 31.4 m/min. They found that at constant speed, the thrust force increased progressively with the increase in feed. This observation was similar to that found by Malhotra [29].

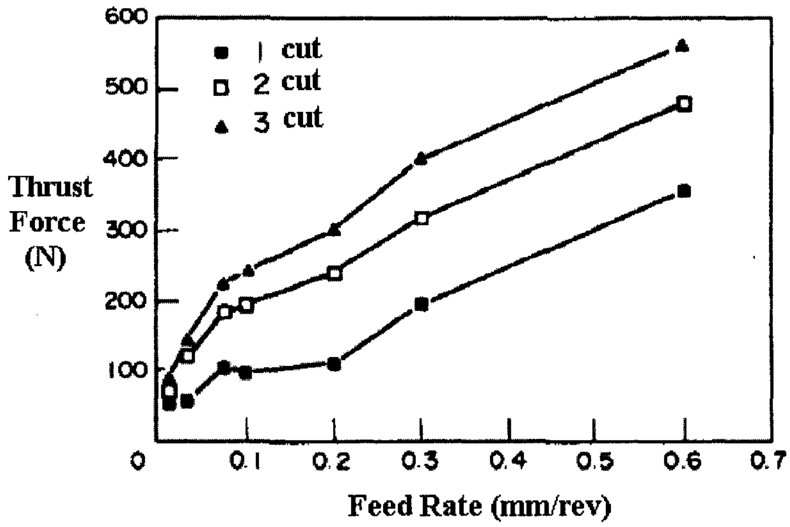

Figure 2.2: Correlation between Thrust Force and Feed Rate [32]

Lin and Chen [34] performed drilling tests on unidirectional carbon fiber epoxy laminate with a volume fraction of 60 % using standard carbide twist drill at ultra high speeds. The cutting conditions used were: (i) feed rate: 0.03 mm/rev, 0.05 mm/rev and 0.07 mm/ rev, (ii) rotational speed: 9,550, 24,100 and 38,650 rpm, (iii) cutting speed: 210, 530 and 850 m/min and (iv) drilled lengths: 13.5, 59.4 and 94.5 mm. They found that the thrust force drastically increased as the cutting speed was increased for each drilled length, while torque increased slightly. Their results were contrary to those reported in [29]. They explained this deviation as a result of extensive tool wear, which occurred at ultra high speeds, thus altering the tool geometry and resulting in higher thrust force and torque. Since the minimum drilled length in their experiments was almost double that reported in [29] and the cutting speeds were almost 10 times greater, the tool wear phenomenon was highly dominant. At constant speed, the thrust force and torque both increased with increase in feed rate and matched the results presented in [14, 15, 32].

In [13], Khashaba conducted drilling tests on glass fiber reinforced plastic (GFRP) composite using standard HSS drills and evaluated their machinability and damage mechanisms. The laminate was made of woven E-glass fiber and epoxy prepreg having a fiber volume fraction of 32.73 % and thickness 3.52 mm. The cutting conditions used were: (i) spindle speed: 455, 875 and 1850 rpm (ii) feed: 0.03, 0.08, 0.15, 0.23, 0.30 mm/rev and (iii) cutting speed: 11.4 to 46.5 m/min. His investigation revealed that at constant spindle speed, both the thrust force and the torque increased with the increase in feed rate as shown in Figure 2.3. This was because of the increase in chip thickness, which results in the increase in the cutting area and the higher thrust force. However, the thrust force and torque were found to decrease with the increase in cutting speed at fixed feed rate as shown in Figure 2.3. This decrease was attributed to higher cutting temperatures generated with the increase in cutting speed combined with low coefficient of thermal conductivity of GFRP composite, which resulted in accumulation of heat around the cutting edges of drill leading to softening of polymer matrix and thus reduction in cutting forces.

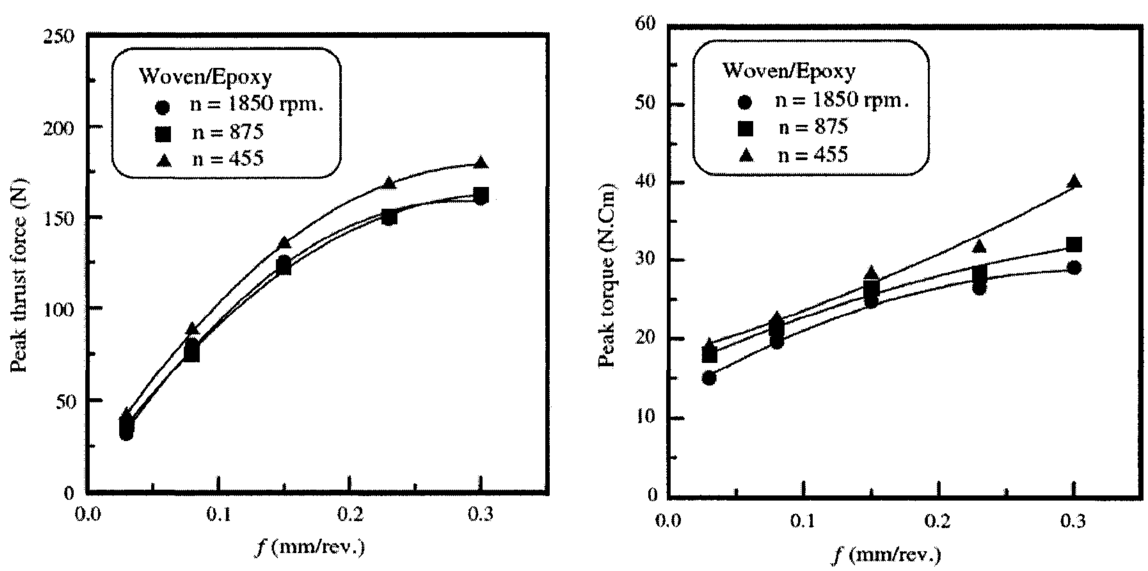

Figure 2.3: Peak Thrust Force and Torque v/s Feed for Glass Fiber Woven Epoxy at Different Spindle Speeds [13]

Another investigation of machinability of GFRP composite using standard HSS drills was carried out in [35]. The laminates produced from glass fiber epoxy prepreg had different fiber volume fractions of 0, 9.8, 13.6 and 23.7 % and constant thickness of 8.5 $\pm$ 0.1mm. The cutting conditions used were: (i) spindle speed: 218, 455, 634 and 1,850 rpm (ii) feed: 0.05, 0.10 and 0.23 mm/rev and (iii) cutting speed: 5.5 to 46.5 m/min. This investigation revealed similar behaviour as observed by Khashaba [13], but contrary to Lin and Chen [34].

2.4 Delamination

Delamination has been found to be the most critical failure mode in laminated composites. It is associated with failure of the weakest part of the composite material – the matrix and the fiber interface or the matrix itself. It has also been found to occur at stress concentration sites such as holes, voids, material discontinuities, ply drop offs, etc.

The study of delamination fracture has been the most challenging phenomenon in composite machining. Dharan [26] used the approach of linear elastic fracture mechanics to establish crack growth in delamination of graphite and aramid epoxy composites. He concluded that the crack propagation is coplanar and along the weak matrix phase.

Later on, Dharan and Saghizadeh [36] worked on the determination in relation to fracture toughness of graphite and aramid composites. They found the fracture toughness of these laminates to be a function of the loading rates, both for unidirectional and woven reinforcements. However, when a comparison was made between the unidirectional and woven fabrics, they found the fracture toughness of the laminate to improve by a factor of 2.5 with the use of woven fabrics as compared to that of the unidirectional ones. This was attributed to the waviness of the weave and associated greater fracture surface area of woven plies as compared to unidirectional ones. Their results proved the superiority of woven prepregs for a multidirectional loading environment.

Tagliaferri et. al. [37] performed drilling experiments on glass fiber reinforced plastic composites having a (0/90/$\pm$ 45) layup, nominal thickness of 1.2 mm and fiber volume fraction of 30 % with 8 mm diameter high speed steel drills in the cutting speed range of 1.5 to 40.2 m/min, to verify the effects of machining parameters on the cut quality. They found the delamination size (D), which was the width of the damage zone around the drilled hole, to increase with the increase in feed but decrease with the increase in speed as shown in Figure 2.4. They also found the delamination damage to decrease to a minimum value for a definite spindle speed (V_r, expressed as rpm) - feed speed (V_t, expressed as tool travel in the feed direction in mm/min) ratio (V_r/V_t), beyond which the damage remained constant. They concluded that the lower values of V_r/V_t produced thicker chips, which in turn produced larger cutting forces during the tool-material interaction, and hence resulted in larger damage. A critical spindle speed - feed speed ratio of 150 was found for this particular GFRP composite.

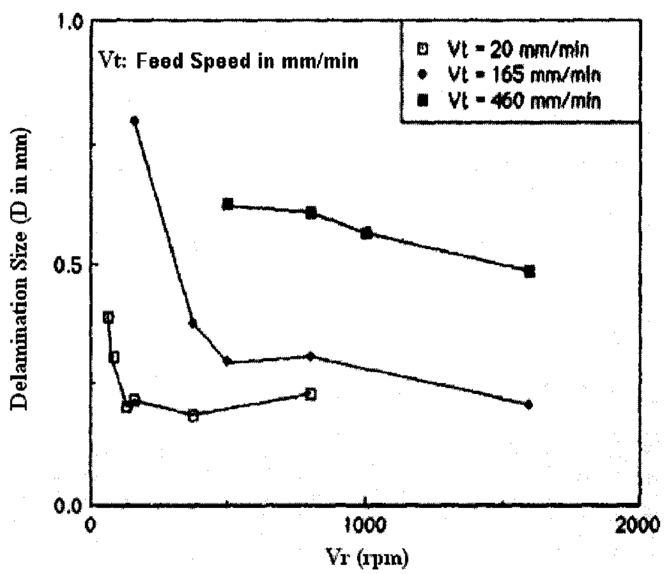

Figure 2.4: Delamination Size "D" at different Spindle Speeds " V_r" and different Feed Speeds "V_t" for GFRP Composite [37]

Caprino and Tagliaferri [20] performed extensive tests on chopped strand glass fiber epoxy composites having a fiber volume fraction of 35 % using 8 mm diameter standard point HSS drills in the cutting speed range of 1.0 to 41.3 m/min. The spindle speeds ranged from 40 to 1,645 rpm and feed rates from 5.7 to 2,630 μm/rev. They found that at very higher feed rates, the failure modes showed features typical of impact damage with step-like delaminations, intralaminar cracks and high-density micro failure as shown in Figure 1.10, which disappeared at lower feed rates. They also established that the number of delamination sites increased considerably along the depth, reaching its maximum near the drill exit. Their findings were in very good agreement with Jain and Yang's [22] delamination model.

In [38], Di Paola et. al. exploited the technology of high speed video imaging to understand the complete crack growth propagation phenomenon during drill exit. They used unidirectional carbon fiber epoxy laminate made of 80 plies with a fiber volume fraction of 62 % and a total thickness of 8.8 mm, using a standard point carbide drill. The spindle speed was fixed at 400 rpm while the feed rate was varied from 50 to 250 μm/rev. They established good correlation between thrust force, delamination and the fiber orientation. Their experimental results proved that at higher feed rates, the resulting higher thrust force produced damage outside the radius of the drill, while at low feed conditions, the cracks were limited within the radius of hole, when examined at varying depths. They highlighted the importance of capturing and modeling cutting forces throughout the drilling cycle for avoiding delamination.

In [39], Enemuoh et. al. used Taguchi's experimental analysis technique and multi-objective optimization criterion for damage free drilling of carbon fiber reinforced thermosets with standard carbide drills. Based on their experimental evaluation and optimization, they recommended high drilling speeds and low feeds for producing delamination free holes. Their conclusions corroborated with the ones made in [20, 37, 38]. In [40] the same authors used design of experiments approach, similar to that used in [39], and investigated the process conditions that minimized delamination damage in thermoplastic (PEEK) composite. They quantified the effects of cutting speed, feed rate, tool material and tool geometry on delamination and surface finish, during the drilling of graphite fiber reinforced composites, and found optimum drilling conditions using analysis of variance technique. Their analysis revealed cutting speed and feed rate as the significant factors affecting surface roughness and thrust force/delamination, respectively.

Davim and Reis [41] performed drilling tests on carbon fiber epoxy composite laminate using 5 mm diameter standard carbide drills for drilling speeds of 1,000, 1,500 and 2,000 rpm and feed rates of 40, 80 and 150 μm/rev. Based on these spindle speeds the cutting speeds ranged from 15.7 to 31.4 m/min. The CFRP laminate was made up of 16 plies with a fiber orientation of 0/90 degrees having 4 mm total thickness. They found the delamination factor (R_d) at exit to be lesser than that at entrance. Their results, however, differed from others [20, 37, 39, 40] as they found delamination to increase not only with feed rate but also with cutting speed, as illustrated in Figure 2.5. No explanation was given for these contrasting results by the authors. So according to the author of this thesis it becomes imperative to reinvestigate these contradictory results in the current experimental work.

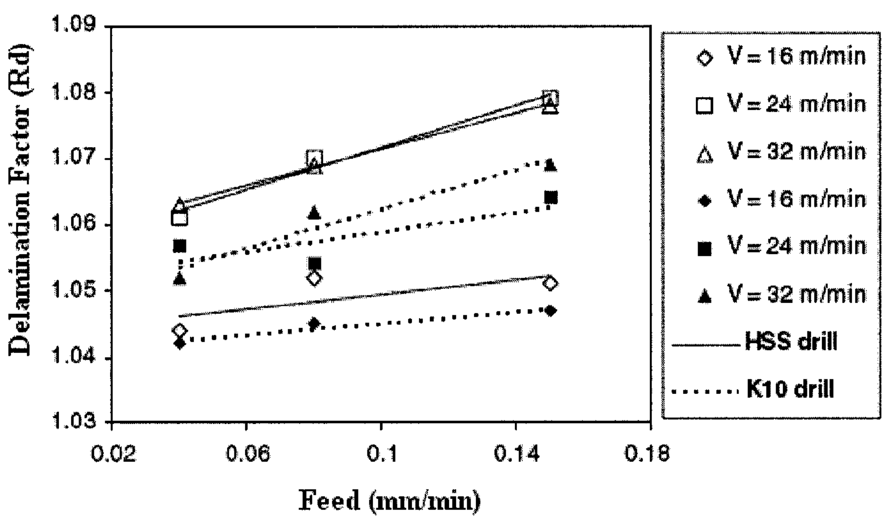

Figure 2.5: Delamination Factor (R_d) as Function of the Cutting Parameters Feed (mm/min) and Cutting Speed (V in m/min) for Two Tool Materials – HSS and Carbide (K10), having Same Geometry [41]

Kim et. al [42] found the delamination length to increase both with feed and cutting speed when drilling of carbon fiber thermoplastics with standard carbide drills. They concluded that higher feed rates generated higher thrust forces, which increased delamination damage. However, the effect of cutting speed was unexplained.

Khashaba [13] performed drilling tests on woven glass fiber epoxy composites having a fiber volume fraction of 32.73 % and total thickness of 3.52 mm with 8 mm diameter standard point HSS drill at different spindle speeds (455, 875 and 1,850 rpm) and feed rates (0.03, 0.08, 0.15, 0.23 and 0.3 mm/rev). The cutting speeds ranged from 11.4 to 46.5 m/min. Figure 2.6 illustrates his results, which depicts the delamination damage to increase with feed rate but decrease with increase in spindle speed. It is, however, noticeable that this trend is not applicable at all feed rates, as slight variations are observed at feed rates less than 0.10 mm/rev. According to the author of this thesis, higher delamination at these low feed rates (f < 0.1 mm/rev) could be attributed to matrix thermal softening at relatively higher spindle speeds.

Sonbaty et. al [35] and Bhattacharya et. al [46] performed drilling tests for different types of composites and found the delamination results to be similar to those reported in [13, 20, 37-40].

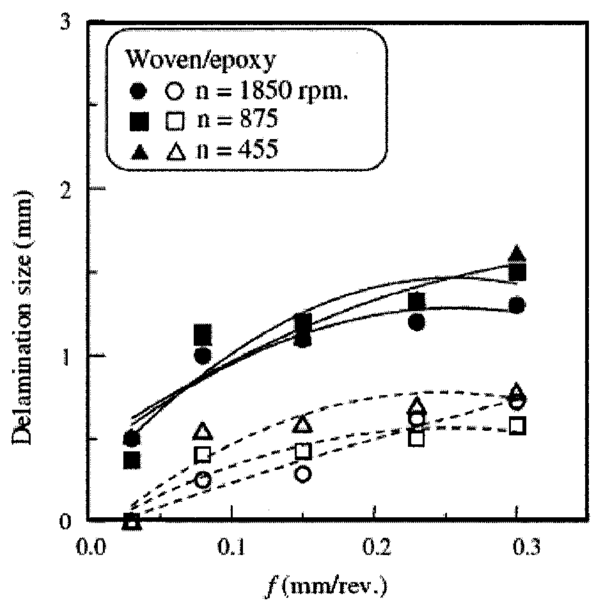

Figure 2.6: Delamination Size for Different Spindle Speeds “n” at Different Feed Rates “f” for GFRP Composite. Dark Symbols Represent Delamination at Exit and White Symbols Represent Delamination at Entry [13]

Some researchers, eg. Tsao and Ho-Cheng [43] worked on developing non-destructive testing techniques for examining delamination. They evaluated ultrasonic "C' scan and computerized tomography techniques to capture not only surface delaminations but also through the thickness delaminations.

2.5 Hole Quality

Hole quality characteristics are evaluated in terms of geometric accuracy and surface roughness. Research has been conducted to define the interaction between the cutting parameters, the tool and the workpiece material to reduce the errors in hole diameter, roundness, cylindricity and improve surface finish.

In [29], Malhotra found the average surface roughness (R_a) to increase with the increase in the number of drilled holes and attributed it mainly to tool wear. He reported an average surface roughness of 3.8 μm for glass epoxy composite laminate at a spindle speed of 1,250 rpm and feed rate of 0.06 mm/rev on account of an average flank wear of 280 μm of HSS drill.

Ho-Cheng and Puw [32] found that at lower feed rates and cutting speeds, the fracture is less violent and more controllable, thus smoother surface is produced. Figure 2.7 shows the correlation established between surface roughness and cutting conditions for carbon epoxy composite laminate.

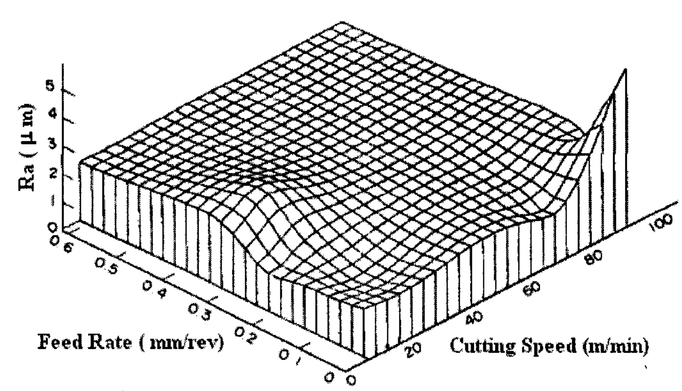

Figure 2.7: Correlation Between Surface Roughness (Ra) and Cutting Conditions (i.e. Feed Rate and Cutting Speed) [32]

Kim et. al. [42] evaluated the machinability of carbon fiber thermoplastics (PEEK). Their evaluation involved spindle speeds in the range of 1,320 to 5,440 rpm and feed rate in the range of 20 to 300 μm/rev. They found that higher feeds produced larger surface roughness (R_a) because of deeper fiber pullouts. A similar response was observed by Ramulu and Kim [44] during their drilling tests on a quasi-isotropic graphite bismalimide (Gr/Bi) composite of thickness 7.2 mm and titanium alloy stacks with standard carbide drills. Surface roughness deteriorated both at high feeds and speeds. However, higher feed rates were found to effect surface roughness more than high cutting speeds. At high feeds, extensive fiber pullout was found to be the main reason for higher roughness. Analysis of the hole diameter revealed oversized holes with standard carbide (C2 grade).

Sonbaty et. al. [35] obtained results similar to Ramulu and Kim [44] for the dependence of surface roughness on feed rate. However, contrasting results were obtained at higher speeds. Their experiments on glass fiber epoxy composite laminates, having different fiber volume fraction of 9.8 %, 13.7 % and 23.7 %, showed an improvement in surface finish at high speeds. Further analysis revealed that the higher fiber volume fraction of glass in epoxy composites increased the thermal conductivity of the laminate, which in turn reduced the thermal damage and hence improved the surface finish with increase in fiber volume fraction.

Konig and Graβ [45] performed experiments to assess the hole quality during the drilling of glass, carbon and aramid fiber reinforced thermosets with carbide and HSS drills. They found the surface roughness to be affected more by the feed rate than the cutting speed especially for unidirectional composites. This dependence was found to be reduced with the increase in the multidirectional plies in the laminate. This was attributed to the reduced interlaminar damage, as the adjacent layers in different directions provided better support to the compressive load while drilling.

Another study on hole drilling of Kevlar (aramid fiber) composites was done by Bhattacharya and Horrigan [46]. They found the average hole surface roughness (R_a) to improve significantly by the use of liquid nitrogen during drilling, which demonstrated the effect of thermal damage in deteriorating the hole surface finish.

Analysis of the hole diameter during drilling of glass fiber thermoplastic composites by Kim et. al. [42] revealed undersized holes when drilled with standard carbide (C2 grade). This was attributed to the spring back capability of thermoplastics, which resulted in diameter errors. However, in drilling of graphite fiber bismalimide (Gr/Bi) composite and titanium alloy stacks with standard carbide drills, Ramulu and Kim [44] found the holes to be oversized for a range of spindle speeds (660 - 1,750 rpm) and feed rates (0.08 - 0.25 mm/rev). This effect was found to increase with both spindle speeds and feeds, as illustrated in Figure 2.8. Hole circularity was found to increase with speed but decrease with feed rate. They attributed this increase in hole diameter and circularity to increased induced vibrations at higher speeds. However, the decrease in hole circularity with feed rate was unexplained. According to the author's knowledge this could be tool and workpiece material dependant.

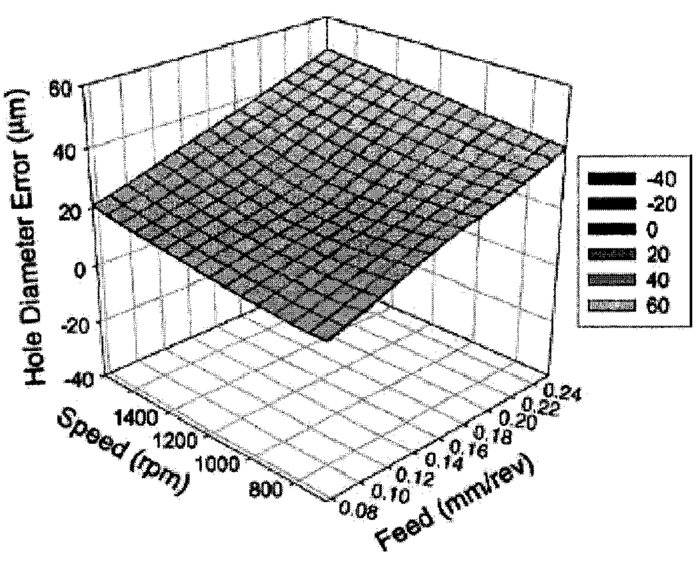

Figure 2.8: Average Diameter Error (μm) for Gr/Bi with various feeds and speeds for standard carbide drill [44]

In [47], Ramkumar et. al. experimentally studied the machinability of quasi-isotropic glass fiber epoxy laminates using uncoated, Titanium Nitride (TiN) coated and Titanium Carbide (TiC) coated HSS tools. They found the form error to be higher for uncoated tools for lesser number of drilled holes (about 25). However, with the increase in the number of holes the uncoated tool provided better form as compared to coated ones. Figure 2.9 shows that TiN coated HSS drills and TiC coated HSS drill performed better up to 37 and 25 holes, respectively, after which they were found to be worse than uncoated HSS drill. They attributed this poor performance mainly to the heat accumulation during continuous drilling, which resulted in peeling off of the coating and thus poor hole circularity.

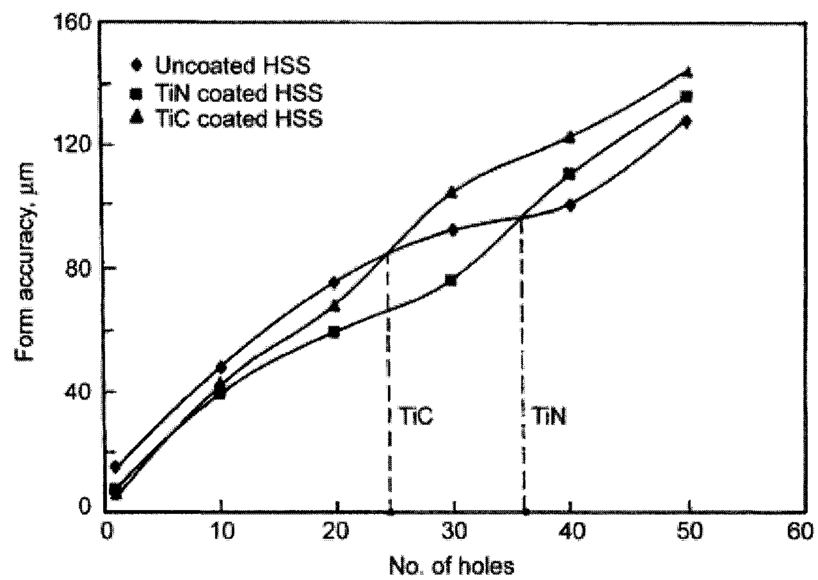

Figure 2.9: Form Accuracy vs. Number of Holes Curves for (0/ +45/90)$_{2s}$ Glass Fiber Epoxy Laminates and Uncoated and Coated Standard HSS Drills [47]

In [48], Brinksmeier and Janseen evaluated the machining characteristics of stacked composites (CFRP/Titanium/Aluminium Stacks). These dissimilar materials introduced a unique set of problems during drilling. Apart from the intense tool wear caused by high fluctuating loads because of drilling dissimilar materials, the erosion and abrasion caused by carbon fibers were also critical. Moreover, the different moduli of elasticity of the materials caused variable elastic deformations, and therefore varying tolerance along the hole depth. Extensive experiments were undertaken to find solutions for economic drilling of these kind of multilayered materials. With a 16 mm standard three fluted drill, deviations in the diameter in the range of 80 μm were observed when dry drilling was performed. However, with the use of minimum quantity lubrication (MQL) with fatty alcohol, diameter tolerance of 17 μm throughout the hole was achieved. Hence, they were able to establish the benefits of MQL in drilling of such kind of multilayered materials for achieving better hole tolerances.

2.6 Tool Wear

Research done on machinability characterization of variety of composite materials highlights the importance of understanding and minimizing tool wear to maintain desired hole quality during a continuous operation. Over the decades, different tool materials like high-speed steel (HSS), carbides, coated HSS, coated carbides and diamond coated carbides have been tested to understand the wear mechanisms for enhancing tool life.

In [29], Malhotra reported the occurrence of both chisel edge and flank wear during drilling of carbon epoxy composite laminate with HSS and Carbide drills at a spindle speed of 1,250 rpm and feed rate of 60 μm/rev. He found the flank wear to be more prominent as compared to the chisel edge wear. This was understandable as most of the cutting happened at the cutting edges while the chisel edge mainly extruded the material. A comparison between the tool materials revealed an average flank wear (V_b) of 800 μm after drilling just 40 holes with a HSS drill. Only 130 μm average flank wear was observed for carbide drill after drilling of 400 holes. He also established a reduction in flank wear with an increase in feed rate from 60 to 190 μm/rev.

In [34], Lin and Chen compared the performance of standard twist drill and multifaceted drills during ultra high speed drilling (up to 38,000 rpm) of CFRP composites. They found aggressive tool wear to be a major problem as it increased significantly at such ultra high speeds. As no quantitative data for tool wear was reported, the evaluation was done qualitatively based on change in tool geometry by microscopic observations. It was observed that as the drilled length increased, wear started at the outer corners, and the outer part of the cutting edge region was ground away. This increased the contact area between the tool and composite, and thus increased the thrust and tangential forces. Table 2.1 provides a comparison between the two tool types used in their experiments. It is evident from the data that the standard point twist drill, which generated lower thrust force at increasing drilled depths, was better than multifaceted drill.

Table 2.1: Comparison of Thrust Force Generated by Two Tool Types at different Drilled Depths during Ultra High Speed Drilling of CFRP Composites [34]

Spindle Speed	Feed Rate	Drilled Depth	Multifaceted Drill Thrust Force	Standard Point Drill Thrust Force
rpm	mm /rev	cm	N	N
38650	0.03	13.5	273.69	105
38650	0.03	59.4	470.38	236.45
38650	0.03	94.5	684.62	284

Ramkumar et. al [47] experimentally evaluated the performance of coated (TiN and TiC) and uncoated HSS tools during drilling of glass fiber epoxy laminates having fiber volume fraction of 40%. The tests done at spindle speed of 1,700 rpm and feed rate of 250 μm/rev revealed better performance of the uncoated tool as compared to the coated one for large number of holes. Coated drill was found to wear faster beyond a certain number of holes. This was mainly attributed to the peeling and chipping off of the coating from the base material.

In [49], Murphy et. al. tested the performance of coated and uncoated tungsten carbide drills in drilling of carbon fiber epoxy composites at spindle speed of 3,000 rpm, cutting speed of 59.8 m/min and feed rate of 48.5 μm/rev. The performance was analyzed in terms of damage to the composite, increase in force, torque and average flank wear. The results of flank wear as illustrated in Figure 2.10 showed a general increase in flank wear with increase in number of drilled holes. A reduction in the flank wear rate occurred around 5-7 holes, which was explained to correspond to a transition from primary to the secondary wear zone. Overall, no extra benefits were gained by the use of coated tool in this investigation of drilling CFRP composites. A comparison of the works of [47] and [49] clearly revealed that uncoated carbides perform much better than HSS tools for both glass and carbon fiber epoxy composites.

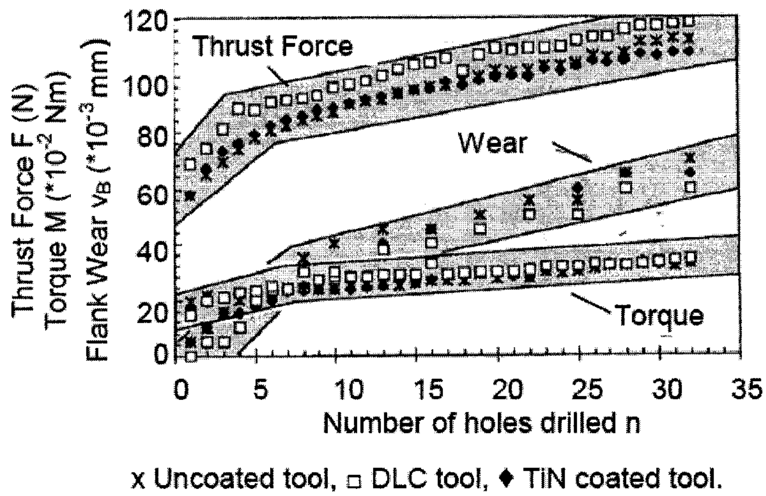

Figure 2.10: Variation of maximum thrust force, torque and tool wear with number of holes [49]

Inoue et. al [50] investigated the influence of tool wear on the internal damage in small diameter drilling of glass fiber epoxy composites. They found higher flank wear to occur at lower feed rates and higher cutting speed.

Velayudham et. al. [51] evaluated the performance of carbide (grade K10) drills in drilling of high volume fraction (about 66 %) glass fiber polymeric composites for a range of cutting speeds from 51.5 to 80.4 m/min. They identified similar wear mechanisms as reported in [29]. They found the average flank wear to increase progressively up to about 300 holes, which was attributed to normal performance of the drill point as shown in Figure 2.11. Beyond 300 holes, however, a rapid increase in tool wear was found to occur. A critical review of their results, by the author of this thesis, indicate an increase in average flank wear with increase in feed rate, and decrease with increase in speeds, which was contrary to the one obtained in [29, 50].

Weinert and Kempmann [52] investigated the effects of using coolant during drilling of high fiber volume fraction glass epoxy composites ($V_f = 70\%$) with uncoated carbide drills. The drilling tests were performed at 7,000 rpm and 260 μm/rev. They observed maximum flank wear (V_{bmax}) of about 100 μm with use of an emulsion as compared to 325 μm V_{bmax} obtained during dry drilling. It was, therefore, recommended to use emulsion to enhance tool life, provided it does not cause a chemical reaction with the composite and affect the hole quality.

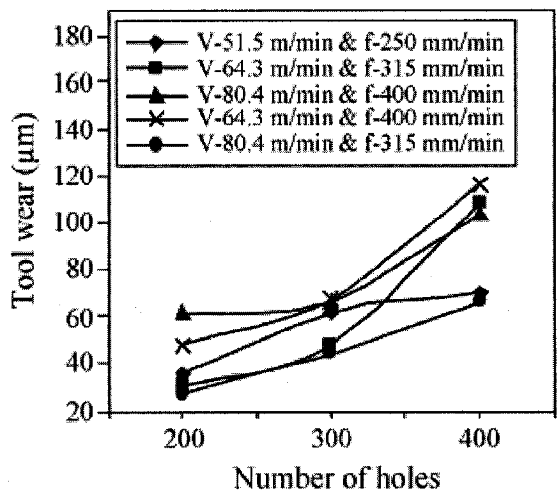

Figure 2.11: Typical Variation in Tool Wear with different Combinations of Cutting Speeds [51]

In [44], Kim et. al. a performance evaluation of HSS and carbide drills was done during drilling of graphite fiber bismalimide (Gr/Bi) composite and titanium alloy stacks. Carbides having higher hot hardness were found to perform better than corresponding HSS drills. The average flank wear was found to increase both with spindle speed and feed rate. The tool wear model developed for standard carbide drill by these authors is described by equation (2.13):

$$Vt^{0.34} f^{-0.68} = 320 \tag{2.13}$$

Where "V" is the cutting speed in m/min, "t" is the tool life in minutes and "f" is the feed rate in mm per rev.

2.7 Cutting Temperature

Machining of fiber reinforced plastics (FRP) in general and drilling in particular is characterized by high cutting temperature. This is mainly due to the poor thermal conductivity of thermoplastics and carbon fibers, which results in low heat being carried away by the chips and the workpiece laminate. Thus the fractional heat load on the tool is significantly higher (up to 55%) in FRP machining than in metals machining (about 20%) [45]. As discussed in previous sections, on one hand the rise in cutting temperature reduces the effort required for cutting by making the material softer, but on the other hand the temperature rise assists in enhancing tool wear and deteriorates hole quality. High cutting temperature also leads to defects like dimensional errors, increased delamination, matrix burning, charring and micro cracking. These defects in turn lead to reduction in the bearing strength of the laminate. Therefore in order to optimize the cutting process it is essential to gain understanding of the cutting temperatures.

Since the geometry of the drill is quite complex, it is difficult to measure temperature at the cutting edge. Also, since the cutting speed required for FRP is high (rarely below 500 rpm) the frequency of contact between the thermocouple, located inside the workpiece, and the cutting lip is very high and thus the contact time is proportionally small. This makes the real time measurement of cutting temperature quite challenging during the drilling process. Researchers have used thermocouples, by locating them on the tool or by embedding inside the laminate, to experimentally measure temperature during the cutting process. However, due to the complexity of the drilling system and tools, very limited literature is available on this subject.

In [53], Nagao et. al. designed a special frequency modulated transmitting torque, thrust force and temperature sensor, which was mounted on the tool holder during drilling. With this setup, they were able to perform cutting tests using a 4 mm diameter HSS drill at cutting speed of 19.1 m/min (N = 1,520 rpm), feed rate of 20 mm/rev and drilled depth of 15 mm on printed circuit boards (PCB). The PCB's were made of thin epoxy, printed circuits and glass fiber epoxy prepreg pressed together. A K-type thermocouple was passed through the coolant-hole of the drill and three other thermocouples were embedded inside the laminate around the drilled hole at two different depths. They found a temperature rise of about 200 ^{o}C at the drill tip. Since the glass transition temperature of epoxy resin is about 130 ^{o}C, the resin softened and solidified again at this temperature. Moreover, the authors found the temperature at the drilling point to rise in proportion to the square root of time and the increase in thickness of the board.

Weinert and Kempmann [52] used a technique similar to that used in [53] for the measurement of temperature during drilling of woven carbon fiber epoxy composite having fiber volume fraction of 70 % with 8 mm diameter carbide (K10/20 grade) at cutting speed of 175.9 m/min. They used inverse drilling kinematics and embedded three thermocouples through the through- coolant-holes close to the cutting edge on the clearance face of the drill. Their results indicated rise in the average tool temperature with both cutting speed and feed, which was basically caused by higher thermal load. In both cases, increasing cutting conditions lead to higher energy transformation and hence higher dissipation of mechanical energy into heat.

Bhatnagar and Ramakrishnan [54] performed experimental investigations to measure the tool tip temperature during the drilling of GFRP and CFRP composites with different tool types (four facet and eight facet carbides). They used a direct technique of cutting the thermocouple embedded in the laminate thereby making a transient hot junction under different feed-speed combinations. They found the temperature to increase with increase in spindle speed but decrease with the increase in feed both for CFRP and GFRP as shown in Figure 2.12. However, the increase for CFRP was more as compared to GFRP as illustrated in Table 2.2. They attributed this effect to the substantially higher value of thermal conductivity of CFRP (4.19 $W/m^{o}K$) as compared to GFRP (0.3 $W/m\,^{o}K$), because of which more heat was taken away by chips than the tool at higher feed rates causing reduced tool tip temperature.

Chen [55] followed the approached used in [53] for measurement of temperature during drilling of CFRP. In his embedded thermocouple technique, he used electrical discharge machining (EDM) process to create a groove and place the thermocouple about 500 μm away from the cutting edge. Measurements of temperature during drilling of unidirectional and multi directional carbon fiber epoxy composite laminates with a 5 mm high speed drill was conducted for two cases:

i. Fixed feed rate = 50 mm/rev and speed range: 35 m/min – 200 m/min.

ii. Fixed Spindle speed = 1370 rpm and feed range: 100 μm/rev – 400 μm/rev.

Table 2.2: Tool Tip Temperature Data for Drilling of CFRP using a Eight Facet Drill [54]

Feed Rate (mm/rev)	**Spindle Speed (rpm)**	**Tool Tip Temperature- Eight facet drill/GFRP (°C)**	**Tool Tip Temperature- Eight facet drill/CFRP (°C)**
22.5	2000	200	425
22.5	4000	225	475
22.5	6000	350	525
7.5	2000	375	650
7.5	4000	425	725
7.5	6000	525	825

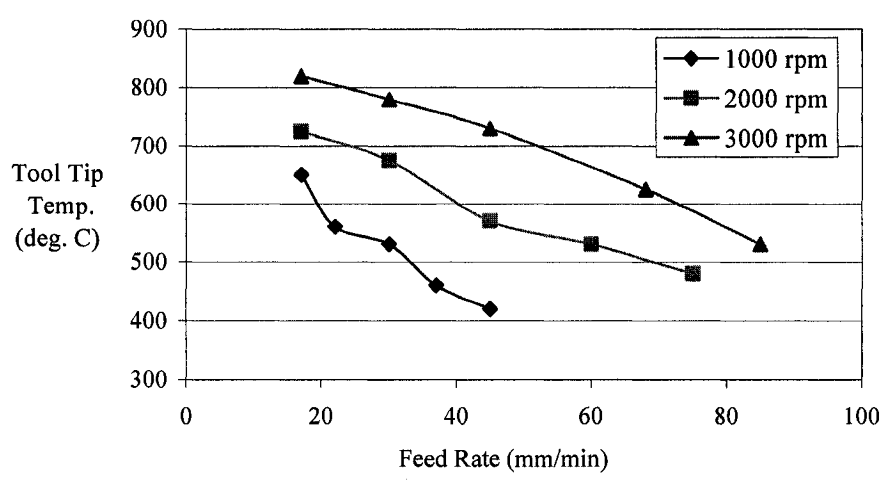

Figure 2.12: Tool Tip Temperature (TTT) for Eight Facet Drill during Drilling of Carbon Fiber Reinforced Plastics (CFRP) [55]

Chen [55] followed the approached used in [53] for measurement of temperature during drilling of CFRP. In his embedded thermocouple technique, he used electrical discharge machining (EDM) process to create a groove and place the thermocouple about 500 μm away from the cutting edge. Measurements of temperature during drilling of unidirectional and multi directional carbon fiber epoxy composite laminates with a 5 mm high speed drill was conducted for two cases:

iii. Fixed feed rate = 50 mm/rev and speed range: 35 m/min – 200 m/min.

iv. Fixed Spindle speed = 1370 rpm and feed range: 100 μm/rev – 400 μm/rev.

His results have been illustrated in Figure 2.13. Empirical results indicated that the flank surface temperature increased with increasing cutting speed but decreased with feed rate. This is in agreement with the results obtained in [54]. However, the results reported by Chen [53] were in contrast to those presented in [52].

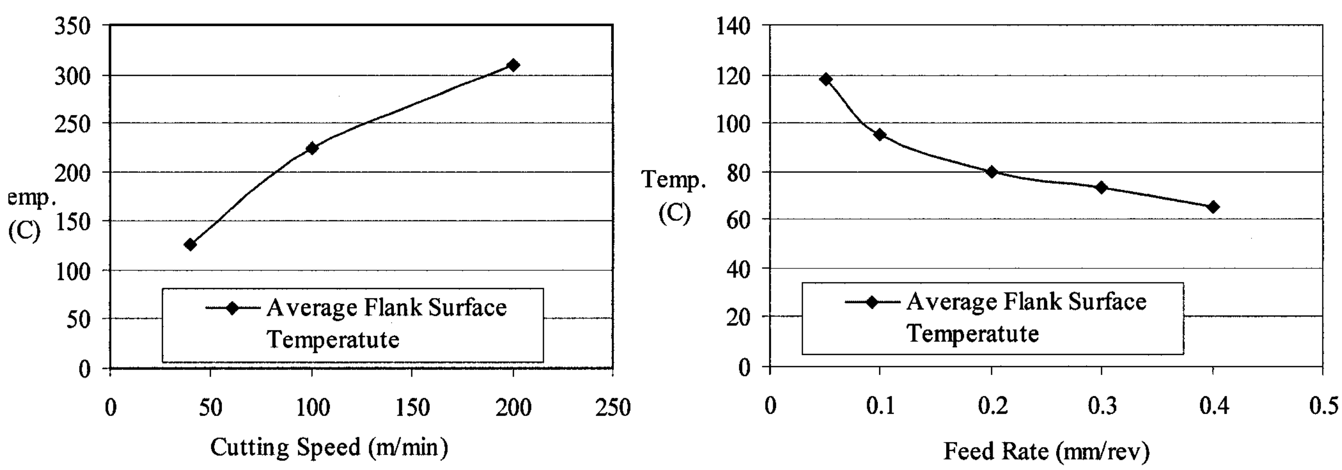

Figure 2.13: Influence of Cutting Speed and Feed Rate on Flank Surface Temperature during Drilling of CFRP [55]

2.8 Conclusions of Literature Review

It is evident from the literature review that sufficient amount of work has been done to define the optimum spindle speed and feed rates for desirable hole quality i.e. close diameter tolerances, better hole circularity, cylindricity, surface finish etc. Lower feed rates have been found to give good hole quality. The role of spindle speed is not very clear as in some cases the results contradict. Also, more work has been done in characterizing the behaviour of unidirectional glass and carbon fiber epoxy composites as compared to woven composites.

In terms of the machine tool capabilities, most of the work available in literature has been carried out in the spindle speed range of 50 to 9,000 rpm and feed range of 6 to 500 μm/rev. One investigation that was carried out for ultra high spindle speed range of 24,000 – 38,000 rpm revealed excessive tool wear and damage to laminate. No work, however, is available in the high spindle speed range of 10,000 to 15,000 rpm and feed range between 500 to 800 μm/rev, which the author plans to address in this research work.

One area that has been addressed widely is delamination of laminated composites. Work has been done to define delamination mechanisms, develop model to relate the controllable cutting parameters, laminate and tool material properties to the extent of delamination damage. Based on these models, delamination avoidance strategies like variable feed along the hole depth have been proposed to avoid exit delamination. However, most of the analytical models discussed are suitable for unidirectional and multidirectional laminates and no evidence of work for woven composites exists to the author's best knowledge.

Limited amount of work has been done in the area of measurement of cutting temperatures. There are few contradictions as highlighted in section (2.7), which if investigated further could make the process more understandable.

The issue of tool wear has been addressed both for HSS and carbide tool materials, but mainly in drilling of unidirectional composites. Uncoated carbide tools have been found to be most suitable in terms of tool life and hole quality. However, little evidence is found in literature that shows the effect of cutting temperature on tool wear. Moreover, most of the tool wear investigations have been in identifying the progression of flank wear with time or number of drilled holes. No work has been done to study the wear regimes, and thus determining the tool replacement strategy during a continuous drilling process as per the author's best knowledge.

This thesis is aimed at addressing some of the issues highlighted above specifically, in the drilling of woven carbon fiber epoxy laminated composite with standard carbide twist drill.

2.9 Thesis Objectives

The following describes the scope of the thesis work:

1. To measure the effect of variation in cutting parameters (spindle speed and feed) on cutting forces, delamination, hole diameter error, hole circularity error and hole surface finish after the drilling operation.

2. To establish the optimum cutting parameters that give no/low delamination and best hole quality (lowest hole diameter error, high circularity and surface roughness) at maximum productivity.

3. To measure temperature during the cutting process and evaluate its effect on cutting forces and hole quality.

4. To establish machinability maps for the range of selected cutting parameters.

5. To examine the mechanisms of tool wear and its progression as a function of time or number of drilled holes. Also evaluate the impact of tool wear on cutting forces, delamination and attributes of hole quality.

Chapter 3

Experimental Setup

3.1 Introduction

This chapter discusses in detail the experimental setup designed to perform machinability drilling tests on woven composites. The entire experimental research task was divided into three phases:

i. Conventional and high speed drilling (HSD) experiments
ii. Temperature measurement during conventional and high speed drilling
iii. Experiments for characterizing tool wear during high speed drilling

The first and second parts were carried out to study the machinability characteristics of the material at low, medium and high speed, and feed cutting conditions. In all the experiments, no coolant was used and hence all tests were performed dry. The responses, for the various desirable outputs, were recorded and used as inputs for the generation of machinability maps. The last part involved study of the tool wear mechanisms and the effect of tool wear on hole quality. The machinability maps created from the first phase were used to decide the cutting conditions for tool wear evaluation.

The experiments were conducted at the Advanced Material Removal Laboratory, Aerospace Manufacturing Technology Centre of the National Research Council of Canada, located in Montreal, Canada. The detailed description of the machine tool, tool holder, tool type, composite laminate and the measurement instruments used for this research work are discussed in the following sections.

3.2 Machine Tool

All the drilling tests were carried out on a 5-axis high-speed, high-power horizontal machining centre Makino A88ε [57], having the following characteristics: 50 kW spindle power, 3 linear and 2 rotary axes, maximum spindle speed of 18,000 rpm, maximum feed rate of 50 m/min, minimum feed setting unit of 1μm, tool clamping force of 19.6 kN and HSK 100A spindle adapter. This machine tool is very versatile and multifunctional for use in milling, drilling, tapping, grinding and honing operations. The large machining envelope (900 x 800 x 970 mm) has the capability to machine medium size components used in aerospace industry. Figure 4.1 shows the Makino horizontal machining center used in this research work.

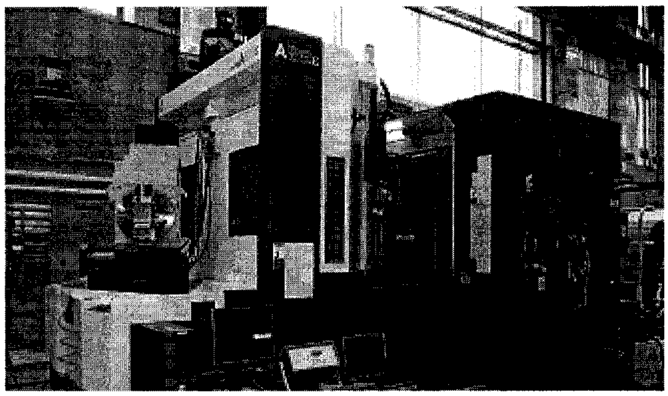

Figure 3.1: Makino A88 ε Horizontal Machining Center

3.3 Dust Extraction System

The machine tool was integrated with a dust collection system to prevent the escape of fine carbon epoxy particles from within the machining envelope to the outside environment and avoid damage to the slideways of the machine tool. This system comprised of two entities:

i. Local dust extraction.

ii. Global dust extraction.

Both systems, fabricated by M/s Nederman, have flexible tubular arrangement for dust removal and are portable in use. The local unit has a maximum airflow of 275 m^3/hr and was located close to the composite laminate holding fixture for evacuation of chips being generated during drilling. The global suction unit was located at one end of the top roof of the machine and was mainly used to sanitize the machining envelope from the carbon chips / dust straying out of the local dust extraction range. Figure 3.2 shows the local dust extraction unit.

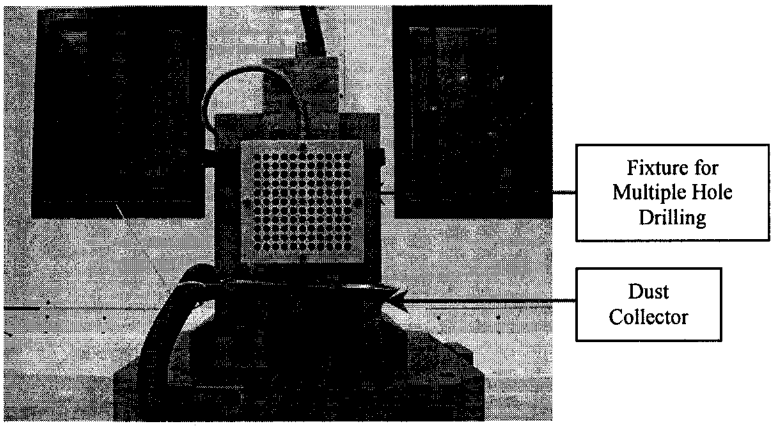

Figure 3.2: Local Dust Collector Used for Chip Evacuation

3.4 Cutting Tool Holder

The tool holder used for phase-1 was a D'Andrea-"Toprun" high speed balanceable tool holder HSK 100A [. Figure 3.3 illustrates the construction of this tool holder. The purpose of tool holder's balancing was to improve the mass distribution of its body (reduce unbalance) in order to produce centrifugal forces within the prescribed limit, when spinning at high spindle speeds. The tool holder is provided with two counter weights in a single plane at fixed distance from the front end of the tool holder. The two counter weights can be moved circumferentially to reduce the imbalance in this single plane. The tool holder can take spring collets for locking the rotary tools like mills, drills, reamers, etc. An assembly drawing of the tool holder used is shown in Figure 3.4.

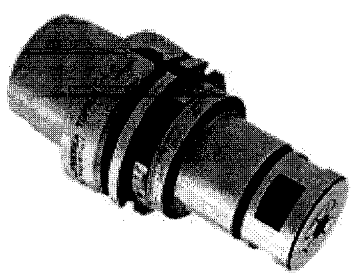

Figure 3.3: Balanceable Tool Holder used for Experimental Work

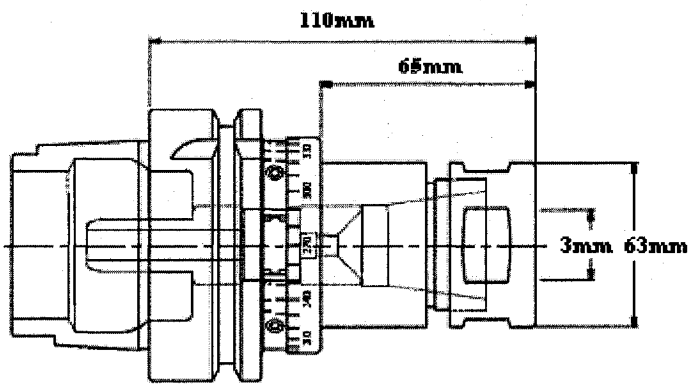

Figure 3.4: Drawing of the D'Andrea Toprun HSK A100 E 40.110 Balanceable Tool Holder Used in Experimental Work

The tool holder, used for temperature measurement experiments, was again a D'Andrea-modular high speed balanceable tool holder with a HSK 100A spindle adapter [58]. This tool holder design was chosen since it was the best suitable one available for mounting the instrumentation used for temperature measurement. Figure 3.5 shows the tool holder (1) having the instrumented tungsten carbide drill (2) and the high speed slip rings (3). The high speed slip has the capability to rotate and transmit the acquired data at spindle speeds up to 15,000 rpm.

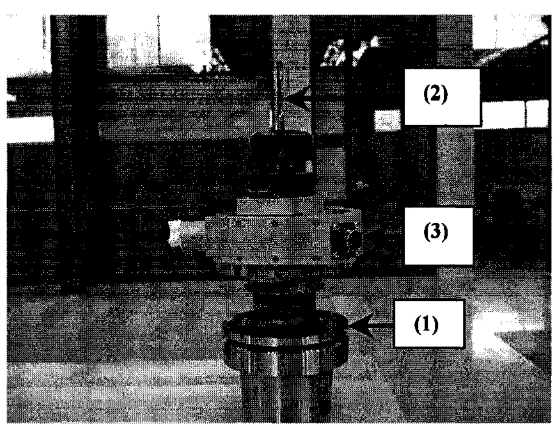

Figure 3.5: Tool Holder Used for Measurement of Temperature with Mounted Slip Ring Assembly and Drill

3.5 Cutting Tool

The drill, used for hole making in the composite plate, was a standard carbide twist drill from Material Removal (M43236), a product of Kennametal Inc [59]. This drill is a 2-

flute, right hand spiral, right-hand cut drill with a 30^o helix angle and 118^o point angle. The fluted length is 44.5 mm and the total length of the drill is 76.2 mm. The carbide grade is ISO K10 - K20 with approximately 7 % cobalt as binder. The drill is shown in Figure 3.6.

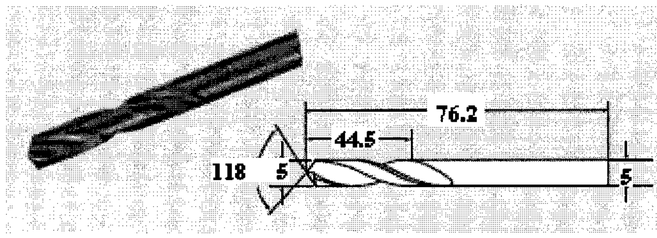

Figure 3.6: Two Flute Standard Point Solid Carbide Twist Drill of 5 mm diameter.

The tool used for measurement of temperature was a Kennametal through-coolant two flute twist drill having 5 mm nominal diameter (B285A05000K715) [60]. A different drill was used since a through-coolant drill was not available in the market from Material Removal. Figure 3.7 illustrates the basic geometry of the drill. This drill has a point angle of 135^o and helix angle of 30^o. The fluted length is 44 mm and the total length of the drill is 82 mm. The carbide grade is ISO K10 - K20 with approximately 7 % cobalt as binder.

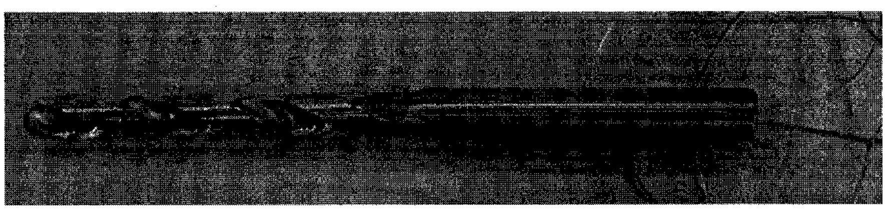

Figure 3.7: Two Flute Standard Point Solid Carbide Twist Drill of 5 mm diameter.

The through-coolant-hole inside the drill was embedded with two K type (Chromel-Alumel) thermocouples and located on the flank face of the drill, with the aid of ceramic cement. Figure 3.8 shows (a) the top face of the drill without any thermocouples and (b) with thermocouples embedded inside the two through-coolant-holes. The thermocouples were precisely located using an optical microscope at about 0.95 -1.00 mm from the cutting edges of the WC drill.

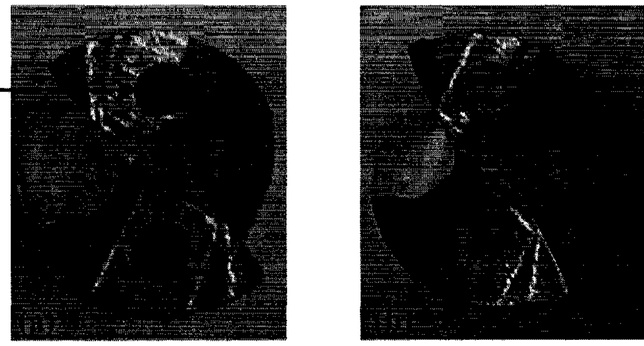

Figure 3.8: Two Flute Standard Point Solid Carbide Twist Drill of 5 mm diameter.

3.6 Workpiece Material

The workpiece comprised of woven carbon fibre as the reinforcements and epoxy as the matrix material. The woven prepreg, L-930 HT 139, used for manufacturing the laminate was supplied by J.D. Lincoln Inc. The woven prepreg was a plain weave fabricated out of T300 graphite fibers each having 3000 filaments. Figure 3.9 illustrates the woven architecture of the prepreg used in manufacturing of the laminate. The physical properties of the ply are illustrated in Table 3.1.

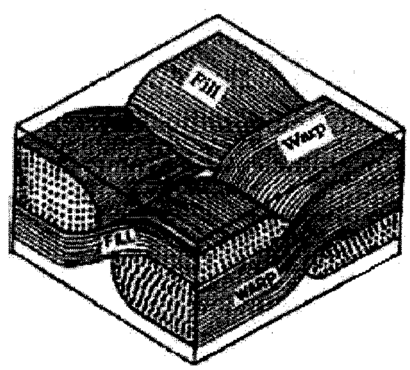

Figure 3.9: Woven Prepreg Ply Architecture Showing the Warp and the Fill Directions

The laminate was designed to have a quasi-isotropic comprising of 28 plies. The lay-up used was $[(0^\circ/-45^\circ/+45^\circ/90^\circ)_3/0^\circ/90^\circ]_s$. The final cured thickness of the laminate was 5.90 $\pm$ 0.02 mm. Figure 3.10 shows the scanning electron microscope image of a section of the laminate, showing the fibers and the matrix phases. It was manufactured by

EADS Composites Atlantic using autoclave molding with a cure time of 60 min at 260°F under 75 psi autoclave chamber pressure.

Figure 3.10: SEM Image of Cross section of Woven Graphite Epoxy Laminate showing the Fiber and Matrix Phase.

Table 3.1: Material Properties of the Fabric Used for the Quasi Isotropic Laminate

Material Properties for Carbon Fabric T300/3k, JD Lincoln L-930HT-139			
Tensile Modulus	E_x	57.92	GPa
	E_y	57.92	GPa
Tensile Strain	n_x	0.01	m in./in.
Tensile Ultimate	X_t	682.59	MPa
	Y_t	682.59	MPa
Compression Ultimate	X_c	526.76	MPa
	Y_c	526.76	MPa
Interlaminar Shear Strength (SBS Test)	S	73.08	MPa
Compression Modulus	C_x,C_y	58.61	GPa
Ultimate Flexture Strength	D_s	784.56	MPa
Fibre Volume Fraction	n_f	60.00	%
Flexture Modulus	D_m	66.88	GPa
Critical Crack Propogation Energy in Mode I Fracture [36]	G_{IC}	266.00	J/m^2

3.7 Workpiece Fixture

A fixture was designed to support the laminate during the drilling process. The fixture has a modular design for quick assembly and disassembly as shown in Figure 3.11 (a) and (b). It comprised of three parts- bottom plate (1), intermediate plate (2) and top plate (3) as shown in Figure 3.11 (a). The bottom plate was bolted on the top face of the dynamometer. The intermediate plate was then assembled on this plate followed by the composite laminate specimen and the top plate. The specimen (4), as shown in Figure

3.11 (a), was sandwiched between the top and intermediate plate and located using two dowel pins placed diagonally for alignment purposes. The laminate was cut into small plates of 6"x 6" size, to carry out drilling of a number of holes in a single setup. The fixture was designed, with the objective of drilling maximum number of holes in the same setup, without interrupting the process.

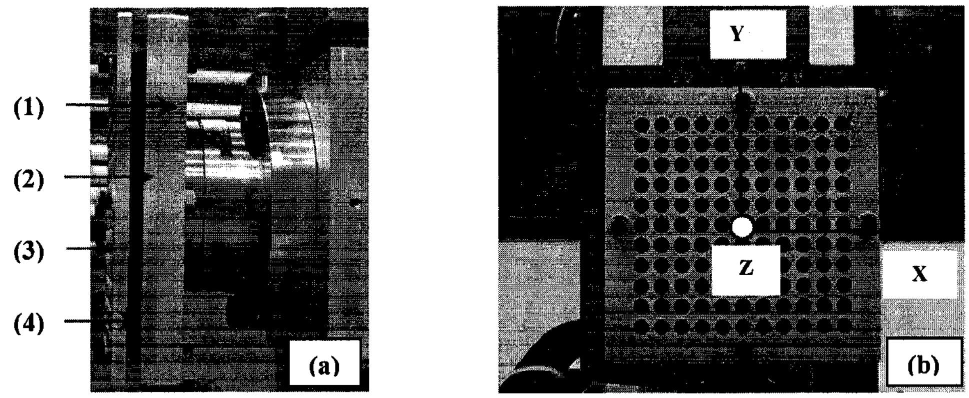

Figure 3.11: Modular Fixture Designed for Multiple Hole Drilling in Single Machine Setup. (a) Side View of the Stack of Top (1), Intermediate (2) and Bottom (3) Plate of Fixture and Specimen (4). (b) Front View of the Fixture

3.8 Force and Torque Measurement

The force and torque signals during the drilling process were measured using a Kistler-four component piezoelectric dynamometer model 9272, which has the capability to measure forces in "X", "Y" and "Z" directions and the torque component in "Z" direction (axis are shown in Figure 3.11(b)). Figure 3.12 shows the piezoelectric dynamometer (1) having the specimen holding fixture (2) mounted on it. As discussed in section (1.8.2), the total thrust force (F_z) measured using the dynamometer is the sum total of the thrust force at the chisel point (F_{ac}), thrust force at the primary cutting edge (F_a) and the thrust force measured at corner of the secondary cutting edge (F_a'), as described by equation (3.1). The cutting force (F_c) was however, derived from the torque (T_z) measured by the dynamometer using the force-torque relation ("R" being drill radius) as illustrated in equation (3.2):

$$F_z = 2F_a + F_{ac} + 2F_a^{'} \tag{3.1}$$

$$F_c = \frac{T_z}{2R} \tag{3.2}$$

The force and torque signals from the dynamometer were sent to a multi channel charge amplifier, filtered with an anti-aliasing analog-to-digital converter, and finally read with an application created in LabView Express. The signals were finally stored as data files that could be processed as required. Technical details and capabilities of the dynamometer and the data acquisition system are elaborated in Table 3.2.

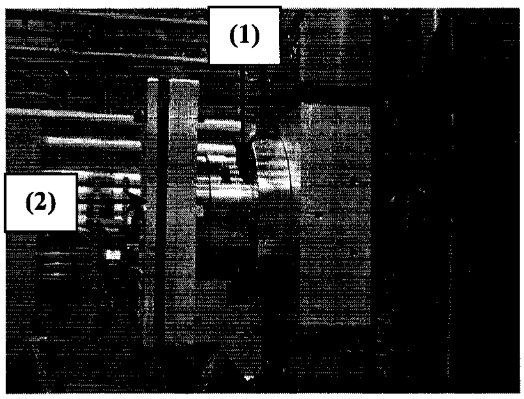

Figure 3.12: Piezoelectric Type Four Component Dynamometer mounted on the machine

Table 3.2: Technical Details of the Instruments Used for Force and Torque Measurement

Force and Torque Measurement Setup				
Instrument Type	**Capability**	**Specifications**	**Make**	**Capability**
Dynamometer	Piezoelectric type	Type 9272	Kistler	4 - component dynamometer Range F_x, F_y -5 to 5 kN F_z = -5 to 20 kN M_z = -200 to 200 kN
Charge Amplifier	Multi Channel Charge Amplifier	Type 5019B	Kistler	No of Channels = 4 Sensor Sensitivity = 0.01-9990 pC/M.U Scale = 0.001-9990000M.U/V
Data Acquisition Card	NI DAQ	PCI 4470	NI	8 -channel Peripheral Computer Interface
Data Acquisition Software	LabView 7.1	Express or 7.1	NI	Virtual Instrument Builder

3.9 Data Acquisition System

The data acquisition system used for the experiments comprised of a data acquisition card fitted inside a PC, and the control was performed by a software application developed in LabView software. According to Shannon's theorem, the data was sampled at more than 2.5 times the cutting frequency to eliminate the aliasing effect. The various experimental sampling frequencies used at different cutting speeds are shown in Table 3.3.

Table 3.3 : Experimental Sampling Frequencies Used for Data Acquisition at Different Spindle Speeds

Spindle Speed (rpm)	**Spindle Speed (rps)**	**Data points/ rev**	**2.5 x Sampling Freq.**	**Experimental Sampling Freq.**
1500	25.0	10	625	2,048
5000	83.3	10	2,083	2,048
8500	141.7	10	3,542	4,096
12000	200.0	10	5,000	8,192
15000	250.0	10	6,250	8,192

3.10 Surface Roughness Measurement

The surface roughness was measured along the depth of the drilled hole. A Form Talysurf series 2 surface profilometer from Taylor Hobsons [61] was used. The measurement procedure was based on IS0 4288:1996 [21]. A cut-off (λ_c) of 0.8 mm and sampling length of 5.0 mm (6 x λ_c) were used. For carrying out measurements along the depth, the specimen was cut along the hole diameter. A diamond stylus, having 0.2 μm radius, was used for carrying out the measurements. Average surface roughness "R_a" and valley void volume ratio of the surface "S_V" were the main parameters measured. The descriptions of "R_a" and "S_V" have already been provided in detail in section (1.10.1.6) and (1.10.1.3), respectively.

3.11 Delamination Measurement

Delamination was measured using an optical stereo microscope (Olympus Model GZX 12). The specimens were inspected both at the entry and exit side of the laminate. The images were captured digitally using the proprietary imaging software "QuadPro 7". The tearing of the top layer, or the separation of the last layer was measured according to the methodology discussed in section (1.10.1.1). The delamination mechanism was finally analyzed using scanning electron microscopy (SEM) measurements.

3.12 Hole Geometry Measurement

The hole geometry parameters i.e. hole circularity and hole diameter error were measured using a "Mitutoyo-Mach 806" coordinate measuring machine (CMM). The specimen was mounted on the table of the CMM, and the measurements were made using the proprietary software GEOPAK CMM V2.4 R9. A "Renishaw-TP7M" ruby-tipped probe of 1 mm diameter was used to perform the measurements at two different planes. For the entry side, the measurements were taken at 1.5 mm below the top of laminate, and for the exit side at 1.5 mm above the bottom face of the hole to eliminate any affect of entry and exit defects.

3.13 Temperature Measurement

Temperature was measured for a set of selected cutting conditions, which will be described in detail in section 3.15. The setup for temperature measurement consisted of a through-coolant-drill, and high speed slip rings mounted on the tool holder (see Figure 3.8). The slip ring, having 3 channels, has the capability to measure temperature at three points simultaneously using K-type thermocouples. The slip ring has two parts, one part is rotary which is locked to the tool holder, while the other part is stationary, where the signal gets conveyed to the data acquisition system. The milli-voltage signal from the thermocouple is conveyed to the high speed slip rings, amplified and then transmitted to the stationary part with the help of carbon brushes. The signal is amplified before transfer to reduce to effect of noise by increasing signal-to-noise ratio. For use at high speeds up to 15,000 rpm, compressed air was used as coolant to avoid heating of the carbon brushes and slip ring rotary components. Figure 3.13 illustrates the temperature measurement setup fitted inside the machine tool.

In order to achieve an appreciable temperature rise during drilling, a stack of four woven carbon epoxy plates was used. The plates were glued together with a double-sided adhesive tape and were held between the top and intermediate plate of the fixture.

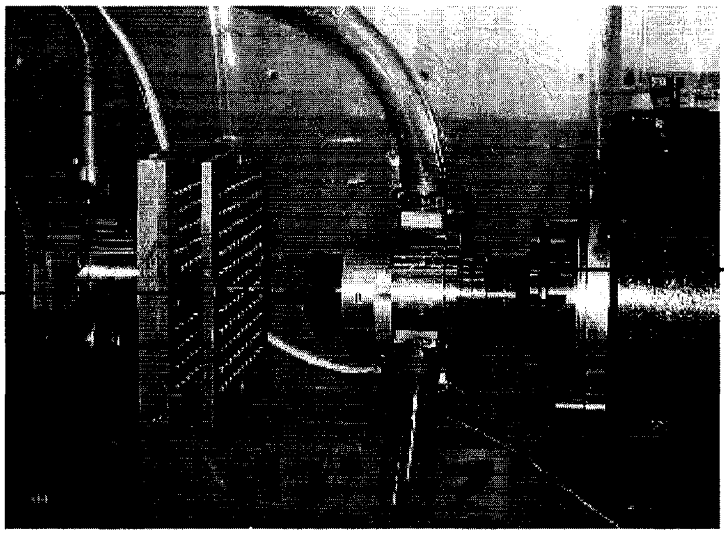

Figure 3.13: Setup of Instrumented Tool Holder with High Speed Slip Rings Mounted on it and Inside Makino Machining center

3.14 Tool Wear Measurement

The tool wear study of the tungsten carbide (WC) drill was carried out in phase three of the experiments. For measurement of wear, an optical stereo microscope (Olympus Model GZX 12) was used. The wear was measured at the flank and rake face sides of the two cutting edges, chisel edge and the two margins. However, since flank wear was found to be the most prominent of all the three types of wear, it was the only one reported. For performing the measurements, the optical microscope was calibrated with a standard scale to 100 % accuracy, and a resolution of one hundredths (1/100) of a micron was set. For wear measurements, the drill was kept mounted on the tool holder. The tool holder was kept vertical for measurement of wear at the chisel edge, and the flank side of the two cutting edges. However, to measure wear at the rake face of the two cutting edges, and the wear at the margins, the tool holder was seated horizontally on a V-block. The drilling tests were discontinued when the average flank wear reached a value of 225 μm, which was 75 μm below the standard value as per ISO 3685 [56]. The worn tool was finally analyzed with the help of scanning electron microscopy for one set of cutting conditions in order to critically examine the wear mechanisms.

3.15 Experimental Matrix

The cutting conditions for first and second phase were selected based on the data available in the literature for the similar composite material and tool type. An effort has been made in this research task to extend the machinability investigations to high speed, and high feed regimes, which have not been addressed so far to the author's best knowledge. As indicated earlier, for the first phase, the cutting conditions were selected to evaluate the machinability of woven graphite fiber epoxy composite laminate in drilling. The cutting conditions for these machinability assessment tests are listed in Tables 3.4.

The second phase involved the measurement of cutting temperature. Since the temperature measurement during drilling was a complex and involving task, only selected range of cutting conditions from phase-1 were used. Since the main objective was to identify the level of cutting temperatures generated at different cutting conditions and understand its effect on hole quality, only the conditions that could result in appreciable temperature rise were selected. Moreover, the constraint on the drilled depth restricted the experiments to be done in the low feed range only. The cutting conditions for the temperature measurement tests are listed in Tables 3.5.

Table 3.4 : Experimental Matrix for Machinability Assessment

Experimental Matrix for Phase 1					
Test Level	**Spindle Speed (rpm)**	**Cutting Speed (m/min)**	**Feed (micron/ rev)**	**Drilled Depth (mm)**	**Tool Diameter (mm)**
1	1500	23.6	20	5.9	5
2	5000	78.5	60	5.9	5
3	8500	133.5	100	5.9	5
4	12000	188.5	200	5.9	5
5	15000	235.6	400	5.9	5
6			600	5.9	5
7			800	5.9	5
Total no of experiments = speed level x feed level =					5 x 7 = 35

Table 3.5 : Experimental Matrix for Cutting Temperature Assessment

Experimental Matrix for Phase 2				
S.No.	**Speed (rpm)**	**Feed (μm/rev)**	**Drilled Depth (mm)**	**Total Drilling Time (sec)**
1	1500	20	23.6	11.6
2	1500	100	23.6	2.3
3	1500	200	23.6	1.2
4	5000	20	23.6	3.5
5	5000	100	23.6	2.8
6	5000	200	23.6	1.4
7	8500	20	23.6	2.0
8	8500	100	23.6	1.6
9	8500	200	23.6	0.8
10	12000	20	23.6	1.5
11	12000	100	23.6	1.2
12	12000	200	23.6	0.6
13	15000	20	23.6	1.2
14	15000	100	23.6	0.9
15	15000	200	23.6	0.5
No of experiments = speed level x feed level =				5 x 3 = 15
Two additional experiments were done at feed rate of 60 μm/rev and spindle speeds of 5,000 rpm and 12,000 rpm				2
Total number of experiments				17

The third phase of experiments focussed on identification of tool wear mechanisms, progression of wear during continuous drilling and the effect of wear on cutting forces, hole quality and productivity. The cutting conditions were selected on the criterion of no delamination, and maximum productivity from the machinability assessment phase. Table 3.6 illustrates the cutting conditions used for assessing tool wear. The two tool wear studies focussed on measurement of wear, forces and hole quality attributes like delamination, hole circularity, hole diameter error, and hole surface roughness for at least 10 data points at each cutting condition. The resources and methodologies used in the machinability assessment phase for measurement of these parameters were also used here.

Table 3.6 : Experimental Matrix for Tool Wear Analysis

Experimental Matrix for Phase 3					
Test Level	**Speed (rpm)**	**Cutting Speed (m/min)**	**Feed (mm/rev)**	**Tool Failure Criterion (Average V_b in microns)**	**Tool Diameter (mm)**
1	12000	188.5	100	225	5
2	15000	235.6	100	225	5
Total N^o of measurements = cutting conditions x N^o of experiments =					2 x 10 = 20

3.16 Conclusions

Experimental test fixture and data acquisition system were developed. The setup used for the machinability assessment and tool wear analysis has been discussed in detail. The instrumentation used and the techniques developed for temperature measurements have been elaborated. Experimental matrices for machinability assessment, cutting temperature and tool wear analysis have been finalized.

Chapter 4

Experimental Results and Discussion on Machinability Assessment and Maps

4.1 Introduction

This chapter discusses in detail the main results of experimental work performed to assess the machinability of woven graphite epoxy composites during drilling. A detailed explanation of the results of high speed and high feed drilling done in this research task is presented.

Section 4.2 of this chapter discusses the results of the machinability assessment of woven carbon fiber epoxy composite during conventional and high speed drilling with a standard tungsten carbide drill. The effect of different spindle speeds and feeds on cutting forces and temperature is measured and analyzed to understand the cutting process in woven composites. Further, the influence of forces and temperature on hole quality and integrity is discussed in detail.

In Section 4.3, the knowledge gained from the machinability assessment is presented in the form of machinability maps. These maps illustrate the effect of cutting parameters on delamination, hole circularity, hole diameter error and hole surface roughness in detail. An example for using these maps for process optimization is provided.

4.2 Machinability Assessment during Conventional and High Speed Drilling

Conventional and high speed drilling tests were performed for the cutting conditions given in Table 3.4 of Chapter 3. The holes were drilled for a fixed depth of 5.9 mm under dry cutting conditions. Data was sampled at more than 2.5 times the cutting frequency as referred to in Table 3.3. However, owing to inhomogeneous structure and brittle nature of graphite fiber, the indenting chisel edge of the drill was found to cause fracture as discussed in section 2.4. Figures 4.1 (a) shows the fracture of hard graphite fibers inside the soft epoxy matrix, observed during the course of this research work. Figure 4.1 (b) highlights the fracture along both the fill and warp directions of the woven graphite fabric. Thus, the cutting process in epoxy composites was found to be entirely based on fracture mechanics, as opposed to shearing phenomenon in metals [26].

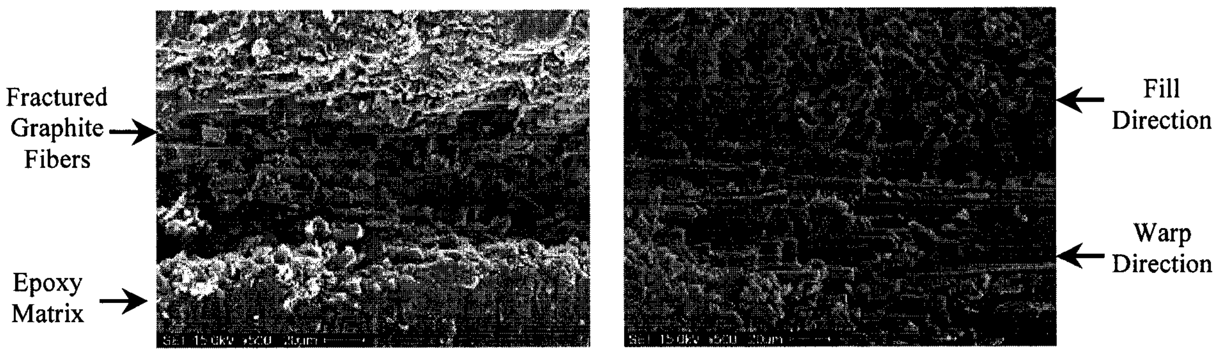

Figure 4.1: SEM Images of Fracture of Hard Abrasive Graphite Fibers in Soft Epoxy Matrix (a) N= 5,000 rpm and f = 20 mm/rev and (b) N = 1,500 rpm and f = 800 mm/rev

During the course of the analysis, specific trends were found to occur at specific spindle speeds and feeds. Therefore, it was decided to classify the cutting parameters into different regimes for a thorough understanding of the process characteristics in those regimes. Moreover, since this research task was specifically focussed on machinability assessment in high speed and feed regimes, a separate category focussed on high speed drilling was created. Hence, the tests conducted have been analysed at three different spindle speed and feed regimes as illustrated in Table 4.1.

Table 4.1: Speed and Feed Categories Investigated During Machinability Assessment

Speed Regime			**Feed Regime**	
Low Speed	1,500 - 5,000 rpm	23.6 - 78.5 m/min	Low Feed	20 - 100 micron/rev
Medium Speed	8,500 rpm	133.5 m/min	Medium Feed	100 - 400 micron/rev
High Speed	12,000-15,000 rpm	188.5 - 235.6 m/min	High Feed	400 - 800 micron/rev

4.2.1 Evaluation of Thrust and Cutting Force

This section discusses in detail the effect of cutting parameters i.e. the spindle speed (N) and feed rate (f) on the thrust (F_z) and cutting force (F_c) in different speed and feed regimes as shown in Table 4.1.

4.2.1.1 Effect of Cutting Parameters on Cutting Forces at Low Speed Drilling (1,500 – 5,000 rpm / 23.6 – 78.5 m/min)

4.2.1.1.1 Effect of Feed and Speed on Thrust Force

At low spindle speed of 1,500 rpm, it was observed that the thrust force increased with the increase in feed rate from 20 to 800 μm/rev as shown in Figure 4.2. The thrust force was found to increase by 35% in the low feed regime as illustrated in Table 4.2. At medium feed rate of 400 μm/rev, the thrust force increased by about 150%, while at high feed rate of 800 μm/rev, the thrust force increased further by about 185%. Thus the thrust force was found to increase with the increase in feed rate for all the three regimes. These results are in agreement with the empirical relation provided by Shaw and Oxford [14, 15] and described by equation (1.5a), which reflects a nonlinear increase in thrust force with the increase in feed per revolution. Similar relation obtained by linear regression for the woven composite drilled at 1,500 rpm is illustrated by the thrust force feed relationship (log-log) in Table 4.5 (refer N = 1,500 rpm). This derived relation shows the nonlinear characteristic of the thrust force feed relation (i.e., $F_z \propto f^{0.6}$). Thus in composite machining, though the chips are formed by fracture as compared to shearing in metal cutting, the generalized equation (1.3) still holds good and reflects the physical significance of feed rate in increasing the thrust force. These trends were found to be in agreement with the results reported in [29, 32, 35]. Similar trend as found at 1,500 rpm were also observed at higher spindle speed of 5,000 rpm.

Thrust forces at 5,000 rpm were found to be lower than those obtained at 1,500 rpm for all the feed regimes as illustrated in Figure 4.2. Also, the reduction in thrust force increased with the increase in feed per revolution. In low feed range (20 – 100 μm/rev) the reduction in the thrust force was in the range of 4 – 19 N, while at high feed range (400 – 800 μm/rev) it increased to about 108 N. The possible reason for this decrease in thrust force could be the thermal softening effect associated with higher spindle speeds as reported in [13]. This effect is discussed in detail in section 4.2.2.

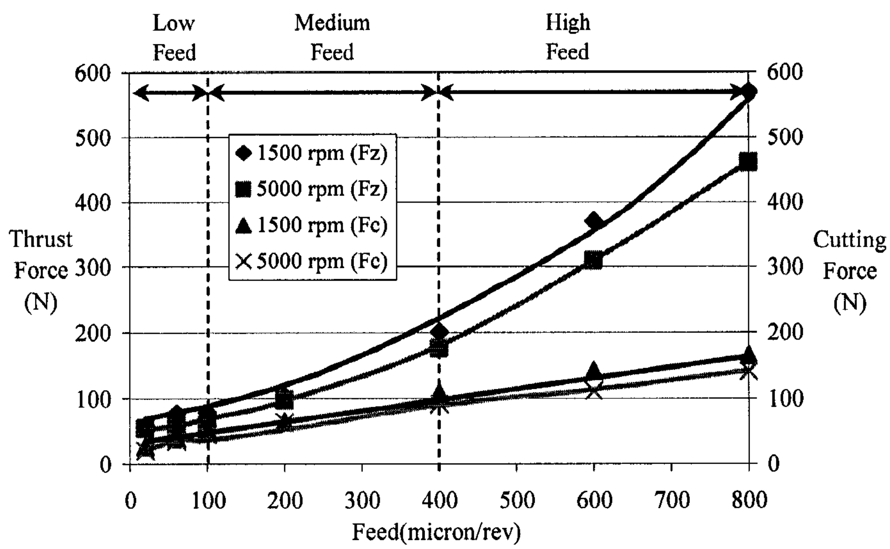

Figure 4.2: Variation of Thrust Force (F_z) and Cutting Force (F_c) with Feed Rate in Low Speed Drilling Regime (1,500 and 5,000 rpm)

Table 4.2: Effect of Increase in Feed Rate (f) and Spindle Speed (N) on Thrust Force (F_z) During Machinability Assessment for Low, Medium and High Speed Drilling

Spindle Speeds		**Thrust Force- F_z (N) at different Feed Rates (μm/rev)**				**Increase in F_z from 20 to 100 μm/rev**	**Increase in F_z from 100 to 400 μm/rev**	**Increase in F_z from 400 to 800 μm/rev**
Regimes	rpm	20	100	400	800			
Low	1,500	58	79	200	570	35%	155%	185%
Medium	8,500	47	67	162	310	43%	142%	91%
High	15,000	30	50	140	147	67%	180%	5%

4.2.1.1.2 Effect of Feed and Speed on Cutting Force

At low spindle speed of 1,500 rpm, it was observed that the cutting force increased with the increase in feed rate, but decreased with the increase in spindle speed from 1,500 to

5,000 rpm as shown in Figure 4.2. The cutting force was found to increase by about 100% in this low feed regime as illustrated in Table 4.3. At medium feed rate of 400 μm/rev, it further increased by about 100%, while at high feed rate of 800 μm/rev, the increase was about 50%. Thus the cutting force was found to increase with the increase in feed rate for all the three feed regimes. These results are in agreement with the empirical relation provided by Shaw and Oxford [14, 15] and described by equation (1.6a), which reflects a nonlinear increase in thrust force with the increase in feed per revolution. Similar relation obtained by linear regression for the woven composite drilled at 1,500 rpm is illustrated by the cutting force feed relationship (log-log) in Table 4.5 (refer N = 1,500 rpm). The derived relation shows good correlation between feed rate and thrust force and highlights its nonlinear behaviour (i.e., $F_c \propto f^{0.51}$). The increase in cutting force with increase in feed rate is due to the increase in cutting area, which increases with increase in feed per revolution when a constant width of cut is maintained in the cutting process. The increased cutting area thus requires more effort, which in turn results in increasing the cutting force.

The cutting force was also found to decrease at higher spindle speed of 5,000 rpm similar to the thrust force as discussed in section 4.2.1.1.1. These results are in agreement with those presented in [13, 29]. The decrease in cutting force, which was about 6 N in the low feed regime increased to about 24 N in the high feed regime, as shown in Figure 4.2. Thus the decrease in cutting force was again found to be directly proportional to the increase in cutting speed, similar to the trend observed in the case of thrust force.

Table 4.3: Effect of Increase in Feed Rate (f) and Spindle Speed (N) on Cutting Force (F_c) During Machinability Assessment for Low, Medium and High Speed Drilling

Spindle Speeds		**Cutting Force-F_c (N) at different Feed Rates (μm/rev)**				**Increase in F_c from 20 to 100 μm/rev**	**Increase in F_c from 100 to 400 μm/rev**	**Increase in F_c from 400 to 800 μm/rev**
Regimes	rpm	20	100	400	800			
Low	1,500	26	53	108	165	104%	104%	53%
Medium	8,500	17	44	87	118	156%	100%	36%
High	15,000	13	32	71	76	146%	122%	7%

Table 4.4: Thrust Force (F_Z), Cutting Force (F_c) and Feed Rate (f) Relationships Obtained By Linear Regression at Low, Medium and High Spindle Speed Regimes

	Thrust Force (F_z) Regression Analysis		**Cutting Force (F_c) Regression Analysis**	
Speed Regimes	**Thrust Force Feed Relationship (Log-Log)**	**Regression Coefficient**	**Cutting Force Feed Relationship (Log-Log)**	**Regression Coefficient**
N = 1,500 rpm	$Ln(F_z) = 0.60\ Ln(f) + 6.5$	$R^2 = 0.85$	$Ln(F_c) = 0.51\ Ln(f) + 5.3$	$R^2 = 0.98$
N = 8,500 rpm	$Ln(F_z) = 0.56\ Ln(f) + 6.0$	$R^2 = 0.90$	$Ln(F_c) = 0.52\ Ln(f) + 5.1$	$R^2 = 0.99$
N = 15,000 rpm	$Ln(F_z) = 0.47\ Ln(f) + 5.3$	$R^2 = 0.95$	$Ln(F_c) = 0.51\ Ln(f) + 4.1$	$R^2 = 0.95$
Generalized Relation between "F_z" and "f" for all speed regimes	$F_z = K_1(f)^{0.54} + K_2$ K_1 & K_2 are constants	Generalized Relation between "F_c" and "f" for all speed regimes	$F_c = K_3(f)^{0.51} + K_4$ K_3 & K_4 are constants	

4.2.1.2 Effect of Cutting Parameters on Cutting Forces in Medium Speed Drilling (8,500 rpm / 133.5 m/min)

4.2.1.2.1 Effect of Feed and Speed on Thrust Force

At 8,500 rpm, the thrust force was found to increase by 43% in the low feed regime as illustrated in Table 4.2. At medium feed rate of 400 μm/rev, the thrust force increased by about 140% and at high feed rate of 800 μm/rev it further increased by about 90% as shown in Table 4.2. Thus, the thrust force was found to increase with the increase in feed rate for all the three regimes, however, in high feed regime the increase was lower.

The results obtained at medium speed drilling are again in agreement with the empirical relation provided by Shaw and Oxford [14, 15] as explained in section 4.2.1.1.1. Similar relation obtained by linear regression for the woven composite laminate, as shown in Table 4.5 (refer N = 8,500 rpm), highlights the nonlinear response (i.e., $F_Z \propto f^{0.56}$) and a very good correlation between the feed rate and thrust force. However, thrust force obtained at 8,500 rpm was found to be lower when compared to low spindle speed of 1,500 rpm as evident from Figure 4.2 and 4.3.

4.2.1.2.2 Effect of Feed and Speed on Cutting Force

At medium speed of 8,500 rpm, the cutting force (F_c) was found to increase with the increase in feed rate as illustrated in Figure 4.3, similar to the trend observed in low speed drilling. The cutting force was found to increase by approximately 150% in the low feed regime as shown in Table 4.3. At medium feed rate of 400 μm/rev, the cutting force increased by about 100% and at high feed rate of about 800 μm/rev, the cutting force increased further by about 36%. The increase in F_c with the increase in feed rate for all the three regimes is again in agreement with the empirical relation provided by Shaw and Oxford [14, 15] as explained in section 4.2.1.1.2. The relation obtained by linear regression between log(F_c) and log(*f*), as shown in Table 4.5 (refer N = 8,500 rpm), highlights the nonlinear response (i.e., $F_c \propto f^{0.52}$) and a very good correlation between the feed rate and thrust force. However, when compared with the low speed drilling case, the cutting forces obtained at medium speed were comparatively lower.

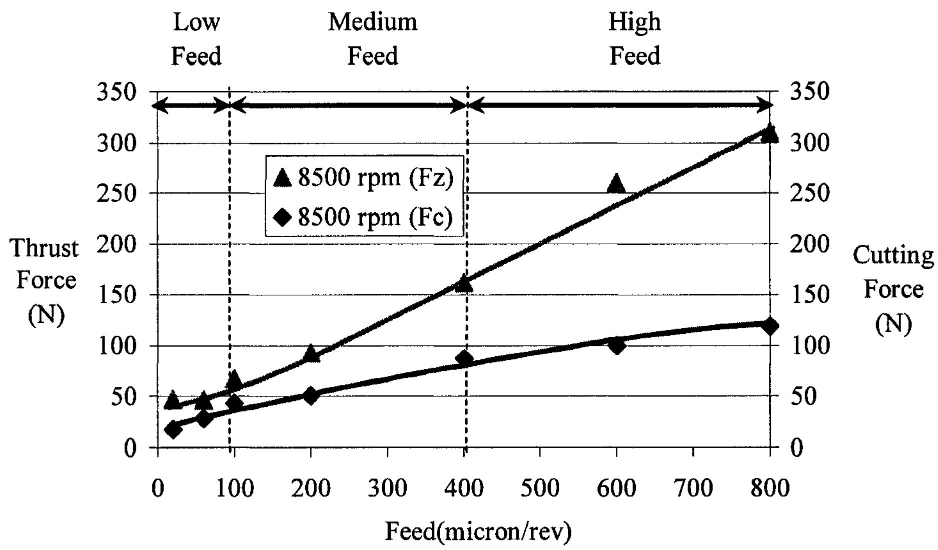

Figure 4.3: Variation of Thrust Force (F_z) and Cutting Force (F_c) with Feed Rate at Medium Drilling Speed of 8,500 rpm

4.2.1.3 Effect of Cutting Parameters on Cutting Forces in High Speed Drilling (12,000 – 15,000rpm / 188.5 – 235.6 m/min)

4.2.1.3.1 Effect of Feed and Speed on Thrust Force

A comparison of Figures 4.2, 4.3 and 4.4 show a substantial reduction in the thrust force at high speeds as compared to the low and medium speed drilling. However, the thrust force was still found to increase with the increase in feed from 20 to 800 μm/rev, as shown in Figure 4.4. The results were found to be in agreement with Shaw and Oxford's models [14, 15] as explained in section 4.2.1.1.1. The linear regression between log(F_z) and log(f), as shown in Table 4.5 (refer N = 15,000 rpm), again highlights the nonlinear response (i.e., $F_Z \propto f^{0.47}$). The thrust force was found to increase by approximately 65% in the low feed range as illustrated in Table 4.2. At medium feed rate of 400 μm/rev, the thrust force increased further by approximately 180%. However, at high feed rate of 800 μm/rev, the thrust force increased by about 5% only. This increase was not so significant when compared to the increase obtained from low to medium feed drilling, which highlights the influence of other parameters mainly cutting temperature at high feed and high speed regime. This suggests that the increasing rate of temperature rise with increase in feed rate, and in turn the thermal softening effect, counteracts the effect of increasing feed rate in increasing thrust force and thus results in insignificant rise in F_Z. To explain the reduction in forces with the increase in spindle speed and not so significant increase in forces at high speed and high feed regime, an investigation of the cutting temperature was done in the second phase as discussed in detail in section 4.2.2.

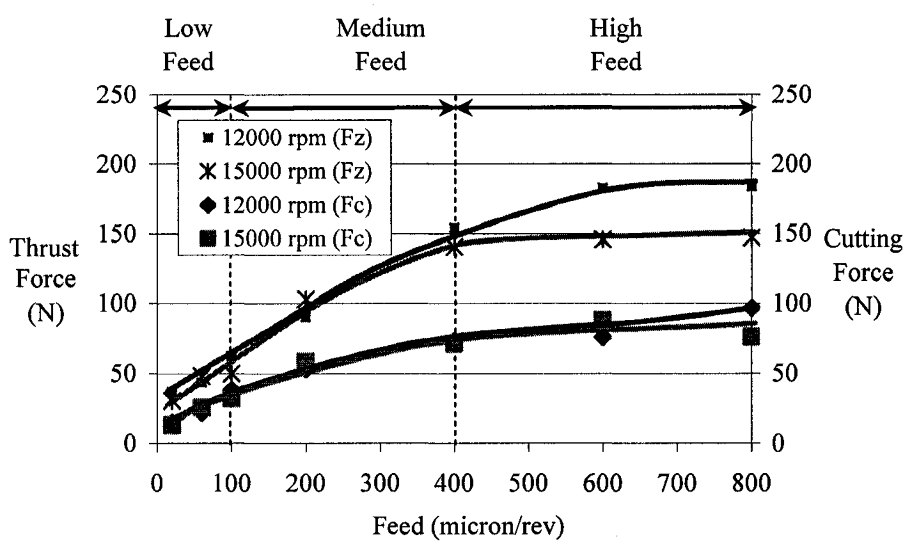

Figure 4.4: Variation of Thrust Force (F_z) and Cutting Force (F_c) with Feed Rate in High Speed Drilling Regime (12,000 - 15,000 rpm)

4.2.1.3.2 Effect of Feed and Speed on Cutting Force

The cutting force was found to increase with the increase in feed rate, similar to the response observed at low and medium speed drilling, as shown in Figure 4.4. The linear regression between log(F_c) and log(f), as shown in Table 4.5 (refer N = 15,000 rpm), highlights the nonlinear response (i.e., $F_c \propto f^{0.51}$), which is again in agreement with Shaw and Oxford's Model [14,15]. The cutting force was found to increase by approximately 145% in the low feed regime as shown in Table 4.3. At medium feed rate of 400 μm/rev, the cutting force increased further by approximately 120%. However, at high feed rate of 800 μm/rev, the cutting force increased by about 7% only. This insignificant increase could again be attributed to thermal softening effect as mentioned in section 4.2.1.3.1. When compared with the low and medium speed drilling, the cutting forces at high speeds were found to decrease for all the feed regimes. A comparison of Figures 4.2, 4.3 and 4.4 illustrate this decrease.

The thrust and cutting force analysis revealed the following main outcomes:

i. Both thrust and cutting force increased with an increase in feed per revolution for low, medium and high speed drilling, except at high speed and high feed, where no significant increase was observed.
ii. The increase in thrust force in low and medium speed was found to be directly proportional to the increase in feed rate in the low, medium and high feed regime, while at high speed it was limited to low and medium feed regime only. So there exists a good physical correlation between the thrust force and feed rate in composite drilling, which is similar to metal cutting as established in [15].
iii. Both the thrust and cutting force decreased as the cutting process advanced from low to high speed drilling. Moreover, in case of high speed drilling the increase in forces was not so significant in the high feed regime. Thus it was evident that the benefits of high speed and high feed could be realized for reduction of forces during drilling.

4.2.2 Cutting Temperature Measurement during Conventional and High Speed Drilling

The measurement of cutting temperature was carried out for all spindle speeds but specific feeds as there was a constraint on drilling larger depths in the medium and high feed regimes. To achieve appreciable amount of temperature rise four composite plates were stacked together, as shown in Figure 3.13, to achieve larger depth of cut. The test matrix for cutting temperature measurement has already been explained in Table 3.4. It was found that at the lowest spindle speed of 1,500 rpm and feed rate of 20 μm/rev a steady state temperature of about 210^0 C was obtained on the flank face of the drill as shown in Figure 4.5 (the measurement point being about 0.95-1.00 mm away from the primary cutting edge). This temperature was found to be in the range of the glass transition temperature for epoxy, which is about 130 °C - 180 °C depending on the type of epoxy used [57, 58]. In [53], cutting temperature of the order of 200 °C was obtained at 1,520 rpm and 20 μm/rev for a 4 mm diameter HSS drill bit, which was found to be much above the glass transition temperature of epoxy being about 130 °C. The temperature time curve in Figure 4.5, shows slight drop in temperature at 27, 38 and 51 sec during the drilling of 4 stack of plates of composite. It is presumed that this drop in temperature was caused by the interfaces of the 4 plates stacked together.

It was further observed that the rate of rise of cutting temperature, from the start to the full entry of drill point, increased both with the increase in feed per revolution and the spindle speed as illustrated in Figure 4.6. At 1,500 rpm, the rate of temperature rise was found to increase from 5 to 63 °C/sec with an increase in the feed rate from 20 to 200 μm/rev as shown in Figure 4.7. At 5,000 rpm, the rate of temperature rise was found to increase from 21 to 55 °C/sec with an increase in the feed rate from 20 to 200 μm/rev as shown in Figure 4.8. At medium spindle speed of 8,500 rpm, the rate of temperature rise was found to increase from 51 to 199 °C/sec for the same increase in feed rate as shown in Figure 4.9. At higher spindle speed of 12,000 rpm, the rate of temperature rise further increased from 86 to 289 °C/sec with an increase in the feed rate from 20 to 200 μm/rev as illustrated in Figure 4.10. Finally at the highest spindle speed of 15,000 rpm, the rate of temperature rise was found to increase to 102 °C/sec at 20 μm/rev and 350 °C/sec at 200 μm/rev as shown in Figure 4.11. It will be shown in section 4.2.2.1 that the increase in slope of the temperature time curves correspond to higher steady state temperatures i.e. above 210 °C.

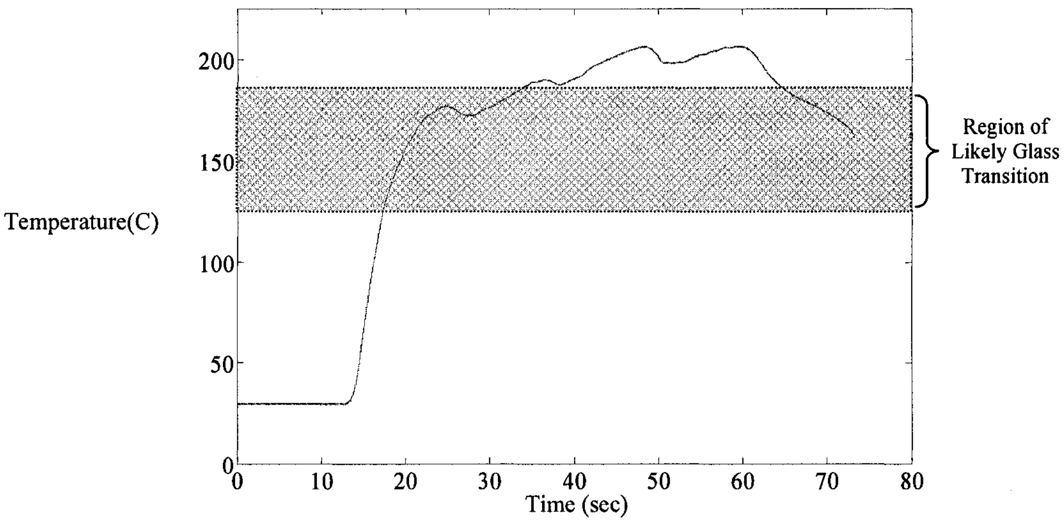

Figure 4.5: Increase in the Cutting Temperature on the Flank Face of the Drill at a N = 1,500 rpm and f = 20 μm/rev

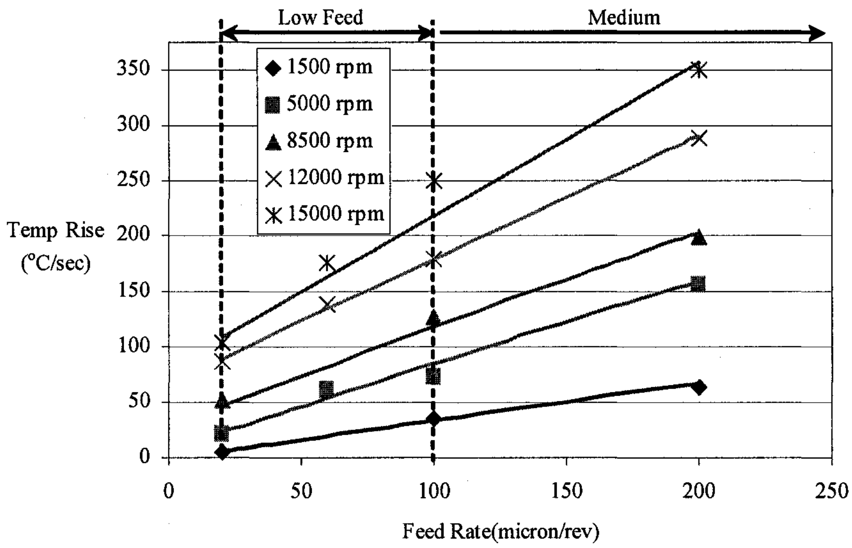

Figure 4.6: Variation in Rate of Temperature Rise with "N" and "f"

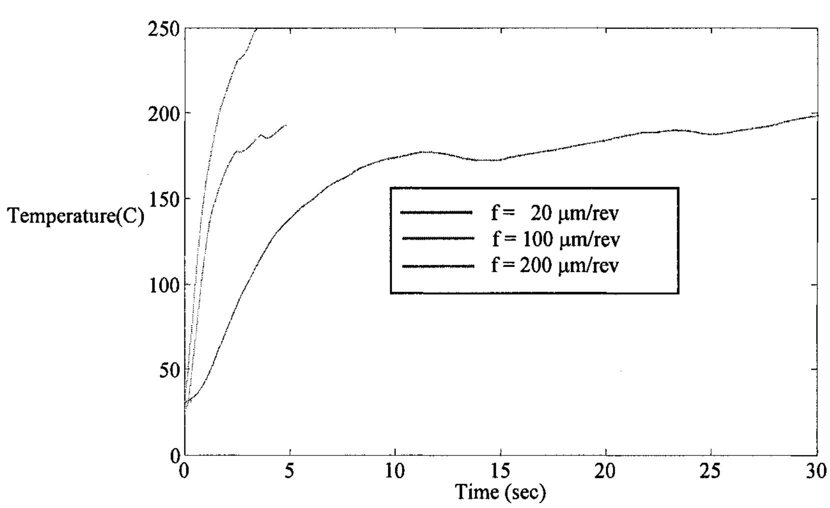

Figure 4.7: Increase in the Cutting Temperature on the Flank Face of the Drill at Spindle Speed (N) of 1,500 rpm and Feed Rate (f) of 20, 100 and 200 μm/rev

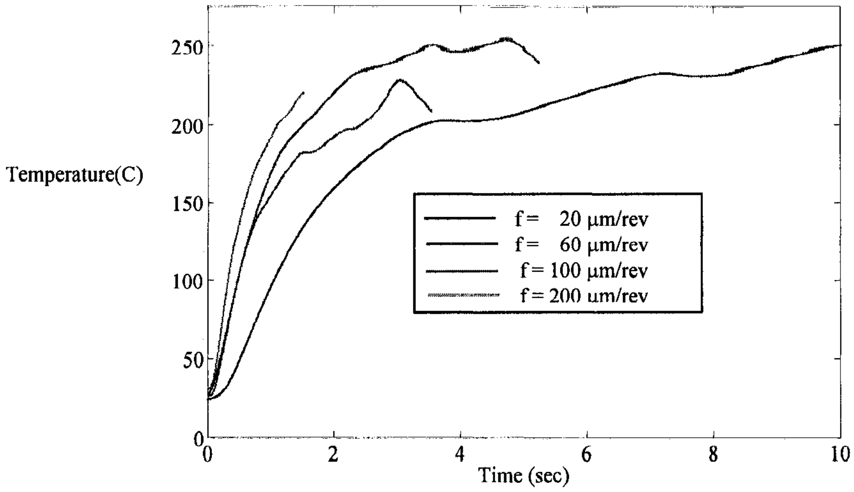

Figure 4.8: Increase in the Cutting Temperature on the Flank Face of the Drill at Spindle Speed (N) of 5,000 rpm and Feed Rate (f) of 20, 60, 100 and 200 μm/rev

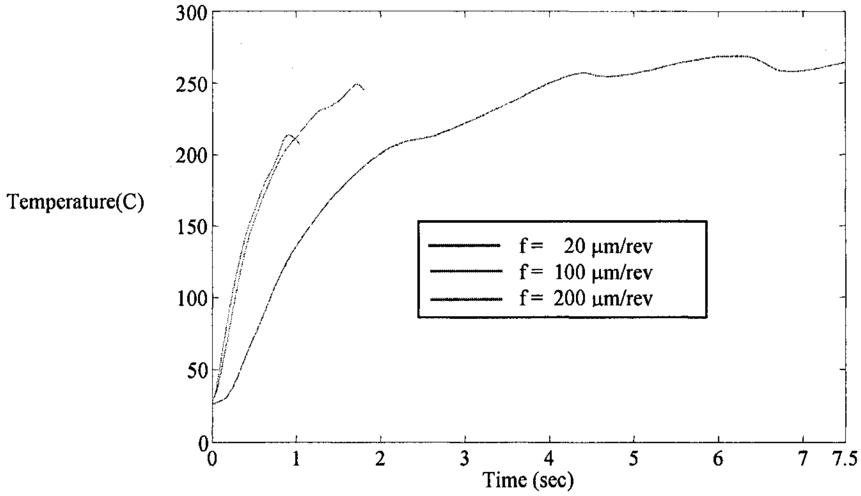

Figure 4.9: Increase in the Cutting Temperature on the Flank Face of the Drill at Spindle Speed (N) of 8,500 rpm and Feed Rate (f) of 20, 100 and 200 μm/rev

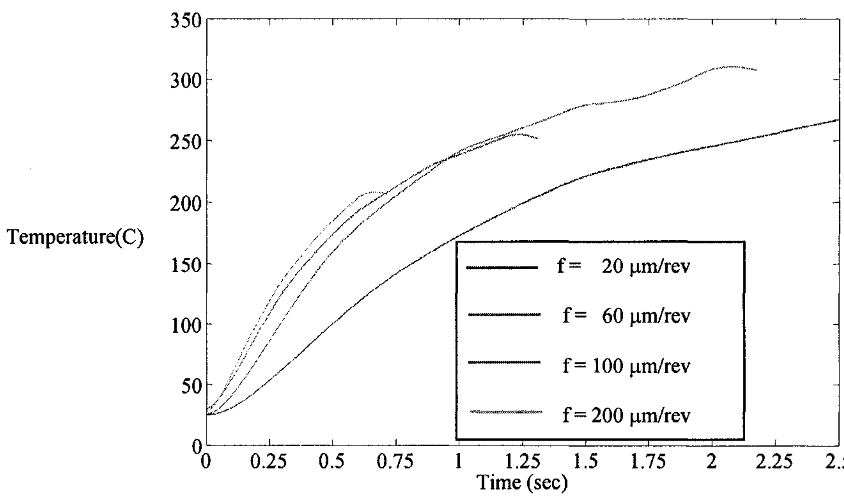

Figure 4.10: Increase in the Cutting Temperature on the Flank Face of the Drill Spindle Speed (N) of 12,000 rpm and Feed Rate (f) of 20, 60, 100 and 200 μm/rev

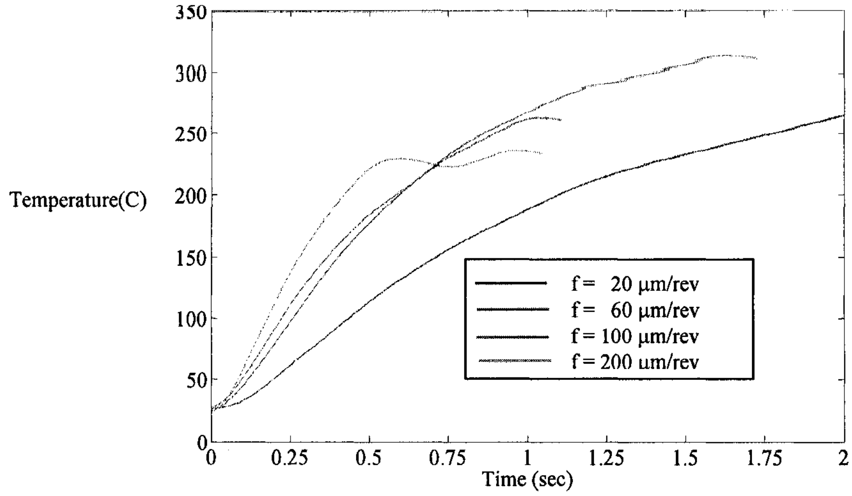

Figure 4.11: Increase in the Cutting Temperature on the Flank Face of the Drill at Spindle Speed (N) of 15,000 rpm and Feed Rate (f) 20, 60, 100 and 200 μm/rev

4.2.2.1 Evaluation of Cutting Temperatures based on a First Order Linear System

Since all the cutting temperature experiments were done for a fixed drilled depth of 23.6 mm, a steady state could not be reached except for the lowest spindle speed of 1,500 rpm and lowest feed rate of 20 μm/rev. So to analytically demonstrate the steady state cutting temperature at other spindle speeds and feed rates, the whole system was treated as a lumped mass and the theory of first order linear system was used. The generalized form of first order linear system, as described by equation (4.1), can be used to define the temperature-time relationship for the drill tool-composite laminate system:

$$\theta = \theta_i + (\theta_s - \theta_i)\left(1 - e^{\frac{-t}{\tau}}\right) \tag{4.1}$$

Equation (4.1) can be reduced to the following normalized form:

$$\bar{\theta} = \frac{\theta - \theta_i}{\theta_s - \theta_i} = \left(1 - e^{\frac{-t}{\tau}}\right) \tag{4.2}$$

where "θ" is the temperature at any time instance "t" having an initial temperature of "θ_i", a time constant of "τ" and steady state temperature of "θ_s". The actual temperature response from experimental data for different set of cutting parameters was used. The unknown parameters, i.e., the steady state temperature 'θ_s' and time constant 'τ_s' were evaluated by minimizing the least square error between the actual temperature and the ideal calculated temperature considering it as a first order linear system. A detailed example, for spindle speed of 8,500 rpm and feed rate of 200 μm/rev, explaining this method with the help of MS Excel Solver tool is provided in Appendix 1. The steady state temperatures obtained using this technique at spindle speed of 1,500 and 8,500 rpm, respectively and feed rate of 20 and 200 μm/rev are shown in Figure 4.12.

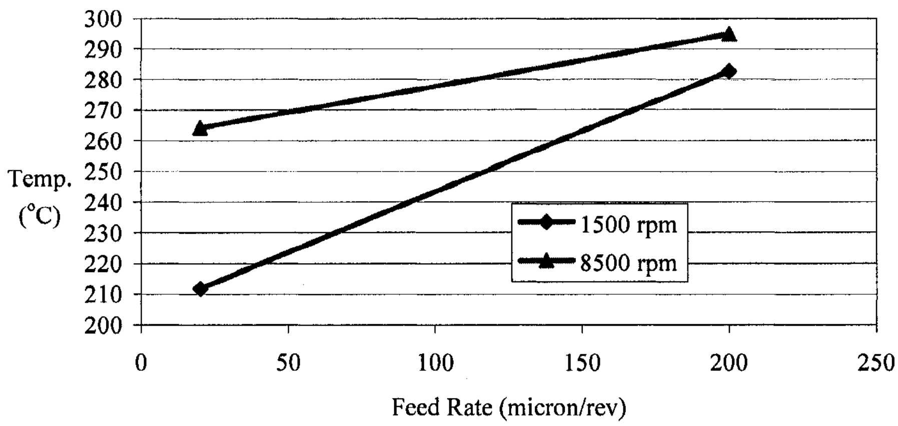

Figure 4.12: Calculated Cutting Temperature on the Flank face of the Drill at Spindle Speed of 1,500 and 8,500 rpm and Feed Rates of 20 and 200 mm/rev

As expected, the cutting temperature at the steady state conditions was found to increase both with the increase in cutting speed and feed rate. Hence, it is estimated that the cutting temperatures at higher feed rates (200 – 800 μm/rev) and higher spindle speeds (12,000 – 15,000 rpm) would be more than 290 °C as calculated at 8,500 rpm and 200 μm/rev.

4.2.3 Effect of Cutting Temperature on Forces

From the analysis of the cutting temperature, it is observed that at the lowest cutting parameters (1,500 rpm and 20 μm/rev), a steady state temperature of about 210 °C is predicted. Moreover, with the increase in spindle speeds and the feed rates, the cutting temperatures were found to increase as illustrated in section 4.2.2.1. It was also observed that the effect of speed was more dominant than that of feed per revolution as shown in Table 4.2. These observations were found to be in agreement with Shaw's evaluation of cutting temperatures during metal cutting, as described by equation (4.5) [5] :

$$\theta_T \propto V^{0.5} t^{0.3} \qquad (4.5)$$

where "θ_T" represents the tool mean face temperature in deg Kelvin, "V" represents the cutting speed in m/min, and "t" represents feed rate in mm/rev. Equation (4.5) highlights the dominating affect of speed as compared to feed. Thus the reduction in both the thrust and cutting force could be attributed to the thermal softening of the matrix due to the increase in cutting temperature at higher spindle speeds. Owing to thermal softening, the resistance to cutting decreases resulting in lower cutting and thrust force.

It was also observed that at a higher spindle speed of 15,000 rpm and at a low feed rate of 20 μm/rev, the higher cutting temperature on the tool results in the matrix burning. Because of the poor heat conductivity of the epoxy matrix, the generated heat is concentrated at the surface of the hole [53] and doesn't transfer to the laminate. This heat concentration results in decomposition or pyrolysis of the polymer i.e. the epoxy matrix [52]. The SEM images of hole drilled at 15,000 rpm and 20 μm/rev, as shown in Figure 4.13 (a) and (b), reveal the matrix burnout or pyrolysis. Hence, high cutting speeds on one hand result in lowering of thrust force on account of thermal softening effect, but on the other hand can result in matrix burning if the feed rate is as low as 20 μm/rev.

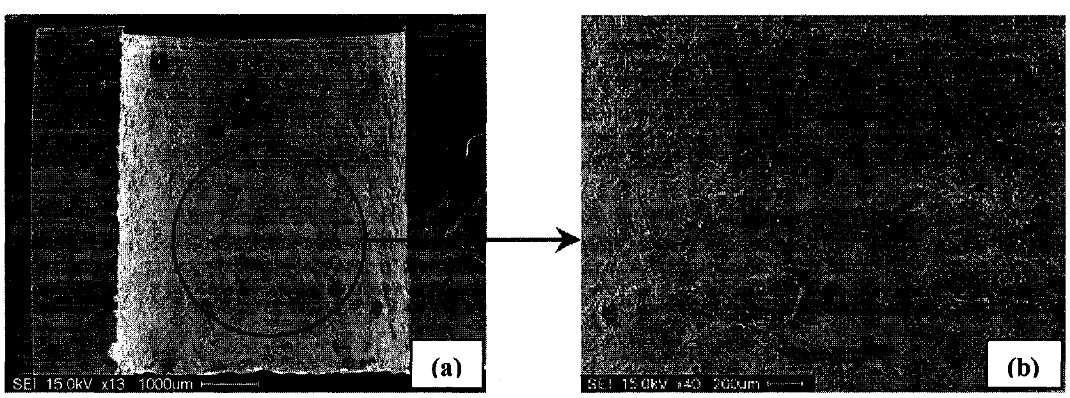

Figure 4.13: Effect of High Spindle Speed of 15,000 rpm and Low Feed Rate of 20 μm/rev on Matrix Burning on Account of High Cutting Temperature. (a) SEM Image of Curved Surface Area of Hole (b) Magnified Image of a Part of the Same Hole

In the high speed and feed regime the cutting temperature increases both on account of the increase in feed rate and the spindle speed. Table 4.5 illustrates an increase of about 50% in the rate of temperature rise on account of increase in feed rate from 100 to 200 μm/rev and at the same time about 480% increase on account of high cutting speed. Also, the increase on account of high speed is almost double as compared to the medium speed regime. Thus, it is evident from these results that thermal softening will result due to the increase in cutting temperatures on account of both high speed and high feed rate. This thermal softening effect will counteract the effect of increasing feed rate in increasing the thrust force. Hence, in the high speed and high feed regime the increase is not so significant for both the thrust and cutting force as shown in Figure 4.4.

Table 4.5: Speed and Feed Categories Investigated During Machinability Assessment

Speed Regimes	**Spindle Speeds (rpm)**	**Rate of Temperature Rise (deg C/sec) at Low and Medium Feeds**		**Increase in Rate of Temperature Rise as compared to Low Speed Regime**		**Increase in Rate of Temperature Rise as compared to Low Feed Regime**
		100 μm/rev	**200 μm/rev**	**100 μm/rev**	**200 μm/rev**	
Low	1,500	30	60			
Medium	8,500	125	200	317%	233%	60%
High	15,000	230	350	667%	483%	52%

4.2.4 Effect of Cutting Parameters on Delamination

Surface delamination was found to occur both at the entry and exit side of the laminate. The delamination was more pronounced at the drill entry side as compared to the exit side. Similar observation was made by Davim and Reis [41]. However, this observation contradicted the results obtained in [20]. Figure 4.14 (a) and (b) shows the entry damage obtained at a spindle speed of 12,000 rpm and feed rate of 400 μm/rev. The SEM examination, as shown in Figure 4.14 (b), provides the evidence of peeling up of top ply of the woven composite laminate.

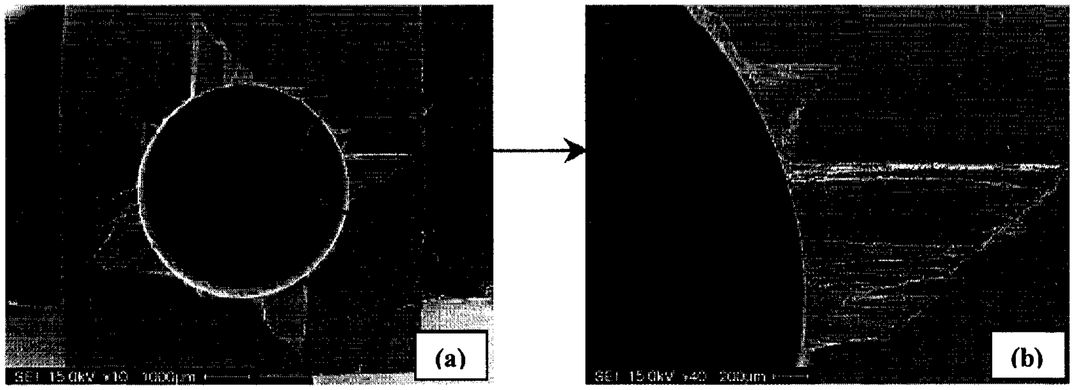

Figure 4.14: SEM Images of Surface Delamination (a) and (b) at the Entry of Drill for a Spindle Speed of 12,000 rpm and Feed Rate of 400 μm/rev

In this research, the delamination at the hole exit could be attributed to an excess layer of resin on the bottom side of laminate as the surface finish was maintained only on the top side. This excess resin acted as a reinforcing layer and thus prevented extensive damage to occur at the hole exit. Delamination damage at entry and exit has been evaluated as per the equation (1.10) described in section 1.10.1.1. The following section discusses the results of the effect of cutting parameters, i.e., "N" and "f" on delamination.

4.2.4.1 Low Speed Drilling (1,500 – 5,000 rpm / 23.6 – 78.5 m/min)

4.2.4.1.1 Exit Delamination

Figure 4.15 illustrates the effect of feed rate on exit delamination and thrust force for the low speed regime. In the low feed range, no delamination was observed with feed rate in the range of 20 to 100 μm/rev and at spindle speed of 1,500 rpm. Similar results have been observed in [18, 59]. The initiation of exit delamination was found to occur in the medium feed regime, i.e., beyond 100 μm/rev. Delamination increased from 8 to 11% in the medium feed regime (100 – 400 μm/rev). It further increased to 24% at 800 μm/rev in the high feed regime. Since thrust force has been identified as the main force causing exit delamination, the increase in delamination was found to occur due to the increase in thrust force with feed rate as explained in section 4.2.1.1.1. Figure 4.16 (a) illustrates the extensive interlaminar damage and high density micro failures caused because of high thrust force of 570 N at 800 μm/rev similar to the observation made in [20]. However, no delamination is observed at low feed rate of 20 μm/rev due to lower thrust force of 58 N as shown in Figure 4.16 (b). These experimental results demonstrate how the increase in feed rate, and consequently thrust force, cause exit delamination.

At 5,000 rpm, the effect of feed rate on delamination damage was found to be similar to that observed at 1,500 rpm. In the low feed regime, no delamination was found to occur up to 100 μm/rev as shown in Figure 4.15. However, delamination increased progressively with the increase in feed rate in the medium and high feed regime. This is again attributed to the increase in thrust force with increase in feed rate as shown in Figure 4.2. Similar trends have been observed in the research work presented in [20, 37, 38, 39].

It was further observed that in the medium and high feed regime, delamination at 5,000 rpm was comparatively lower than the one obtained at 1,500 rpm. These findings are similar to the ones observed in [13, 37, 39, 46]. However, these observations contradict the results obtained in [41, 42], where the delamination was found to increase with increase in spindle speed. Since the thrust force was found to decrease with increase in spindle speed, as explained in section 4.2.1.1.1 and illustrated in Figure 4.2, the occurrence of lower delamination is expected. It is also observed that the delamination starts to occur beyond a critical thrust force, which corresponds to a particular feed rate. This significance of critical thrust force will be discussed in detail in section 4.2.5.

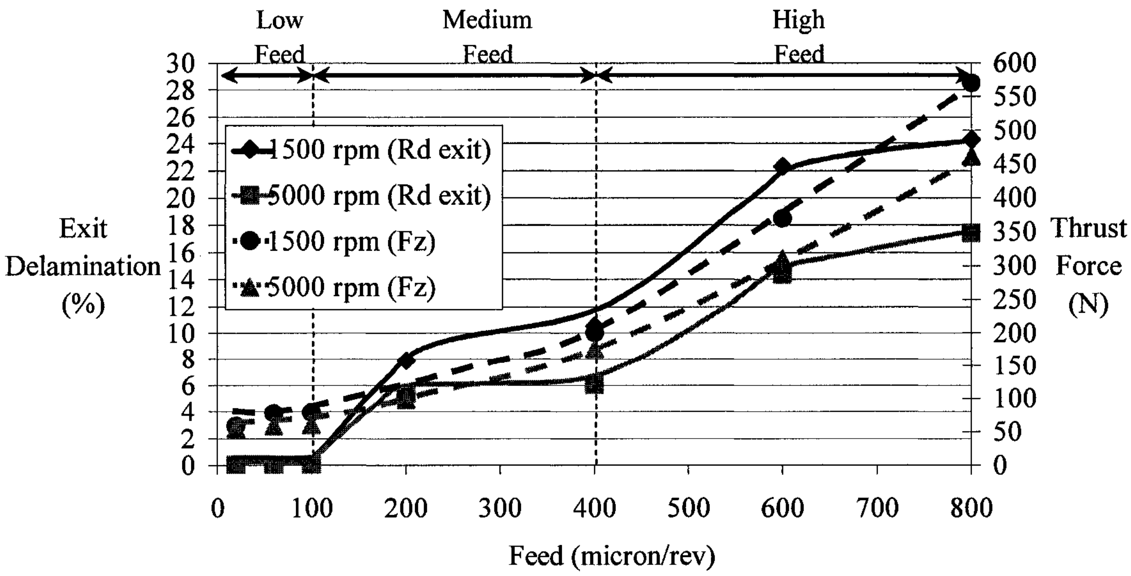

Figure 4.15: Variation of Exit Delamination with Feed Rate (20 – 800 μm/rev) during Low Speed Drilling (1,500 – 5,000 rpm)

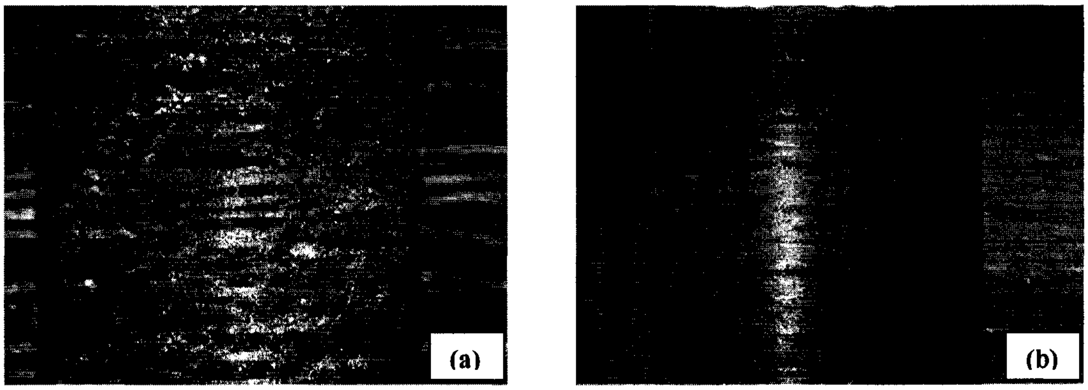

Figure 4.16: Effect of Feed Rate on Internal Delaminations at a Spindle Speed of 1,500 rpm (a) Extensive Micro Delaminations at Ply Interface During High Feed Rate Drilling at 800 μm/rev (b) No Interlaminar Delamination at Feed Rate of 20 μm/rev

4.2.4.1.2 Entry Delamination

Entry delamination, which is basically ply peel up, is caused by the effect of the cutting force at the entry point of the drill. During the axial movement of the drill, depending on the feed rate, the first few plies are cut by the primary cutting edges and made to flow on the rake face along the helical fluted path of the drill. This action generates a peeling force in the direction of drill axis and thus can cause entry delamination to occur.

Figure 4.17 shows the effect of feed rate on entry delamination and cutting force in the low speed drilling regime. No delamination was found to occur up to 100 μm/rev at spindle speeds of 1,500 rpm and 5,000 rpm as shown in Figure 4.18 (a). The initiation of delamination was found to start in the medium feed regime (i.e., above 100 μm/rev) and increased progressively up to 29% at 400 μm/rev. With increase in feed, delamination further increased to 48% at 800 μm/rev in the high feed regime. Figure 4.18 (b) shows the entry delamination of about 48% obtained at these cutting conditions. Overall in the low speed drilling regime, the entry delamination was found to increase from 22 - 25% at medium feed rate of 200 μm/rev to 40 - 48% at high feed rate of 800 μm/rev. This increase in entry delamination is attributed to the increase in cutting force with increase in feed rate as shown in Figure 4.1 and Figure 4.17. Similar trends were also observed in [20, 37, 38].

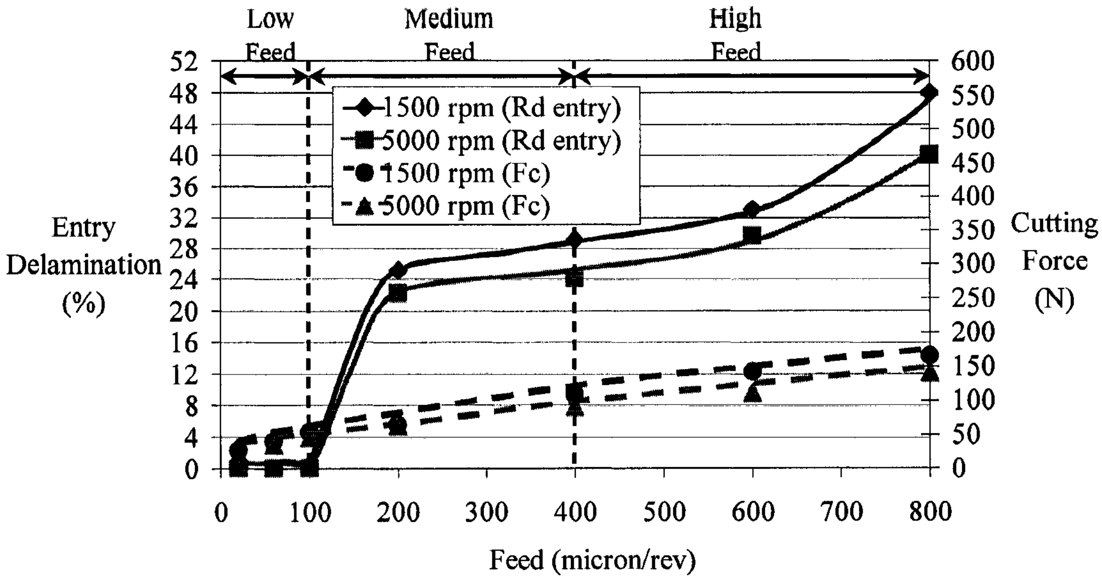

Figure 4.17: Variation of Entry Delamination and Cutting Force with Feed Rate in Low Speed Drilling Regime (1,500 – 5,000 rpm)

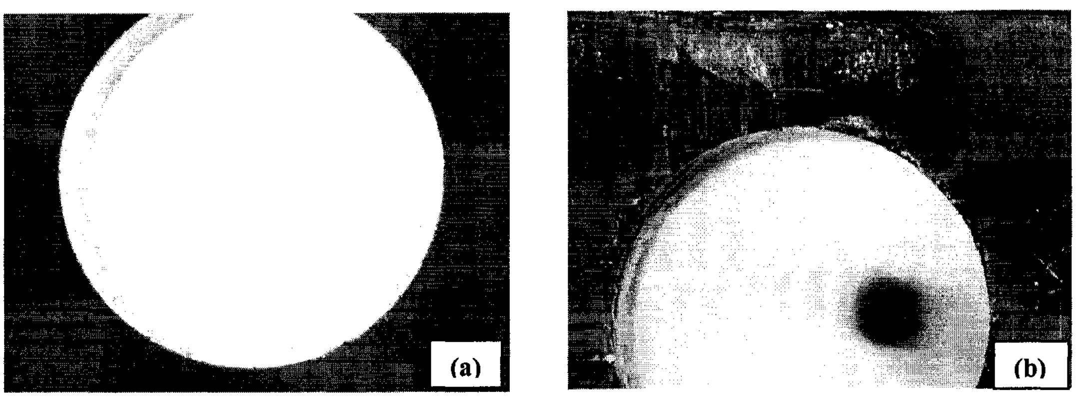

Figure 4.18: Entry Delamination at Spindle Speed of 1,500 rpm and Feed Rates of 20 µm/rev and 800 µm/rev (a) No delamination at 20 µm/rev (b) 48% Delamination at 800 µm/rev.

Entry delamination was also found to decrease with the increase in spindle speed from 1,500 to 5,000 rpm similar to exit delamination. Since the cutting force which caused entry delamination was found to decrease with increase in spindle speed, due to thermal softening as explained in section 4.2.3, the exit delamination also decreased.

4.2.4.2 Medium Speed Drilling (8,500 rpm / 133.5 m/min)

4.2.4.2.1 Exit Delamination

No delamination was found to occur up to 100 μm/rev as shown in Figure 4.19. A good quality hole produced at 20 μm/rev without any indication of delamination is shown in Figure 4.20 (a). Beyond 100 μm/rev, the exit delamination increased progressively, reaching a maximum of 6% in the medium feed regime. It further increased to about 11% with increase in feed to 800 μm/rev in the high feed regime. Figure 4.20 (b) shows the 11% exit delamination obtained at high feed rate of 800 μm/rev. Similar to the low speed drilling case, the increase in exit delamination in the medium speed drilling regime is attributed to the increase in thrust force, which was found to increase with increase in feed rate. Figure 4.19 shows the progressive increase of thrust force and the resulting delamination with increase in feed rate. It is also observed that beyond a feed rate of 100 μm/rev delamination starts to occur. Hence the thrust force at this particular feed rate is referred to as critical thrust force. This critical thrust force will be discussed in detail in section 4.2.5. Moreover, both thrust force and exit delamination were found to decrease with increase in speed from low to medium speed regime, which is evident from the comparison of Figures 4.19 and 4.15.

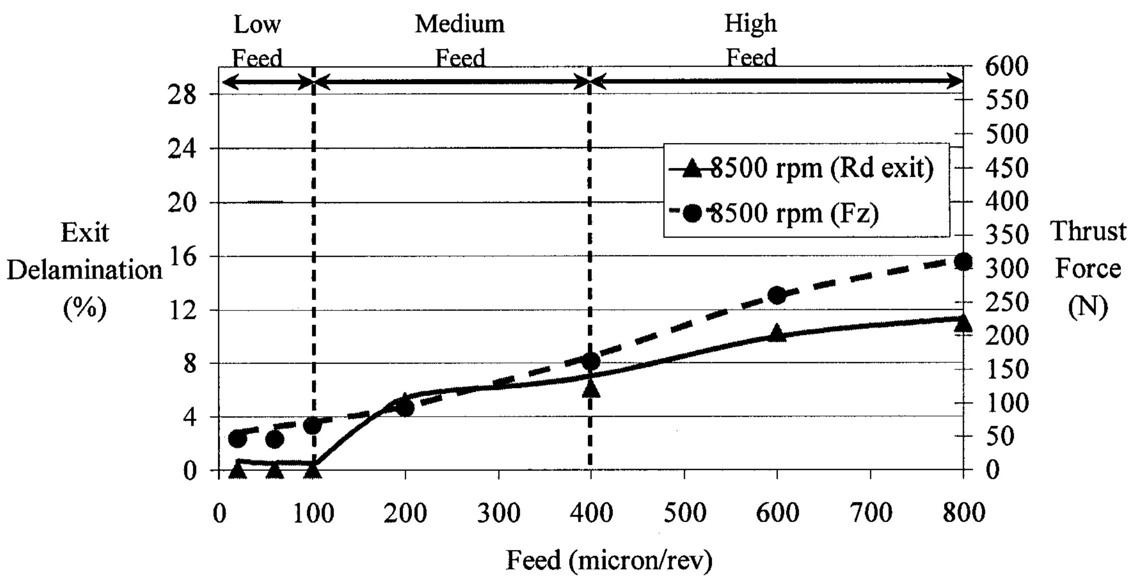

Figure 4.19: Variation of Exit Delamination and Thrust Force with Feed Rate during Medium Speed Drilling Regime

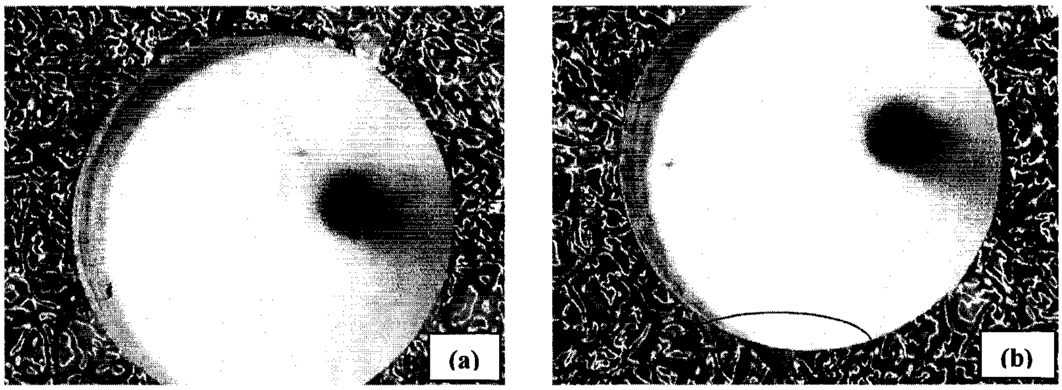

Figure 4.20: Exit Delamination at spindle speed of 8,500 rpm and Feed Rates of 20 and 800 μm/rev (a) No delamination at 20 μm/rev (b) 11% Delamination at 800 μm/rev

4.2.4.2.2 Entry Delamination

At a medium spindle speed of 8,500 rpm, no delamination was found to occur with the increase in feed rate from 20 to 100 μm/rev, as illustrated in Figure 4.21. The initiation of delamination started in the medium feed regime (i.e., beyond 100 μm/rev) and increased progressively up to 26% at 400 μm/rev. Further the entry delamination increased to 38% at 800 μm/rev in the high feed regime. Figure 4.22 (a) shows the evidence of no delamination at 20 μm/rev, while Figure 4.22 (b) shows the occurrence of 38% delamination at high feed rate of 800 μm/rev.

As in the case of low speed drilling, the increase in entry delamination at medium speed drilling is also related to the increase in cutting force with the increase in feed, as shown in Figure 4.21. It is also observed that the entry delamination in the medium speed drilling is lower than that observed in low speed drilling, as shown in Figures 4.21 and 4.17. This is again associated with the reduction in cutting force with the increase in spindle speed (see Figure 4.2 and 4.3).

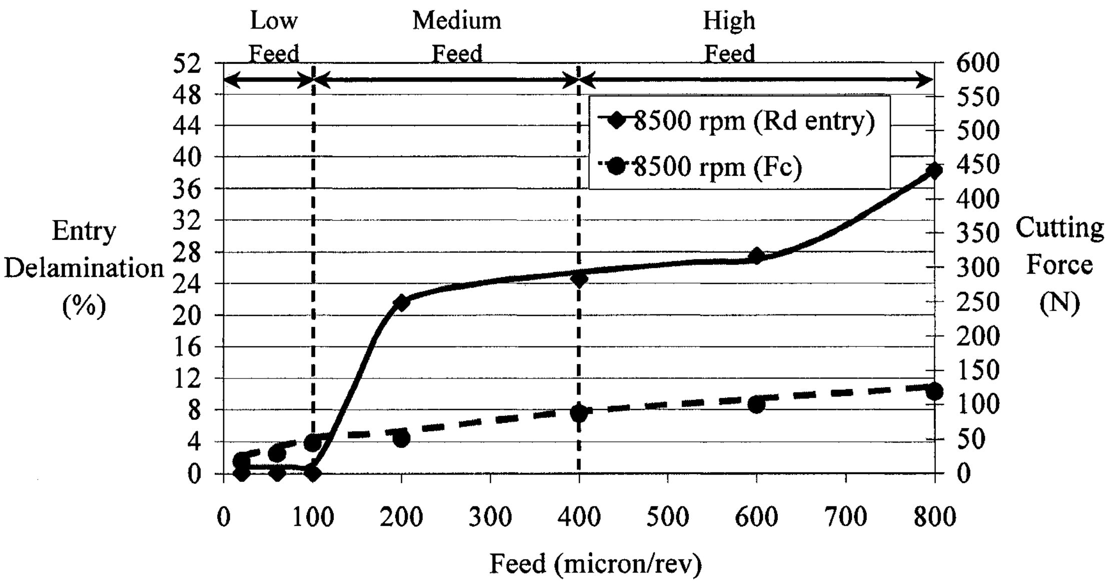

Figure 4.21: Variation of Entry Delamination and Cutting Force with Feed Rate during Medium Speed Drilling of 8,500 rpm

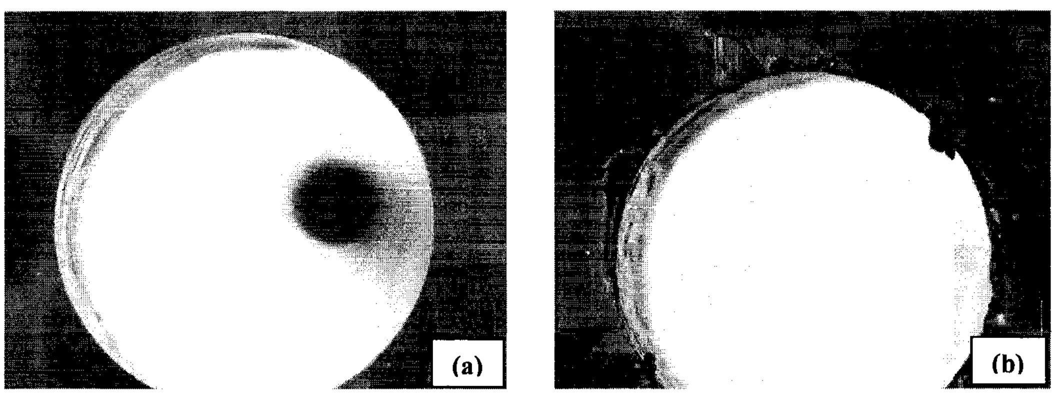

Figure 4.22: Entry Delamination at N = 8,500 rpm and f = 20 and 800 μm/rev (a) No delamination Observed at 20 μm/rev (b) 38% Delamination Observed at 800 μm/rev

4.2.4.3 High Speed Drilling (12,000 - 15,000 rpm / 188.5 – 235.6 m/min)

4.2.4.3.1 Exit Delamination

Figure 4.23 shows the effect of increase of feed rate and spindle speed on exit delamination and thrust force in the high speed drilling regime. At 12,000 rpm, no delamination was found to occur up to 100 μm/rev, as shown in Figure 4.23. However, at the highest spindle speed of 15,000 rpm and the lowest feed rate of 20 μm/rev an exit delamination of about 7.5% was found to occur. This could be attributed to high cutting temperature generated at 15,000 rpm and relatively longer time of contact between the cutting edges and the hole surface leading to softening of the epoxy matrix at the ply interface. Due to this thermal softening, exit delamination can occur under the influence of thrust force. This type of delamination has been referred as "thermal effect dominated mode" of delamination [28]. However, between 60 to 100 μm/rev no delamination was found to occur. After 100 μm/rev, the exit delamination increased progressively reaching a maximum of 5% at 800 μm/rev. The increase in delamination with feed rate is again due to the increase in thrust force as explained in the low and medium speed drilling regime. However, the delamination at high speed of 15,000 rpm was found to be lower than the one obtained at low and medium speed and is evident from the comparison of Figures 4.15, 4.19 and 4.23.

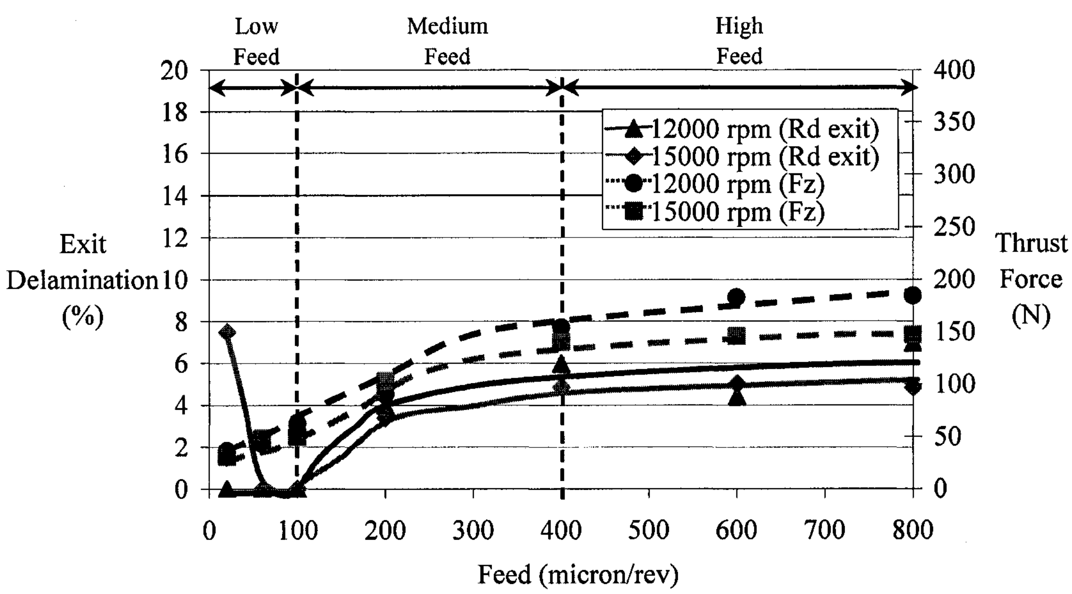

Figure 4.23: Variation of Exit Delamination and Thrust Force with Feed Rate during High Speed Drilling Regime (12,000 – 15,000 rpm)

4.2.4.3.2 Entry Delamination

The delamination at entry was found to give similar response as the exit delamination with the increase in feed rate. Figure 4.24 illustrates the effect of increase in feed on entry delamination and the cutting force. Delamination of about 8% was found to occur at highest spindle speed of 15,000 rpm and lowest feed rate of 20 μm/rev as shown in

Figure 4.25 (a). This is similar to the thermal effect dominated mode of delamination obtained at hole exit. Further, the delamination was found to increase to 15 – 20% at 200 μm/rev in the medium feed regime and finally to 34 – 37% at 800 μm/rev in the high feed regime. Figure 4.25 (b) shows the 35% entry delamination obtained at 800 μm/rev and spindle speed of 15,000 rpm. The increase of entry delamination with feed rate is again due to the increase in cutting speed. It was, also observed that the magnitude of delamination decreased with the increase in cutting speed. This was again attributed to lower cutting force generated with increase in spindle speed, as can be seen from the comparison of Figures 4.17, 4.21 and 4.24.

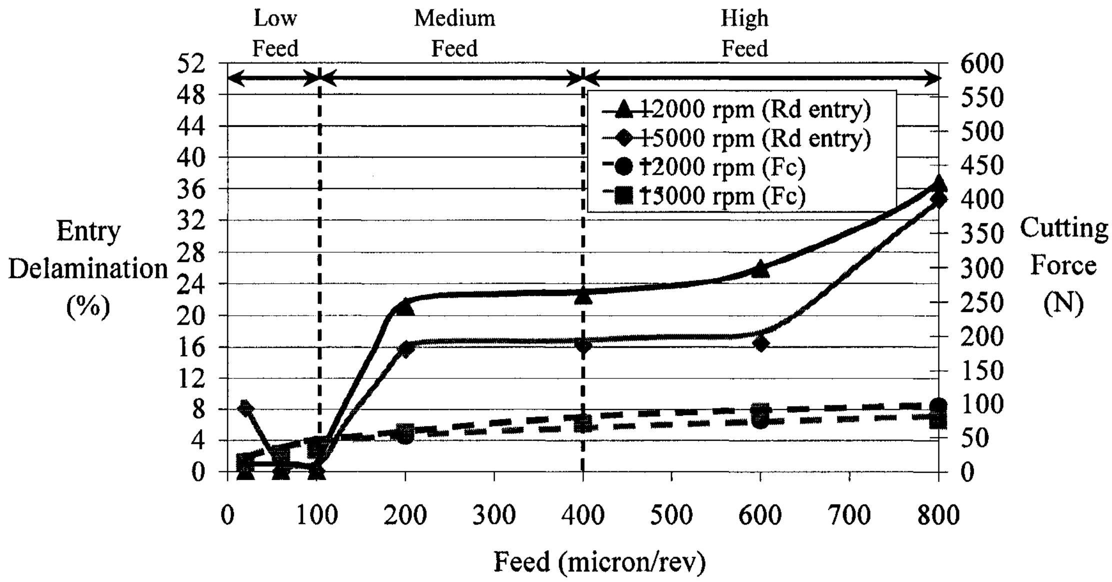

Figure 4.24: Variation of Entry Delamination and Cutting Force with Feed Rate during High Speed Drilling at 12,000 – 15,000 rpm

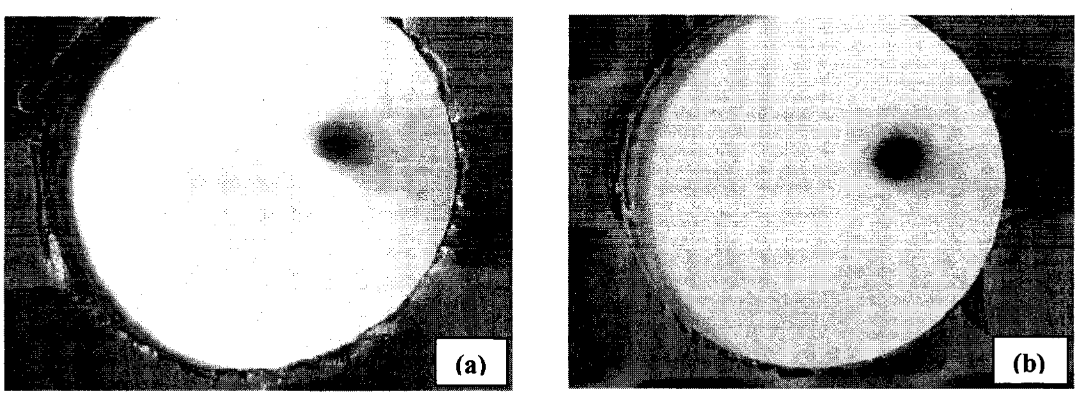

Figure 4.25: Entry Delamination at Spindle Speed of 15,000 rpm and Feed Rates of 20 and 800 μm/rev (a) 8% Delamination Observed at 20 μm/rev (b) 35% Delamination Observed at 800 μm/rev

From the entry and exit delamination investigation, it is evident that delamination can be avoided without sacrificing the process productivity by performing drilling at low feed rates and high spindle speeds. Figures 4.26 (a) – (d) show good quality holes obtained without any delamination in the low feed range of 60 – 100 μm/rev and from low spindle speed of 1,500 rpm to high spindle speed of 15,000 rpm.

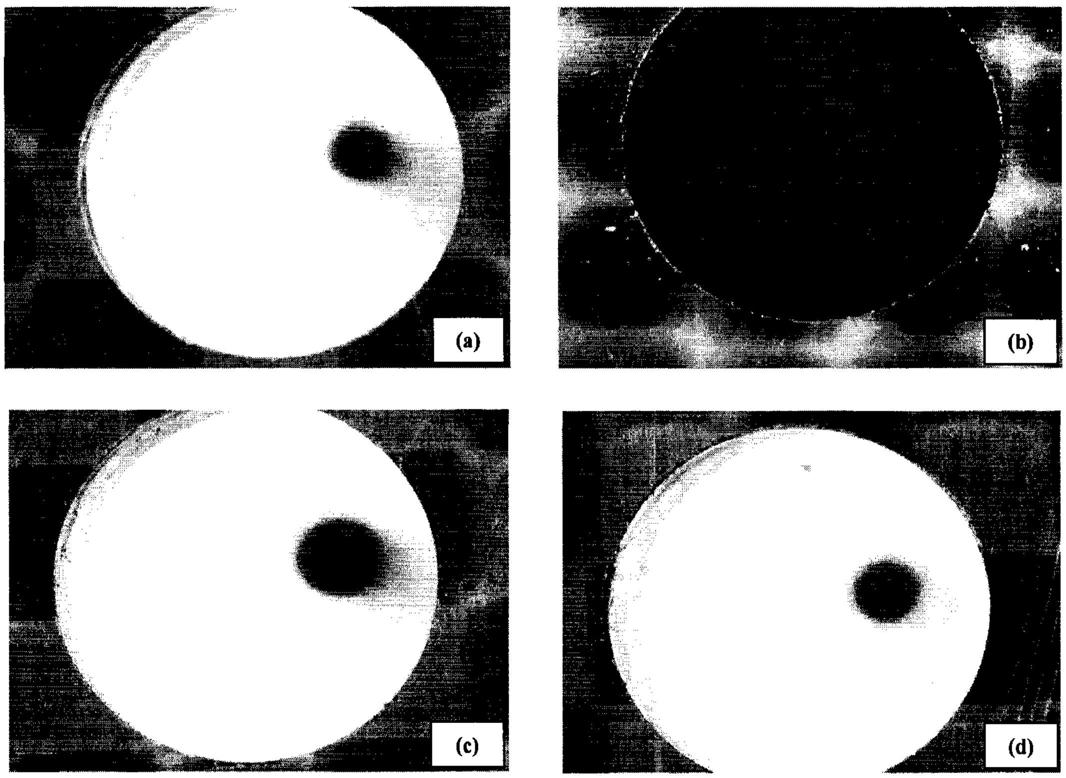

Figure 4.26: Holes with no Surface delamination at Different Speed Regimes and Low Feed Regimes. (a) N = 15,000 rpm & f = 60 μm/rev (b) N = 12,000 rpm & f = 60 μm/rev (c) N = 8,500 rpm & f = 100 μm/rev (d) N = 1,500 rpm & f = 100 μm/rev

4.2.5 Correlation between Forces and Delamination

The experimental results of delamination signify the importance of cutting force and thrust force at the hole entry and exit, respectively. It is also evident from the discussion that there exists a critical thrust and cutting force, which when exceeded delamination damage is observed. This section discusses in detail the physical correlation between forces and delamination. Also, the critical forces obtained from the experimental data are compared with the critical forces evaluated from the Ho-Cheng and Dharan Force Model [18].

4.2.5.1 Evaluation of Critical Thrust and Cutting Force using Ho-Cheng and Dharan Model

The various force and delamination models discussed in section 2.2 of Chapter 2, highlight the occurrence of delamination once the critical forces are reached [18, 22-25]. However, so far no model has been developed for the evaluation of critical force during the drilling of woven composites. In this research task the pioneering and the most simplistic Ho-Cheng and Dharan delamination model [18] has been used to evaluate the critical forces for the woven quasi-isotropic laminate used in this research work. A detailed explanation of this model, the assumptions used and its conservative nature has already been presented in section 2.2. Though this model is conservative in its approach, it is still useful in providing a basic idea about the forces that could be critical to this woven laminate.

The critical thrust force and cutting force have been found to depend on the energy release rate per unit area in mode 1 failure "G_{IC}", highest ply stiffness "E_I" and the Poisson's ratio"v" [18]. Knowing these properties for the woven graphite epoxy laminate, the critical forces evaluated are shown in Table 4.6. A detailed calculation of these forces has been provided in Appendix 2. Thus according to calculated values shown in Table 4.6, the exit delamination, i.e., push out should occur at the cutting parameters (spindle speed and feed rate), which generate a thrust force of about 65 N and the entrance delamination, i.e., peel up should occur when the cutting force reaches 44 N.

Table 4.6: Critical Thrust "F_z^*" and Cutting Force "F_c^*" for woven graphite epoxy laminate as calculated using Ho-Cheng and Dharan Force Model

Material	E_1 (GPa)	G_{IC} (J/m2)	F_z^* (N)	F_c^*(N)
Woven Graphite/Epoxy	57.9	266	65	44

4.2.5.2 Exit Delamination

Figure 4.27 shows the progressive increase in exit delamination with increase in thrust force. At low speed drilling of 1,500 and 5,000 rpm no delamination is observed up to a thrust force of 78.5 N and 60 N, respectively. These experimental critical thrust forces are about 20% higher (in case of 1,500 rpm) and 8% lower (in case of 5,000 rpm) than the calculated critical thrust force of 65 N (shown as shaded area in Figure 4.28). Beyond these forces the delamination was found to increase with increase in thrust force.

In the medium speed range of 8,500 rpm, no delamination was found to occur up to a thrust force of 67 N, as shown by the shaded region in Figure 4.28. However, as the thrust force increased beyond this value, the exit delamination was also found to increase. This experimental critical thrust force was nearly as the calculated thrust force given in Table 4.6.

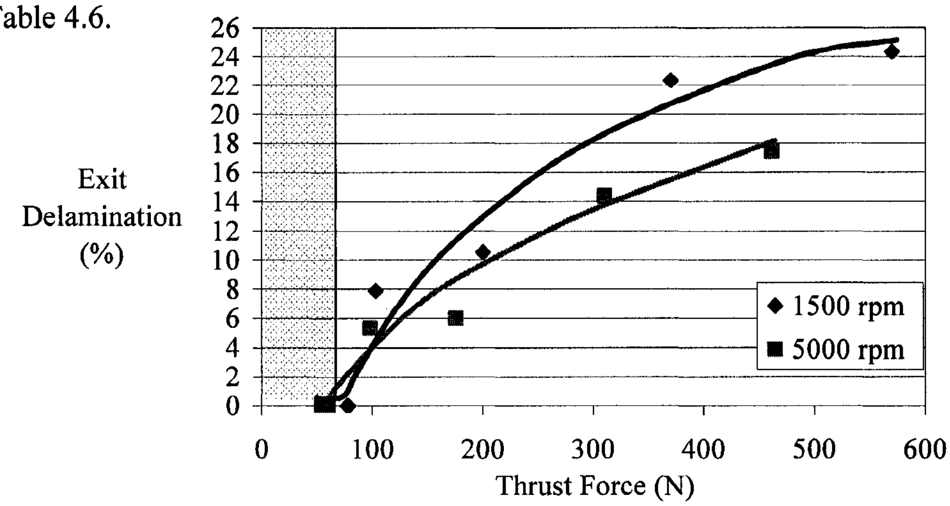

Figure 4.27: Correlation between the Exit (Push Out) Delamination and Thrust Force During Low Speed Drilling (1,500 – 5,000 rpm)

Figure 4.29 illustrates the change in exit delamination with increase in thrust force in the high speed regime. The experimental critical thrust force was found to be 62 N and 50 N at spindle speeds of 12,000 rpm and 15,000 rpm, respectively. These are about 5% and 23% lower than the calculated critical thrust force. At a high speed of 15,000 rpm, delamination of about 7.5% was found to occur at a thrust force of 30 N, though the critical thrust force was much higher. On examination of this type of delamination, it was concluded that high cutting temperature generation during high speed drilling resulted in thermal induced delamination, i.e. not due to the thrust force. Figure 4.13 (a) and (b) illustrate the observed thermal damage along the depth of the curved surface of the hole. It was further observed that with the increase in spindle speed from the low to high speed regime, the extent of delamination is reduced as a result of the reduction in the thrust force. This is evident from the comparison of Figures 4.27, 4.28 and 4.29. One can conclude that the experimental critical thrust force has a variation of about $\pm$25% as compared to the theoretical critical thrust across the different spindle speed regimes. There is roughly a proportional decrease in exit delamination by 80%, resulting from 74% reduction in thrust force, as the spindle speed is increased from 1,500 to 15,000 rpm, as shown in Table 4.7.

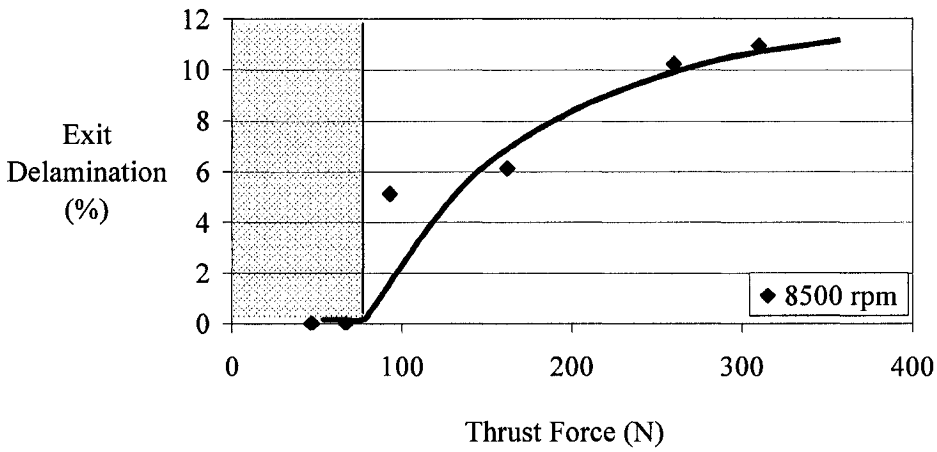

Figure 4.28: Correlation between the Push Out Delamination and Thrust Force During Medium Speed Drilling of 8,500 rpm

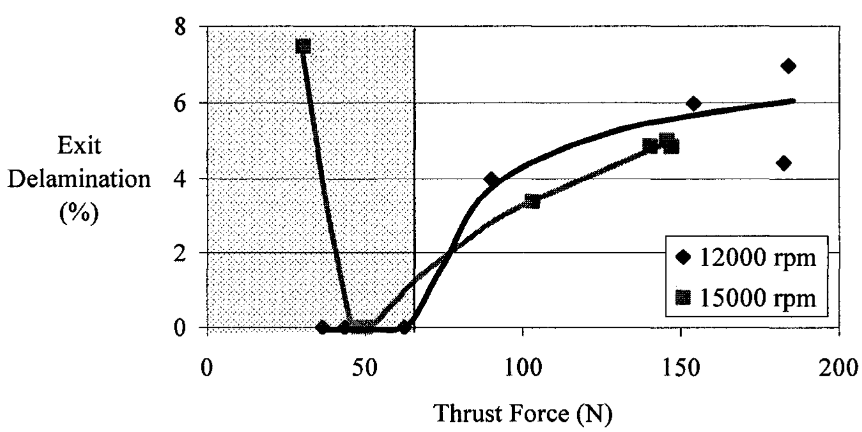

Figure 4.29: Correlation between the Push Out Delamination and Thrust Force During Medium Speed Drilling of 12,000 – 15,000rpm

Table 4.7: Effect of the Increase in Spindle Speed on Reduction in Thrust Force and Exit Delamination

Spindle Speed (rpm)	Feed Rate (μm/rev)	Thrust Force (N)	Exit Delamination (%)	Decrease in Thrust Force	Decrease in Exit Delamination
1,500	800	570	24.31		
15,000	800	147	4.85	74%	80%

4.2.5.3 Entry Delamination

Figure 4.30 illustrates the change in entry delamination with the increase in cutting force. At low speed drilling of 1,500 and 5,000 rpm, no exit delamination was found to occur up to a thrust force of 53 N and 45 N, respectively as shown by the shaded region. Beyond these critical forces, the delamination started to increase and showed good physical correlation with the increase in cutting force. These experimental critical forces are about 20% and 2% higher than the calculated critical cutting force of 44 N given in Table 4.6.

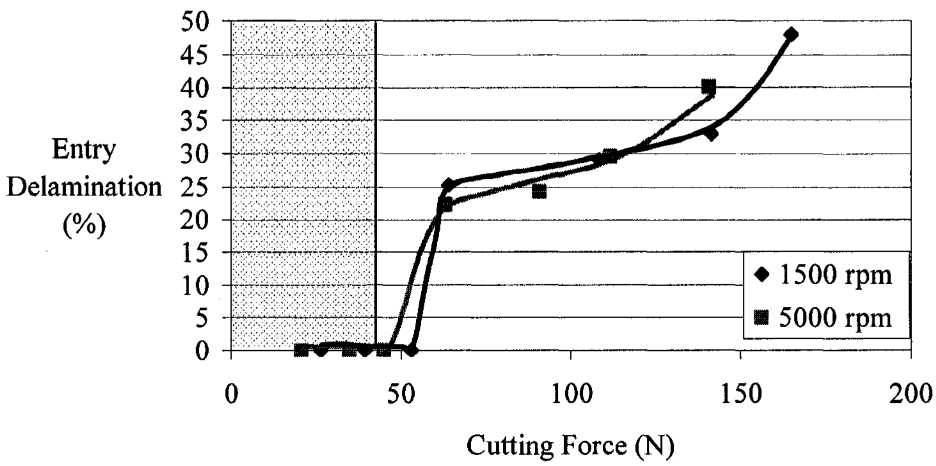

Figure 4.30: Correlation between the Peel Up i.e. Entry Delamination and Cutting Force During Low Speed Drilling (1,500 – 5,000 rpm)

In the medium speed range of 8,500 rpm, no delamination was found to occur up to a thrust force of 44 N as shown by the shaded region in Figure 4.31. As the thrust force increased beyond this critical value, the entry delamination was also found to increase. The experimental critical force was found to be close to the calculated critical force of 44 N.

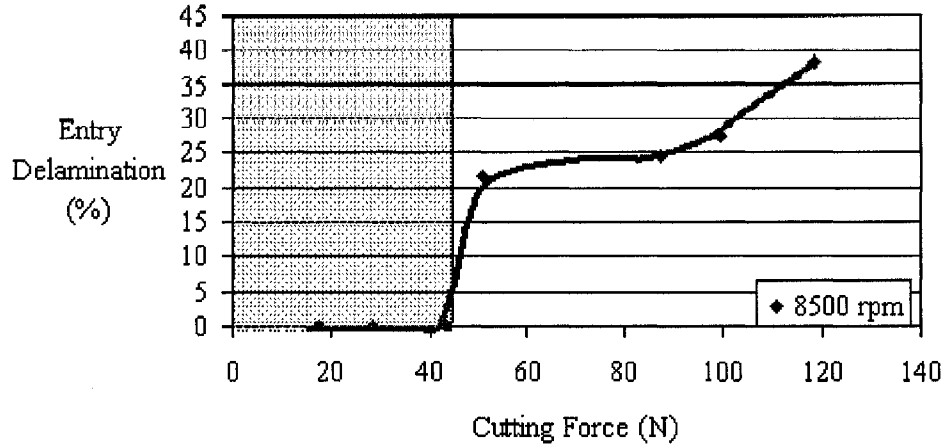

Cutting Force (N)

Figure 4.31: Correlation between Peel Up i.e. Entry Delamination and Cutting Force During Medium Speed Drilling of 8,500 rpm

Figure 4.32 illustrates the progressive increase in entry delamination with increase in cutting force in the high spindle speed regime. The experimental critical force was found to be 38 N and 32 N at spindle speeds of 12,000 and 15,000 rpm, respectively as shown by the shaded region. However, at 15,000 rpm delamination of about 8% was found to occur at a much lower cutting force of 13 N. As explained in section 4.2.4.3, this unusual delamination is attributed to the higher cutting temperature generated during high speed drilling, which softened the matrix phase resulting in "thermal effect dominated mode" of delamination [28]. The critical forces were found to be about 27% and 12% lower than the calculated critical force at 12,000 and 15,000 rpm, respectively.

It was also observed that with the increase in spindle speed, the extent of entry delamination is reduced. This reduction was on account of decrease in the cutting force as evident from the comparison of Figures 4.30, 4.31 and 4.32. There is about 28% reduction in entry delamination due to 54% reduction in the cutting force as the spindle speed increased from 1,500 to 15,000 rpm, as illustrated in Table 4.8.

Table 4.8: Effect of the Increase in Spindle Speed on Reduction in Thrust Force and Exit Delamination

Spindle Speed (rpm)	**Feed Rate (μm/rev)**	**Cutting Force (N)**	**Entry Delamination (%)**	**Decrease in Cutting Force**	**Decrease in Entry Delamination**
1,500	800	164.78	47.95		
15,000	800	76.02	34.69	54%	28%

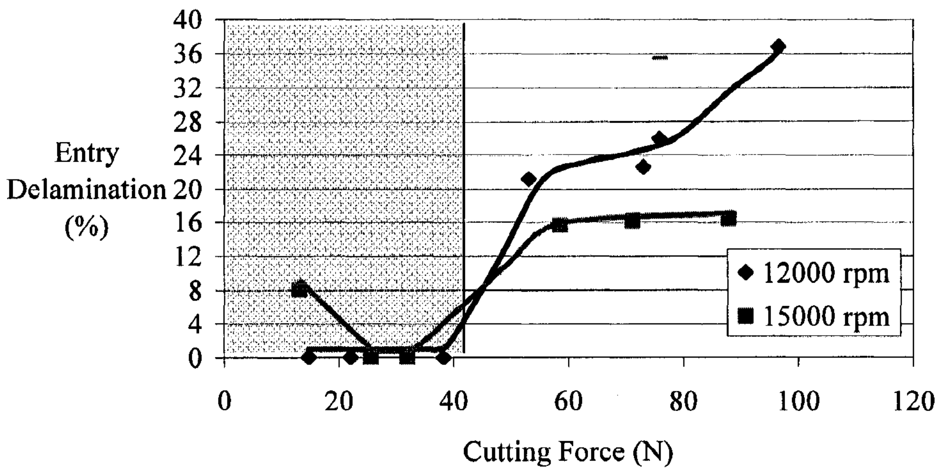

Figure 4.32: Correlation between Peel Up i.e. Entry Delamination and Cutting Force During High Speed Drilling (12,000 – 15,000 rpm)

4.2.6 Effect of Cutting Parameters on Hole Circularity Error

Hole circularity is one of the critical hole geometry factors that is responsible for accurate assembly of bolted joints. A roundness (circularity) criterion specifies a tolerance zone bounded by two concentric circles within which each circular element of the surface must lie and applies independently at any plane [44]. In this work hole circularity has been measured using the Coordinate Measuring Machine as described in section 3.12. Hole circularity error has been found to be influenced by the cutting variables, i.e., "N" and "f" during the drilling process [42, 44, 46]. This section discusses in detail the effect of cutting variables on hole circularity error both at the entry and exit side of hole.

4.2.6.1 Low Speed Drilling (1,500 – 5,000 rpm / 23.6 – 78.5 m/min)

At 1,500 rpm, the hole circularity error was found to be within 0.05 - 0.25% of the hole diameter as shown in Figure 4.33. The hole circularity error at entry was found to increase from 0.05% at low feed rate of 20 μm/rev to about 0.18% at high feed rate of 800 μm/rev. Similarly, the hole circularity error at exit was found to increase from 0.07% at low feed rate of 20 μm/rev to about 0.20% at high feed rate of 800 μm/rev. A similar trend was found to occur at 5,000 rpm.

Figure 4.34 shows the increase in hole circularity error, both at entry and exit, with increase in feed rate. A comparison of hole circularity error at the entry and exit of laminate revealed slightly higher circularity error at the hole exit than at the entrance. The hole circularity error at exit was found to increase from 0.11% at 20 μm/rev to 0.45% at 800 μm/rev. The hole circularity error at entry was also found to increase with increase in feed rate.

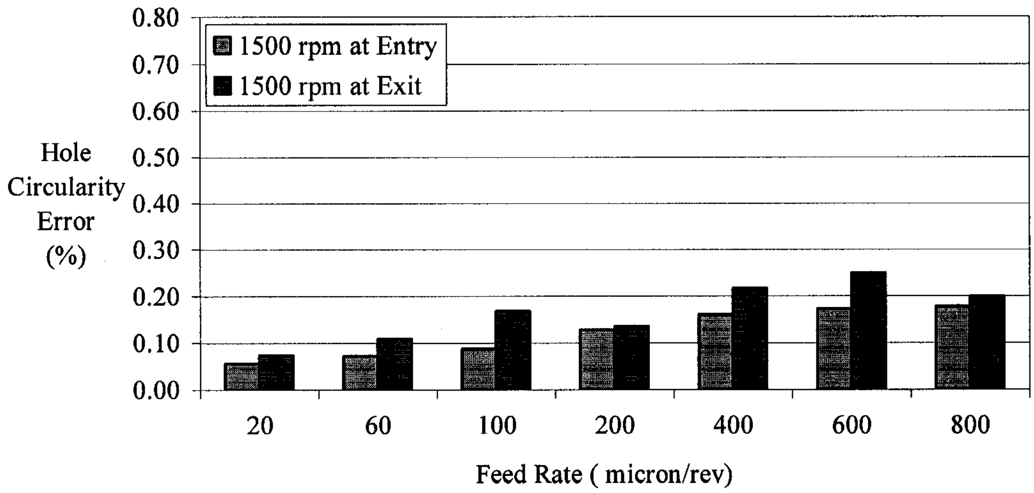

Figure 4.33: Variation in Hole Circularity Error at Entry and Exit with Feed Rate during Low Speed Drilling of 1,500 rpm

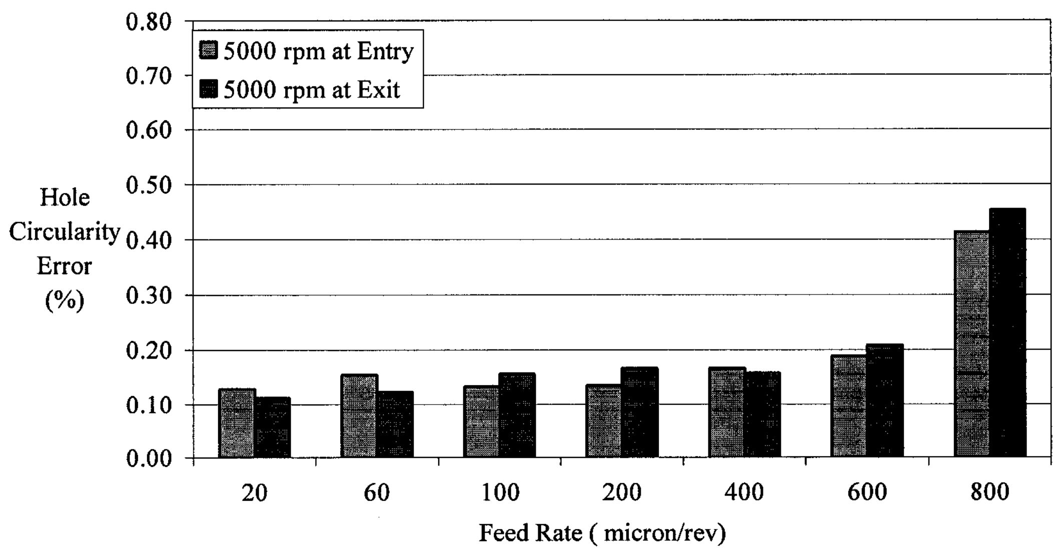

Figure 4.34: Variation in Hole Circularity Error at Entry and Exit with Feed Rate during Low Speed Drilling of 5,000 rpm

4.2.6.2 Medium Speed Drilling (8,500 rpm / 133.5 m/min)

Figure 4.35 shows the increase in hole circularity error with increase in feed rate for medium spindle speed of 8,500 rpm. The hole circularity error at entry was found to increase from 0.14% at low feed rate of 20 μm/rev to about 0.55% at high feed rate of 800 μm/rev. Similarly, the hole circularity error at exit was found to increase from 0.10% at low feed rate of 20 μm/rev to about 0.24% at high feed rate of 800 μm/rev. However, at the medium speed of 8,500 rpm, the hole circularity error was found to be worse on the entry side as opposed to the better hole circularity at the entrance in low speed regime.

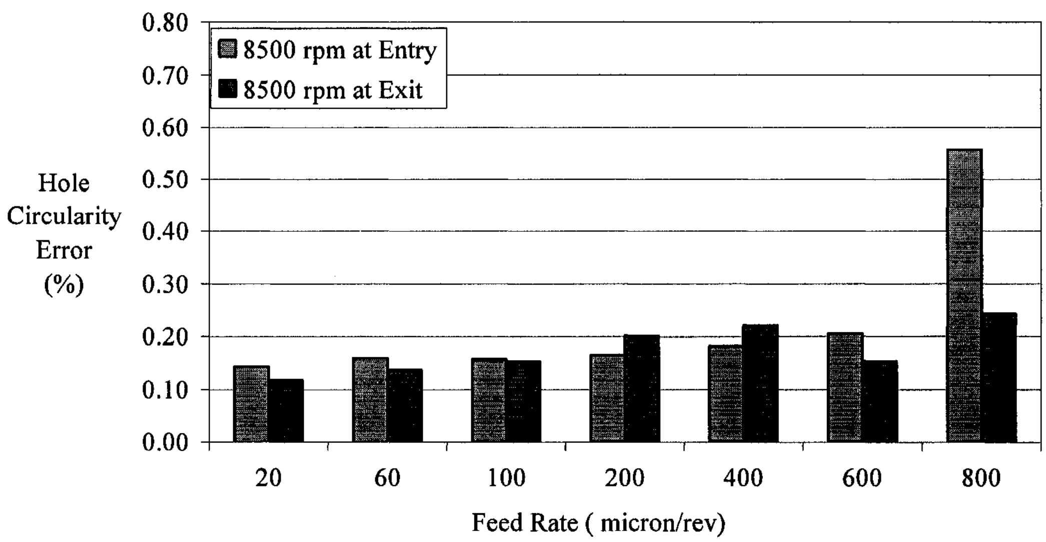

Figure 4.35: Variation in Hole Circularity Error at Entry and Exit with Feed Rate during Medium Speed Drilling of 8,500 rpm

4.2.6.3 High Speed Drilling (12,000 -15,000 rpm / 188.5 -235.6 m/min)

Figures 4.36 and 4.37 illustrate the change in hole circularity error with increase in feed at 12,000 & 15,000 rpm, respectively. The hole circularity error was found to be higher at the hole entry than at the exit as opposed to the low speed drilling, where hole circularity error at exit was found to be worse. Also at high spindle speeds, the hole circularity error was found to be in the range of 0.10 – 0.75%, which was comparatively higher as compared to the hole circularity error at low and medium speeds. The hole circularity error both at entry and exit was found to slightly improve at feed rate of 60 μm/rev in the low feed regime. Beyond 60 μm/rev, the hole circularity error at entry increased from 0.10% to a maximum of 0.75% at spindle speed of 15,000 rpm. However at 12,000 rpm, the hole circularity error at entry was in the range of 0.15 - 0.65% for the feed range of 60 – 800 μm/rev, and thus was slightly lower.

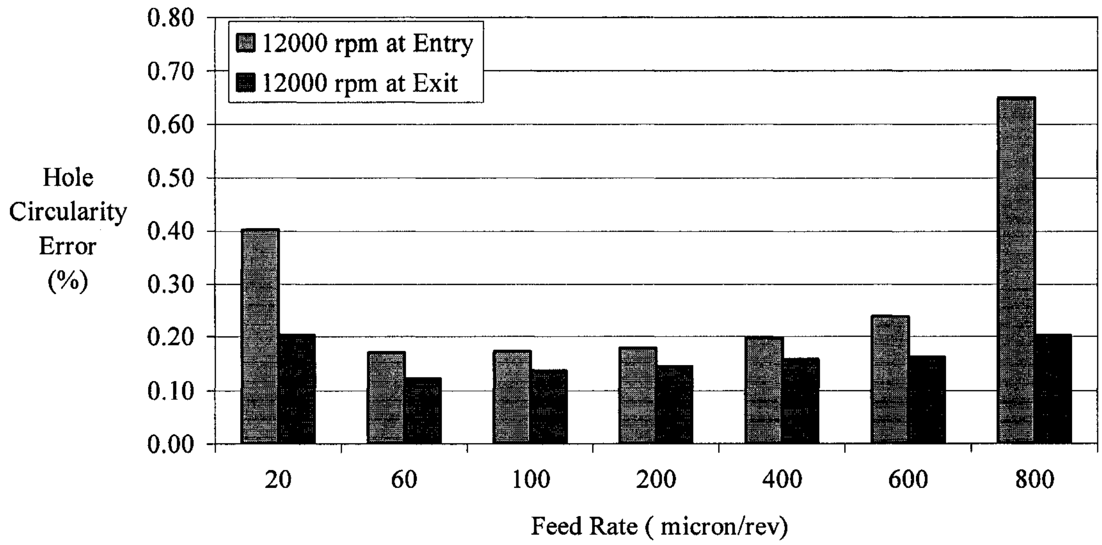

Figure 4.36: Variation in Hole Circularity Error at Entry and Exit with Feed Rate during High Speed Drilling of 12,000 rpm

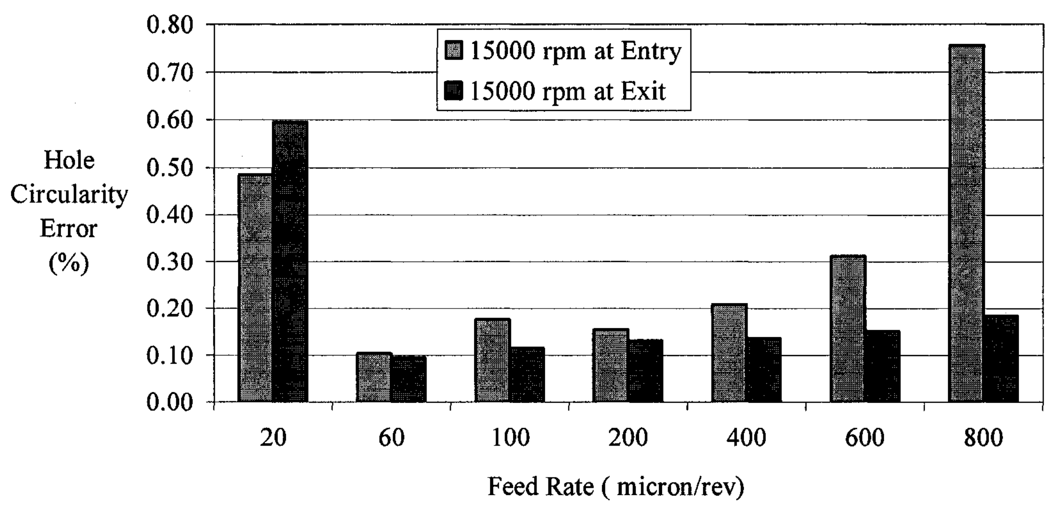

Figure 4.37: Variation in Hole Circularity Error at Entry and Exit with Feed Rate during High Speed Drilling of 15,000 rpm

The following conclusions can be been drawn for the affect of cutting parameters, i.e., spindle speed and feed rate on hole circularity error:

i. Hole circularity error was found to increase with increase in feed rate for all spindle speeds with the exception of high speed drilling, where it goes through at minimum at 60 μm/rev. The increase in hole circularity error with increase in feed rate could be attributed to the increase in thrust force (as shown in Figures 4.2-4.4). With increase in feed rate from low to high feed regimes, the action of the drill penetrating the laminate at hole entry becomes more of an impact action thus resulting in higher resistance. This high thrust force could result in off-centring the drill chisel edge, resulting in poor hole circularity at the entrance. Figure 4.38 illustrates the effect of increasing thrust force on the hole circularity error at the entrance. Each point on the spindle speed curve (which corresponds to a particular thrust force and hole circularity error) represents a particular feed rate, and the data points at higher thrust force levels represent higher feed rates as already established in section 4.2.1. It is evident from this figure that for a range of thrust force between 50 - 150 N (as shown bounded by the two broken lines), the hole circularity error produced was within 0.20% of the hole diameter for all the speed regimes. However, beyond 150 N the hole circularity error started to deteriorate becoming worse with the increase in cutting speed.

ii. The observed increase in hole circularity error with the increase in spindle speed was in agreement with the results reported in [44], though a graphite bismalimide thermoset was used at relatively low speed range of 660 – 1,750 rpm. It was identified during the drilling experiments that, with increase in spindle speed, the vibrations induced during the drill entry also increased. These induced vibrations combined with lower thrust forces at higher speeds made the tool workpiece (laminate) system less rigid and thus resulted in poor hole circularity at higher spindle speeds. Figure 4.38 illustrates the effect of lower thrust force at higher spindle speeds in producing large circularity errors. However, the extent of hole circularity error is system dependant, i.e. varies with drill size and rigidity of tool holder and spindle.

iii. At low feed rate of 20 μm/rev, large hole circularity error was observed especially for higher spindle speeds of 12,000 and 15000 rpm as shown in Figures 4.36 and 4.37. This could be attributed to higher cutting temperatures observed at higher spindle speeds (12,000 - 15,000 rpm) as established in Figure 4.6. These higher cutting temperatures coupled with longer contact time of tool with laminate at low feed rate of 20 μm/rev resulted in softening of the matrix. This thermal softening effect along with high induced vibrations at higher spindle speeds produced poor hole circularity in the high speed and low feed regime as shown in Figure 4.38.

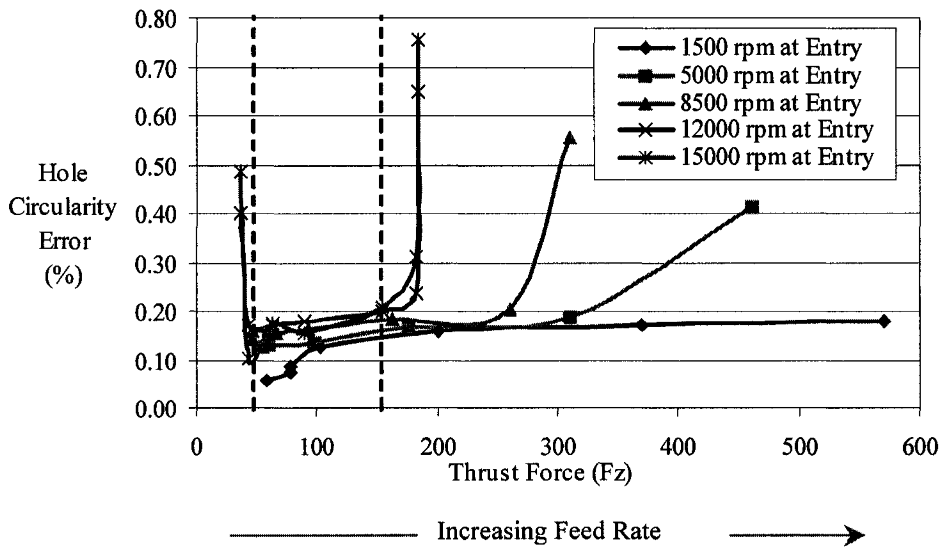

Figure 4.38: Effect of Thrust Force on Hole Circularity Error at the Drill Entry for all Different Spindle Speeds (1,500 – 15,000 rpm)

4.2.7 Effect of Cutting Parameters on Hole Diameter Error

Hole diameter is another key geometry parameter that must be controlled during the drilling in order to avoid the production of oversized holes that cannot be repaired and can result in the part being scrapped. In [49], the authors investigated the hole diameter error in accordance to the H8 tolerance limits set on the hole, produced by drilling. In this research task, ISO h8 shaft tolerance set on the tool by the tool manufacturer (M/s Material Removal, a subsidiary of Kennametal Inc.) was used to evaluate the effect of speed and feed on the hole diameter. The ISO h8 shaft tolerance for the 5 mm standard point drill, used in these experiments, limits the tolerance to +0 to -0.018 mm, i.e., a maximum hole undersize of about 0.36%. Hole diameter error in this experimental work has been calculated as per equation (1.12) using Coordinate Measuring Machine (CMM). The experiments produced holes within the h8 tolerance standards on the drill diameter, except for a few exceptions at low feed rate and high spindle speeds. These exceptions and their dependence on cutting parameters, i.e., spindle speed and feed rate are discussed in detail in this section

Figures 4.39 and 4.40 illustrate the change in hole diameter error with feed rate at low spindle speed range of 1,500 - 5,000 rpm. The holes were found to be within the tolerance limits for feed rates in the range of 60 to 600 μm/rev. At high feed rate of 800 μm/rev and spindle speed of 5,000 rpm, the holes were found to be undersized by about 1.10% of the hole diameter. However, at low feed rate of 20 μm/rev the hole diameter was found to be slightly oversized by about 0.15% at 5,000 rpm. These results were found to contradict those presented in [44], where the hole diameter error was found to increase from less oversize to more oversize with increase in feed rate during drilling of a graphite bismalimide thermoset at spindle speed range of 660 – 1,750 rpm and feed range of 80 – 240 μm/rev. One reason could be that the particular carbide drills used for experiments in [44] was designed to produced oversized holes, and the oversize increased further both with speed and feed.

At medium speed of 8,500 rpm and feed rate between 60 - 800 μm/rev, the holes were found to be within tolerance i.e. undersized as shown in Figure 4.41. However, at the lowest feed rate of 20 μm/rev the hole diameter was found to be oversized by 0.20%. Moreover, the undersize reduced in magnitude as compared to low speed drilling regime and is evident from the comparison of Figures 4.39 and 4.41.

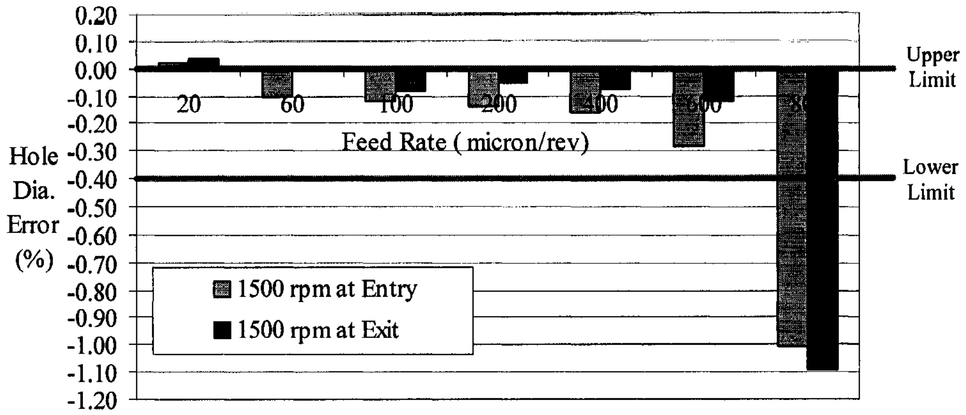

Figure 4.39: Effect of Feed Rate on Hole Diameter Error at Drill Entry and Exit for Spindle Speed of 1,500 rpm

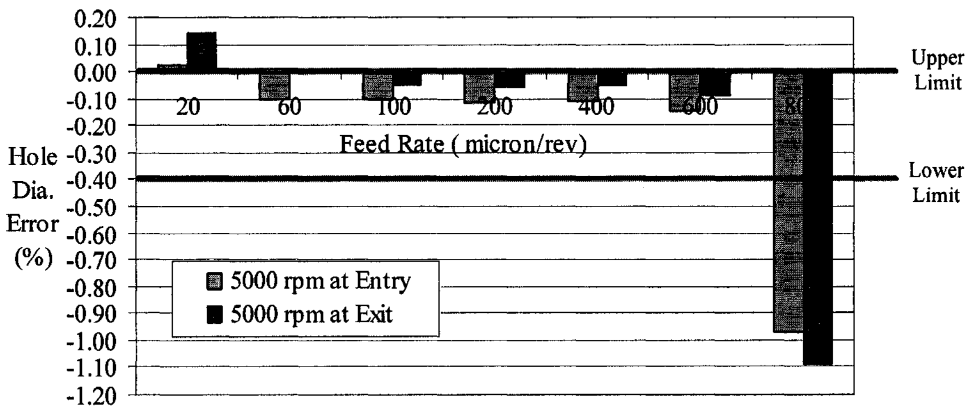

Figure 4.40: Effect of Feed Rate on Hole Diameter Error at Drill Entry and Exit for Spindle Speed of 5,000 rpm

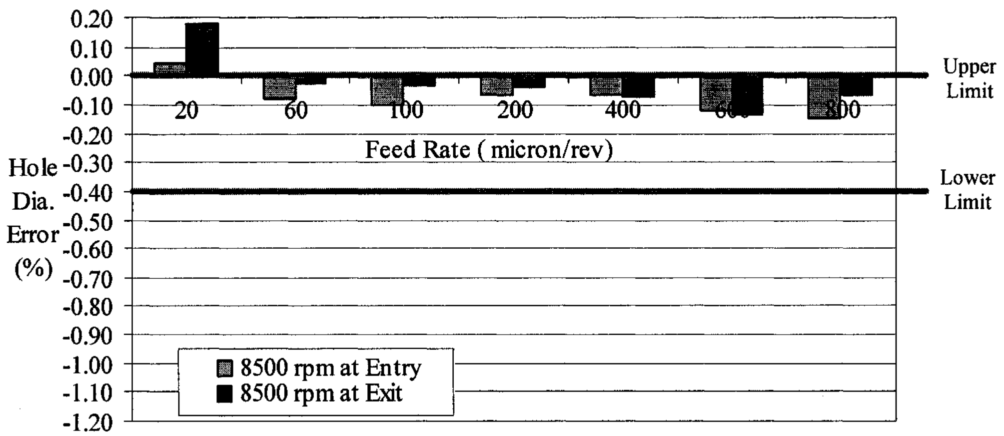

Figure 4.41: Effect of Feed Rate on Hole Diameter Error at Drill Entry and Exit for Spindle Speed of 8,500 rpm

Figures 4.42 and 4.43 illustrate the effect of increase in feed and speed on hole diameter error in the high speed regime. At 12,000 rpm, the holes were found to be within tolerance in the medium and high feed regime (200 - 800 μm/rev). In the low feed regime of 60 - 100 μm/rev and spindle speed of 12,000 rpm, oversized holes were produced only at exit side, while at 20 μm/rev oversized holes were produced both at entry and exit. At higher spindle speed of 15,000 rpm, the holes produced were oversized by about 5.75% at feed rate of 20 μm/rev, while in the feed range of 60 – 200 μm/rev the holes were slightly oversized by less than 0.21%. As the feed rate increased to high feed regime, i.e., 800 μm/rev slightly undersized holes were produced mainly on the exit side.

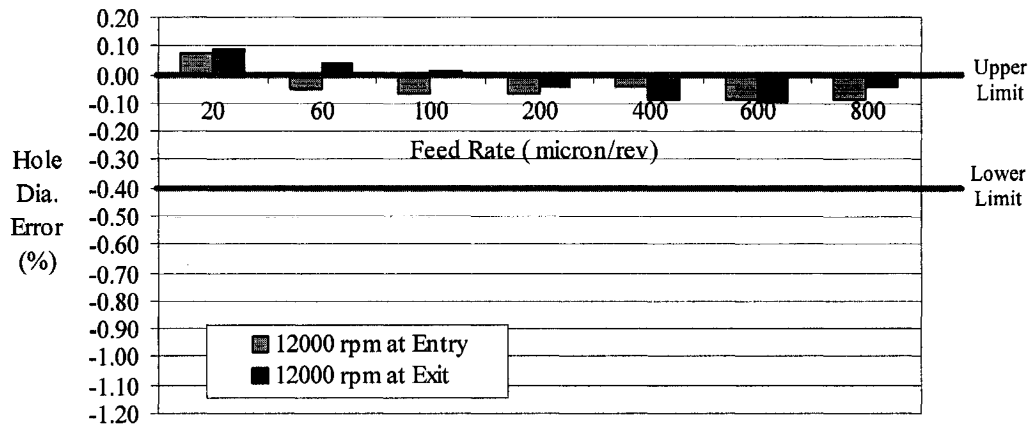

Figure 4.42: Effect of Feed Rate on Hole Diameter Error at Drill Entry and Exit for Spindle Speed of 12,000 rpm.

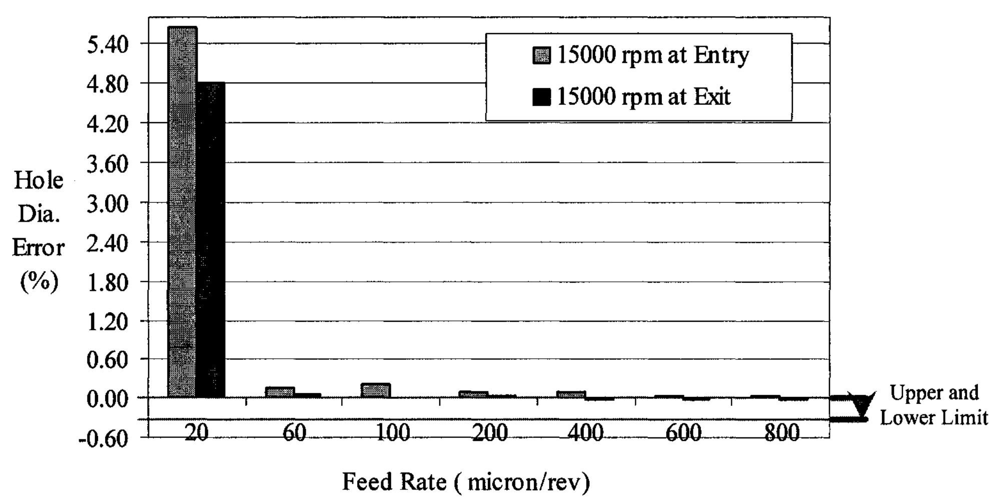

Figure 4.43: Effect of Feed Rate on Hole Diameter Error at Drill Entry and Exit for Spindle Speed of 15,000 rpm

At low and medium spindle speeds, the undersized holes produced were within the design tolerance of the drill except at lowest feed rate of 20 μm/rev, where the holes produced were oversized as evident from Figures 4.39 – 4.41. This could be attributed to the higher thermal expansion of WC tool as compared to composite laminate under the effect of higher cutting temperatures, i.e., greater than 265 °C estimated at a spindle speed of 8,500 rpm. Since the thermal conductivity of WC drill is about 3.2 times the thermal conductivity of graphite epoxy laminate, as shown in Table 4.9, most of the generated heat during cutting goes to the WC drill. Also the coefficient of thermal expansion of WC is about 250 times more than the composite laminate, as shown in Table 4.9; hence as the tool expands it produces slightly oversized holes. At higher speeds of 15,000 rpm, where comparatively higher cutting temperature were produced, highly oversized holes of the order of 5.50% were produced. With increase in feed rate the holes continued to be oversized, however, the magnitude of oversize was found to decrease. This could be attributed to lower contact time between the cutting tool and the hole surface, which could have resulted in less time for WC drill to expand owing to its thermal inertia and thus lower oversized holes at higher feeds.

Table 4.9: Thermal Properties (Thermal Conductivity and Coefficient of Thermal Expansion) of Tungsten Carbide/Cobalt and Carbon Epoxy [1, 5]

Material	**Thermal Conductivity (W/m °K) (measured at room 25°C)**	**Coefficient of Thermal Expansion (μm/m)/°K**
Tungsten Carbide / Cobalt (WC 94/Co 6)	80.00	5.00
Carbon/Epoxy (T300/5208)	25.00	0.02

Apart from thermal effects, the induced vibrations at higher spindle speeds were also found to produce oversized holes [44]. At high spindle speeds and low feed rates, lower thrust forces were generated as shown in Figure 4.4. Under the influence of low thrust force, the tool laminate system would be less stiff as compared to higher feed rate conditions where the reaction forces were found to be higher. This could results in higher vibrational effects at low feeds as compared to higher feed rates and thus makes the holes oversized.

Figures 4.44 and 4.45 show a good physical correlation between the hole diameter error at entry and the thrust force and hole diameter error at exit and the cutting force. Each point on the spindle speed curve (which corresponds to a particular thrust/ cutting force and hole diameter error) represent a particular feed rate, and the hole diameter error data points at higher force levels represent higher feed rates as already established in section 4.2.1. It is evident from Figure 4.44 that for a thrust force between 50 - 300 N (as shown bounded by the two dotted lines), the hole diameter error at entry was within $\pm$0.25% of the hole diameter for all the speed regimes. However, beyond 300 N the holes produced are undersized beyond the lower tolerance limit of -0.40 % at low speed drilling regime (1,500 – 5,000 rpm). Similarly from Figure 4.45, it is evident that for a cutting force between 25 - 115 N (as shown bounded by the two dotted lines), the hole diameter error at exit was within $\pm$0.20% of the hole diameter for all the speed regimes.

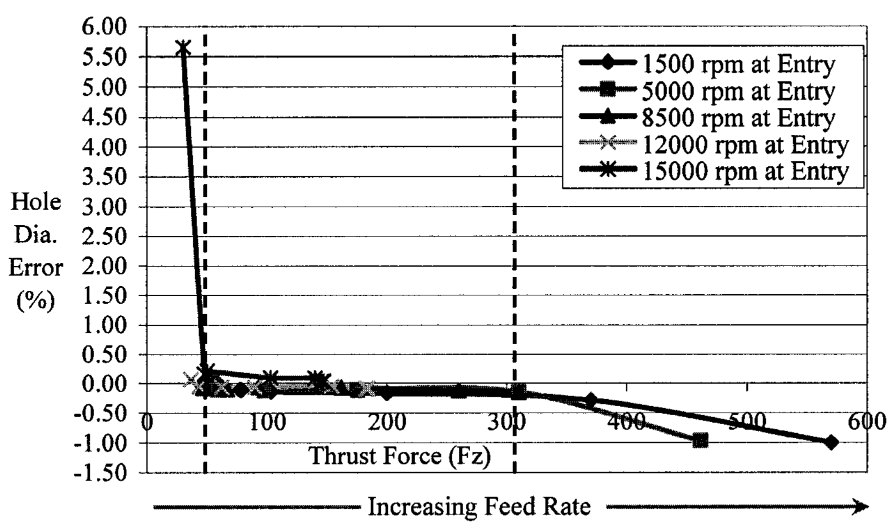

Figure 4.44: Effect of Thrust Force on Hole Diameter Error at the Drill Entry for all Spindle Speeds (1,500 – 15,000 rpm)

At cutting force lower than 20 N, obtained at high spindle speed and low feed rate, oversized holes of up to 4.75% were produced. Within the cutting speed range of

1,500 – 5,000 rpm and high feed rates the cutting forces exceed 115 N and undersized holes are produced. The reason for oversized holes at high spindle speed and low feed rate has already been explained above. The undersized holes produced at higher forces could be due high fiber pull out and extensive interlaminar delamination damage observed at low spindle speeds and high feeds. These damages are evident from surface micrographs shown in Figure 4.46 (a) and (b). The rough surfaces produced at high feed rate of 800 μm/rev and speed range of 1,500 – 5,000 rpm could have influenced the hole diameter measurements and thus resulted in more undersized holes.

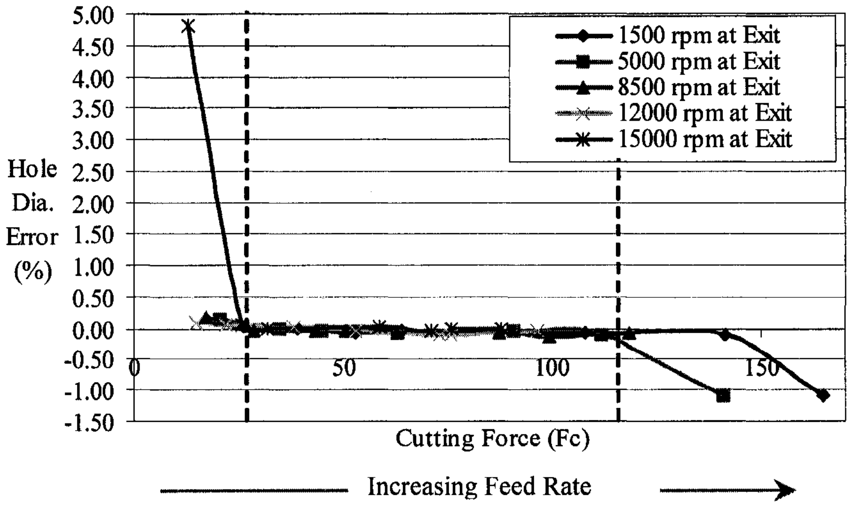

Figure 4.45: Effect of Cutting Force on Hole Diameter Error at the Drill Exit for all Spindle Speeds (1,500 – 15,000 rpm)

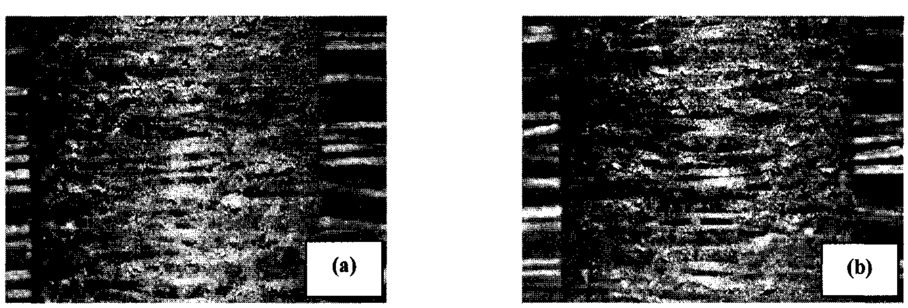

Figure 4.46: Average Surface Roughness "R_a" of 2.5 μm (a) and 2.0 μm (b) for Holes Drilled at f = 800 μm/rev and (a) N = 1,500 rpm and (b) N = 5,000 rpm

4.2.8 Effect of Cutting Parameters on Surface Roughness

The drilling process of graphite fiber epoxy thermoset composites results in series of mini-fiber fractures, matrix burnout, fiber pull outs and interlaminar delaminations as shown in Figures 4.1, 4.13 and 4.16, respectively. The cutting parameters, i.e., spindle speed "N" and feed rate "f" have been found to influence all these damage mechanisms, which in turn affect the surface roughness of the produced hole. Figure 4.47 illustrates the extensive fiber pull out that occurred at 1,500 rpm and 800 μm/rev during the course of this research. This section discusses in detail the effect of cutting parameters on hole surface roughness, which was measured using a surface profilometer as already discussed in section 3.10.

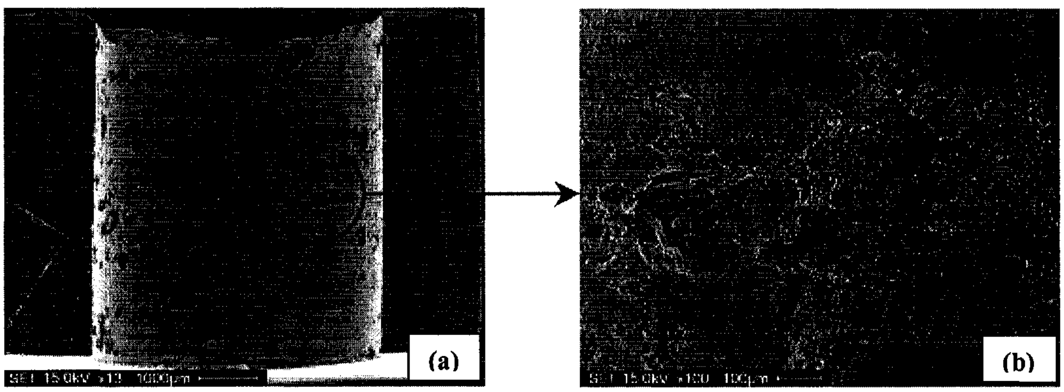

Figure 4.47: Fiber Pull-Out Observed On a Hole Surface at Spindle Speed of 1,500 rpm and Feed Rate of 800 μm/rev

Figures 4.48 and 4.49 show the effect of spindle speed and feed rate on average surface roughness. For all spindle speeds (1,500 – 15,000 rpm), the average surface roughness "R_a" was found to increase with increase in feed rate. Figures 4.50 (a) - (h), show the increase in surface roughness with increase in feed rate from 20 μm/rev to 600 μm/rev for each investigated spindle speeds. These results were found to be in agreement with [32, 35], where the surface roughness was also found to increase with speed and feed. At a particular spindle speed, the increase in average surface roughness 'R_a' with increase in feed from 60 – 800 μm/rev was attributed to the increase in both the thrust and cutting force, as already shown in Figures 4.2 – 4.4. The increasing thrust force caused damage at the ply interface resulting in interlaminar delaminations, while the increasing cutting force coupled with low feed rates resulted in fiber pull out. The surface roughness thus deteriorated due to these two factors.

At low feed rate of 20 μm/rev, the surface roughness deteriorated with increase in spindle speed from 1,500 to 8,500 rpm. This was on account of increase in fiber pull out with increase in spindle speeds as shown in Figures 4.50 (a) and (c). It was observed that with increase in spindle speed, the cutting temperature increased as illustrated in Figure 4.12. Owing to higher cutting temperature at higher speeds, the matrix softening occurred and as a result graphite fibers instead of being cut, they were pulled out from the relatively soft matrix, resulting in higher fiber pull out and thus higher surface roughness. However, at higher spindle speed 15,000 rpm the surface roughness was found to improve, when compared to medium speed of 8,500 rpm as shown in Figure 4.49. This was due to burning of epoxy matrix observed at high spindle speed of 15,000 rpm, which smeared the hole surface, as evident from the SEM image illustrated in Figure 4.13 and optical image of hole surface shown in Figure 4.50 (g). This smearing action resulted in filling of the fiber pulled out cavities, thus giving better R_a. At very high feed rates of 600 and 800 μm/rev, the surface roughness was found to slightly improve with increase in spindle speeds as shown in Figure 4.49. This was again due to the thermal softening effect, which resulted in decrease of thrust and cutting forces, thus producing less interlaminar damage and improved surface roughness. A comparison of Figures 4.50 (d), (f) and (h) illustrates the reduction in interlaminar damage with increase in spindle speed from 8,500 rpm to 15,000 rpm at feed rate of 600 μm/rev.

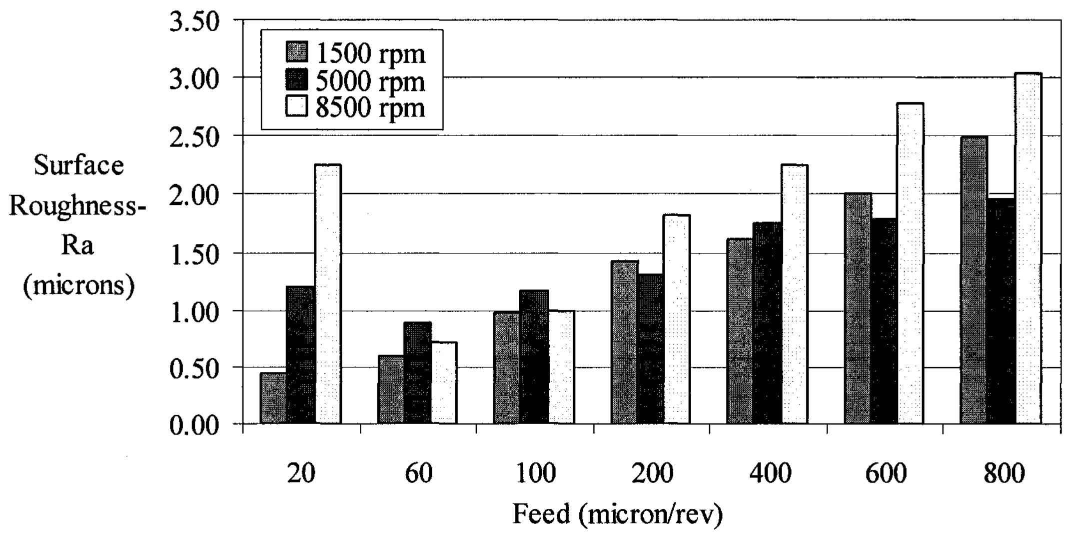

Figure 4.48: Effect of Feed Rate and Spindle Speed on Average Surface Roughness at Low and Medium Speed Drilling (1,500 – 8,500 rpm)

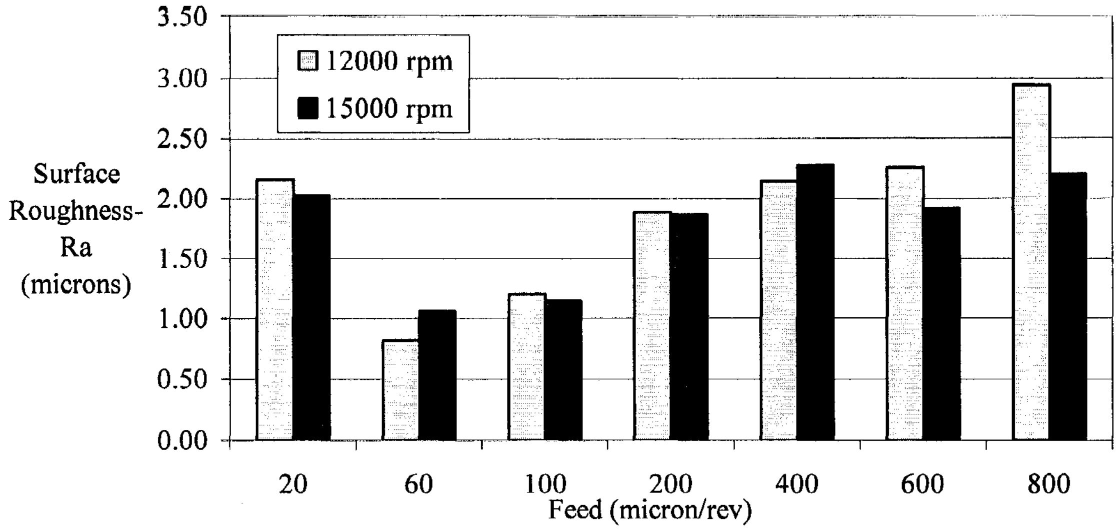

Figure 4.49: Feed Rate and Spindle Speed on Average Surface Roughness at High Speed Drilling (12,000 – 15,000 rpm)

The machinability assessment revealed the importance of thrust force, cutting force and cutting temperature in causing the damage mechanisms namely delamination, fiber pull out, hole surface roughness and hole geometry attributes like hole circularity and hole diameter error. High speed drilling (12,000 - 15,000 rpm) investigation highlights the importance of thermal softening effect in reducing the thrust and cutting force, and eventually the delamination damage for a range of low feed rates. Also surface roughness has been found to improve at high speeds and low and medium feeds, again due to the reduction in forces which in turn reduce fiber pull out and interlaminar delamination. However, at the same time high speed regime was found to be detrimental to hole geometry attributes. At low feed rates and high speeds, large hole circularity and diameter errors were found to occur mainly due to lower reaction forces. Thus, this investigation clearly highlights the physical significance of cutting forces and temperature in controlling the composite part quality. Since the effects might contradict, as seen at high spindle speeds, there was a need to present the information in the form of readily usable maps which could help in optimizing the drilling process. The next section provides the concept of machinability maps and their use.

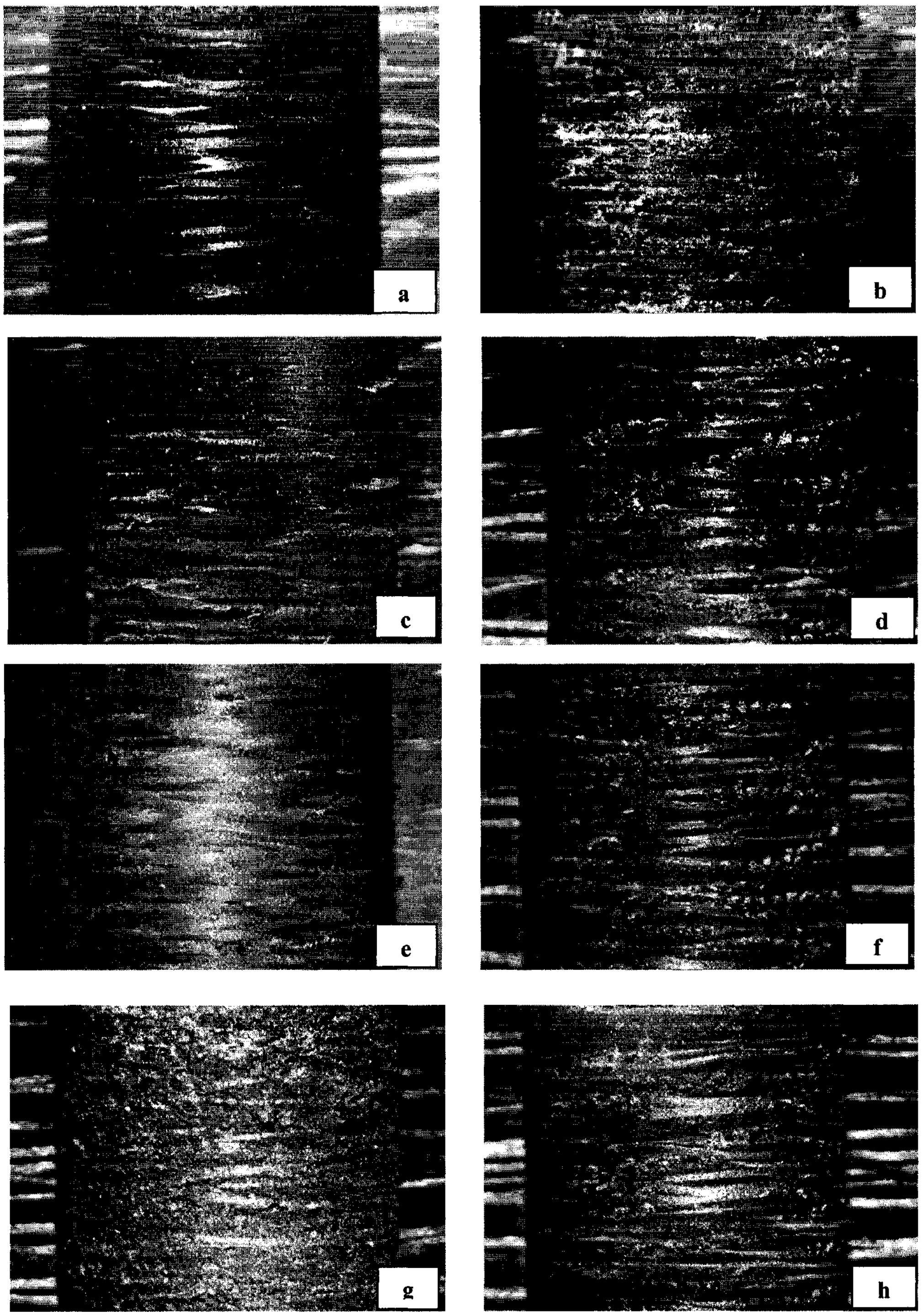

Figure 4.50: Average Surface Roughness at Different Spindle Speeds and Feed Rates (a) Ra = 0.5 μm at 1,500 rpm and 20 μm/rev (b) Ra = 2.0 μm at 1,500 rpm and 600 μm/rev (c) Ra = 2.2 μm at 8,500 rpm and 20 μm/rev (d) Ra = 2.8 μm at 8,500 rpm and 600 μm/rev (e) Ra = 2.1 μm at 12,000 rpm and 20 μm/rev (f) Ra = 2.3 μm at 12,000 rpm and 600 μm/rev (g) Ra = 2.03 μm at 15,000 rpm and 20 μm/rev (h) Ra = 1.9 μm at 15,000 rpm and 600 μm/rev

4.3 Machinability Maps

The machinability assessment of the graphite epoxy laminate established the material behaviour characteristics with regards to delamination, hole circularity, hole diameter error and hole surface roughness, for different speed and feed regimes (low, medium and high speed). Hole quality characteristics are found to be strongly dependent on the cutting forces and temperatures generated during the drilling process as analysed in section 4.2. During the physical drilling process these intermediate variables can be directly monitored and thus can be used to control the process by adjusting the input cutting parameters. Thus, having already established the effect of cutting variables on the forces and temperature, the approach of the machinability maps was used to represent the effect of change of input variables on the output parameters. Since the data obtained was discrete, the machinability maps are plotted for the worst case of each output parameter, i.e., delamination, hole circularity, hole diameter error and hole surface roughness for a particular range of input parameters, i.e., the spindle speed and feed rate. Moreover, obtaining good results for some desirable parameters like delamination, might require cutting condition that may badly affect other parameters, therefore optimization requires superposition of all the maps. This section also provides a brief example about the use of these machinability maps for optimization.

4.3.1 Machinability Map for Delamination

Delamination was identified in section 4.2 as one of the factors that strongly depends on both the forces and cutting temperature. Delaminations at the entry and exit of laminate were found to increase with increase in cutting force and thrust force, respectively. It was also identified that with increase in spindle speed, the cutting forces decreased as a result of thermal softening leading to reduced delamination damage. However, at high spindle speeds (12,000 – 15,000 rpm) and low feed rate of 20 μm/rev thermal induced delamination was found to occur.

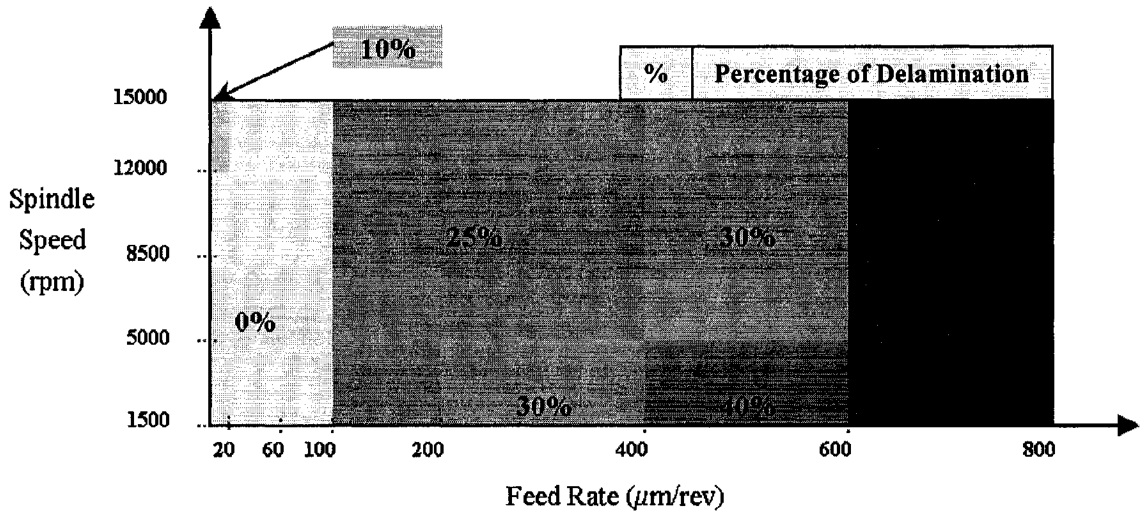

Figure 4.51: Machinability Map Showing the Effect of Spindle Speed and Feed Rate on Delamination

Figure 4.51 shows the effect of the feed rate and spindle speed on the delamination damage in the form of delamination damage machinability map. It is evident from this map that with increase in feed rate there is increase in delamination damage as discussed in section 4.2.4. However, with the increase in spindle speeds there is reduction in delamination damage for medium (100 – 400 μm/rev) and high feed regime (400 – 600 μm/rev). It is also evident from the machinability map that high spindle speed of 15,000 rpm and feed rates between 20 and 100 μm/rev will result in no delamination. The delamination machinability map thus gives a combined effect of both the cutting parameters on delamination damage, and hence can be used as a tool for selecting drilling parameters to avoid damage or minimize delamination.

4.3.2 Machinability Map for Hole Circularity Error

Figure 4.52 presents the machinability map developed to show the effect of cutting parameters, i.e., spindle speed and feed rate on hole circularity error. It shows the effect of high spindle speeds and high feed rates (600 – 800 μm/rev) in producing holes with large hole circularity errors. Also the deteriorating effect of medium and high speeds

(8,500 – 15,000 rpm) combined with low feed rates (20 – 60 μm/rev) is evident from this machinability map for the reasons already explained in section 4.2.6. It is also evident from the machinability map that high spindle speed of 15,000 rpm and feed range of 60 – 200 μm/rev will result in best hole circularity of about 0.2 % without sacrificing process productivity.

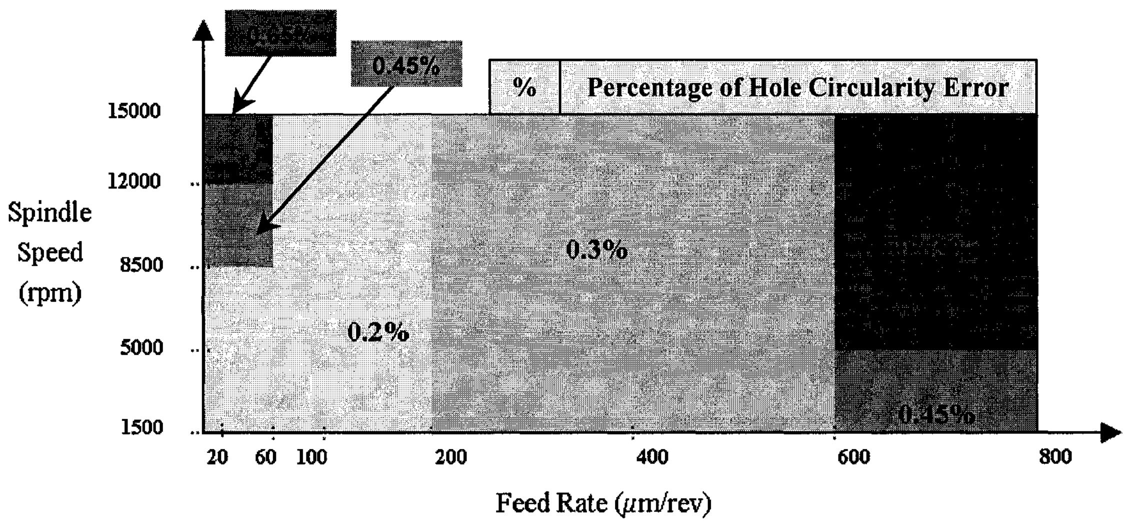

Figure 4.52: Machinability Map Showing the Effect of Spindle Speed and Feed Rate on Hole Circularity Error

4.3.3 Machinability Map for Hole Diameter Error

Figure 4.53 illustrates in detail the effect of cutting parameters on the hole diameter error in the form of hole diameter error machinability map. Hole diameter error was found to strongly depend on the thrust force at the hole entry, as already explained in section 4.2.7. At higher spindle speed range of 12,000 - 15,000 rpm and low feed rate of 20 mm/rev, the thermal softening effect resulted in lowering of the thrust force. The lower thrust force coupled with high induced vibration because of high spindle speeds, produced highly oversized holes. This machinability map makes it evident that the high spindle speeds result in production of oversized holes for all the investigated feed ranges. Thus, the high speeds might not be the best cutting conditions to maintain hole diameter, unless the diameter error falls within the design tolerance, or undersized drills are used.

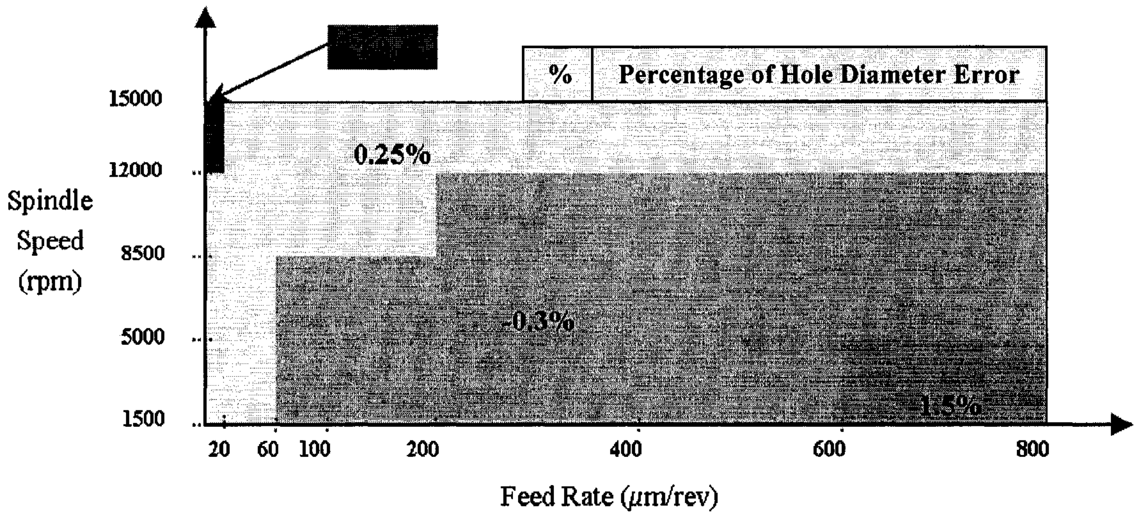

Figure 4.53: Machinability Map Showing the Effect of Spindle Speed and Feed Rate on Hole Diameter Error

4.3.4 Machinability Map for Surface Roughness

The machinability map of surface roughness, shown in Figure 4.54, illustrates the effect of cutting parameters, i.e., spindle speed and feed rate, on the average hole surface roughness, i.e., R_a. The surface roughness was found to increase both with feed rate and spindle speed in the low and medium speed regime, as analyzed in section 4.2.8. The dependence of surface roughness on both the thrust and cutting force was also established. Since these forces were found to increase with feed rate, as described in section 4.2.1, the surface roughness was expected to show similar response. However, exceptions were found to occur at high spindle speeds of 15,000 rpm and low feed rate of 20 μm/rev and high feed rate of 400 – 800 μm/rev, where the surface finish was found to improve slightly for the reason already explained in section 4.2.8. The surface roughness machinability clearly highlights this effect of high spindle speeds. This map can again be used as a tool for better surface roughness control without sacrificing process productivity.

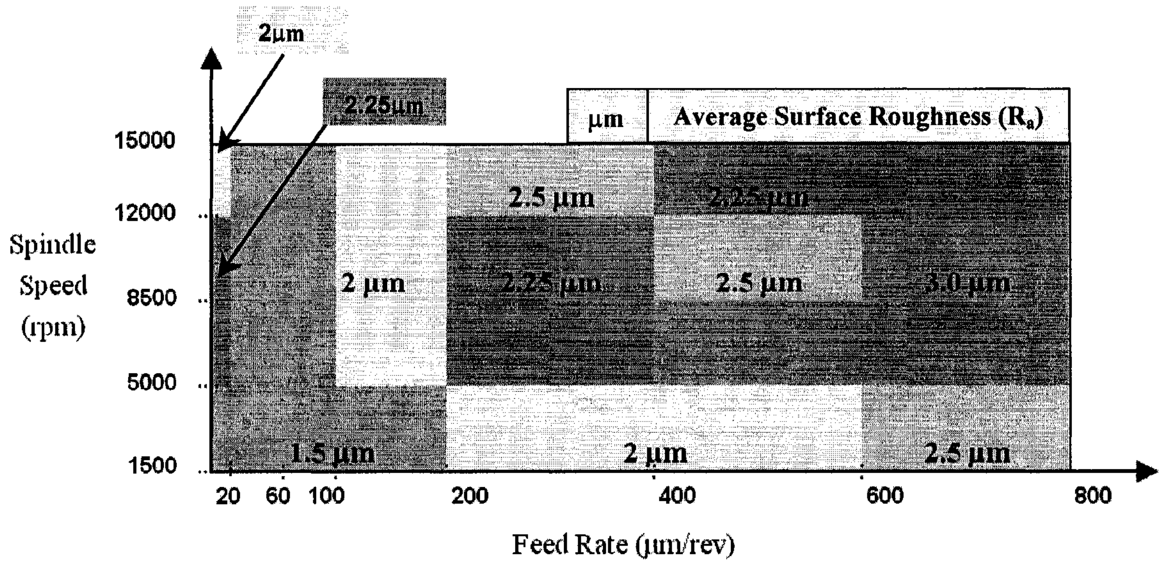

Figure 4.54: Machinability Map Showing the Effect of Spindle Speed and Feed Rate on Hole Surface Roughness (R_a)

4.3.5 Example of the Use of Machinability Maps

This section illustrates the methodology of superimposing different machinability maps to meet predefined hole quality objectives. For this example assume that the predefined objective criteria are: no delamination, maximum hole circularity error of 2.50%, maximum hole diameter error of -0.30% and maximum surface roughness of 2 μm. In order to identify the most optimal cutting conditions meeting all these objectives, each criterion is evaluated individually and then the maps are superimposed to achieve the optimum cutting conditions meeting all the objectives. For example, from the delamination machinability map, a maximum spindle speed of 15,000 rpm and feed rate up to 100 μm/rev can be selected from the machinability map for delamination (Figure 4.51) to meet the objective of no delamination. Similarly, the cutting conditions meeting other objective criteria are highlighted and superimposed, as shown in Figure 4.55, to achieve the most optimal cutting conditions meeting all the objectives in totality. In this example, as shown in Figure 4.55, spindle speed of 8,500 rpm and feed rate of 100 μm/rev are found to be the most optimal cutting conditions to meet the predefined objectives and to ensure maximum productivity.

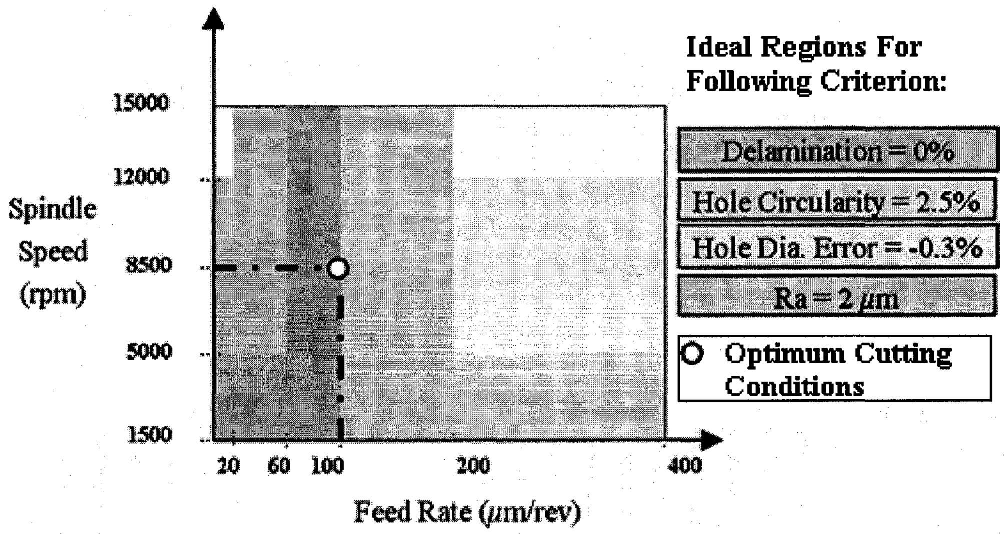

Figure 4.55: Machinability Map Showing the Methodology to Identify the Most Optimal Cutting Parameters Meeting Predefined Objective Criterion

4.4 Conclusions

This chapter presented in detail the results of the experimental work done for machinability assessment of woven graphite epoxy composite and the developed machinability maps for better process control. It was established that the forces and cutting temperature generated during drilling have strong physical significance in determining the machined hole quality. High speed drilling approach produced contrasting results as spindle speed of 15,000 rpm was found to reduce delamination damage and improve surface roughness but deteriorate the hole circularity and diameter. The machinability map concept was introduced and its use is demonstrated to achieve certain hole quality attributes while ensuring maximum productivity. Detailed conclusions have been presented in Chapter 6.

Chapter 5

Tool Wear Mechanisms and Their Effect on Hole Quality in High Speed Drilling

5.1 Introduction

This chapter discusses in detail the main results of experimental work done to assess tool wear of tungsten carbide (WC) drills during high speed machining of woven graphite epoxy composites. Section 5.2 of this chapter discusses the basic wear mechanisms observed during the course of tool wear assessment and analysis. In the section 5.3, the effect of progression of tool wear on delamination, hole quality attributes and productivity have been analyzed in detail.

5.2 Tool Wear Analysis

Machinability assessment of woven graphite epoxy composite laminate provided us the basic understanding about the interaction between the cutting parameters, forces, and temperatures. The knowledge of these interactions was used to design the machinability maps, as a tool to be used for process planning and control. However, since the cutting tool is subjected to severe rubbing with the abrasive graphite fibers, it was essential to establish the understanding of the wear behaviour of the WC drill, and consequently the impact of tool wear on hole quality and process productivity. To evaluate tool wear mechanisms, and its impact on hole quality attributes, the cutting conditions which gave maximum productivity with no delamination, were selected. These cutting conditions are as follows:

i. Spindle speed = 15,000 rpm, Feed rate = 100 μm/rev

ii. Spindle speed = 12,000 rpm, Feed rate = 100 μm/rev

The following section explains in detail the various wear mechanisms identified and their impact on hole quality.

5.2.1 Tool Wear Mechanisms

The standard point two-fluted twist drill is subjected to aggressive abrasive action in the presence of hard graphite fibers embedded inside the soft epoxy matrix. Owing to the inhomogeneous nature of composite laminate (soft matrix and hard graphite fibers), the cutting edges experience fluctuating chip load. This results in completely different wear characteristics of the WC drills when used for drilling woven graphite epoxy composites as compared to metals. The main mechanisms observed during high speed drilling were:

i. Chipping
ii. Abrasion
iii. Adhesion of burnt carbon

During the start of the drilling process chipping was observed at the following locations on the drill:

i. The rake face relieved along the chisel edge (Figure 5.1(a))
ii. The rake face of the cutting edge (Figure 5.1(b))
iii. The corner of the drill and secondary cutting edges (Figure 5.1(c))

The chipping at the corner, the rake face of primary cutting edge, and the secondary cutting edge occurred during the start of drilling, when the edges were sharp and the stresses were high. Tungsten carbide, being brittle in nature, is unable to sustain these high stresses and thus undergoes chipping. Figures 5.1 (a), (b), and (c) illustrate the chipping mechanisms observed during the course of tool wear study at 15,000 rpm. The crater and cracks created because of chipping were found to worn away with increase in wear during continuous drilling.

During the cutting process, abrasion was found to occur mainly on the rake and flank face of the cutting edge of WC drill similar to those observed in [48]. Figures 5.2 (a) and (b) illustrate the abrasive wear observed at the flank and the rake face of the cutting edge, respectively. For the case of drilling woven composite, abrasive wear was found to be more severe on the flank face of the two primary cutting edges. This could be because of the type of chips produced during drilling of epoxy based composites. Unlike metals, where the chips are continuous, segmental, or discontinuous, machining of thermoset composites generates chips mostly in the form of powder or flakes. The types of chips generated during 1,500 and 15,000 rpm, and 20 and 800 μm/rev have been shown in detail in Appendix 3. The powdery chips formed at low feed rates and high spindle speeds rub against the flank face, which is in constant contact with the laminate during drilling of the hole, and thus cause an abrasive action resulting in wear. The presence of fine powdery chips between the cutting edges and the abrasive graphite fibers could results in "three-body" abrasive wear mechanism, where the loose fine graphite coated epoxy chips cause abrasion of both the tool and the hole surface. Moreover, due to the powdery form the mobility of the chips increases as it moves along the drill flutes, and as a result the abrasive action on the rake face is not as aggressive as on the flank face.

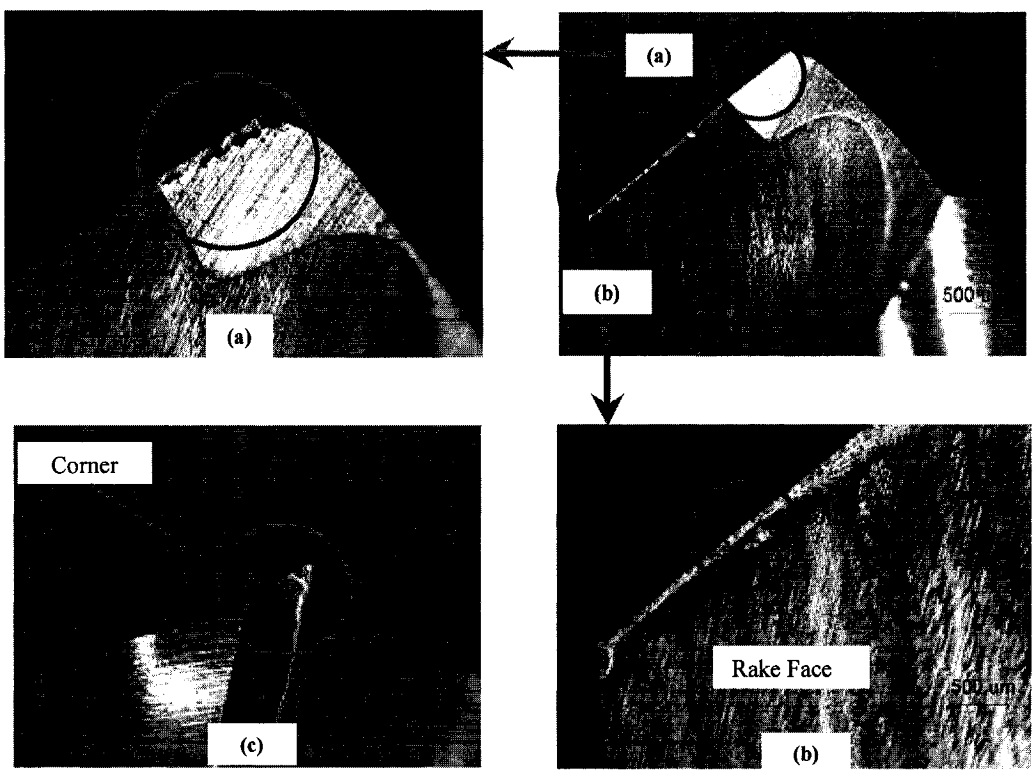

Figure 5.1: Wear mechanisms of the Drill Bit during High Speed Drilling (15,000 rpm) and Low Feed Rate of 100 μm/rev (a) Chipping on the Rake Face along the Chisel Edge after Drilling of 10 holes (b) Chipping on the Rake Face after Drilling of 100 holes (c) Chipping at the Corner and Margin of the Drill after Drilling of 50 holes

Further, it was found that with continuous drilling the heat built up on the tool resulted in melting and subsequent burning of the epoxy. Carbon residues of the burnt epoxy were found adhered to secondary clearance on the rake face as shown in Figure 5.2 (a).

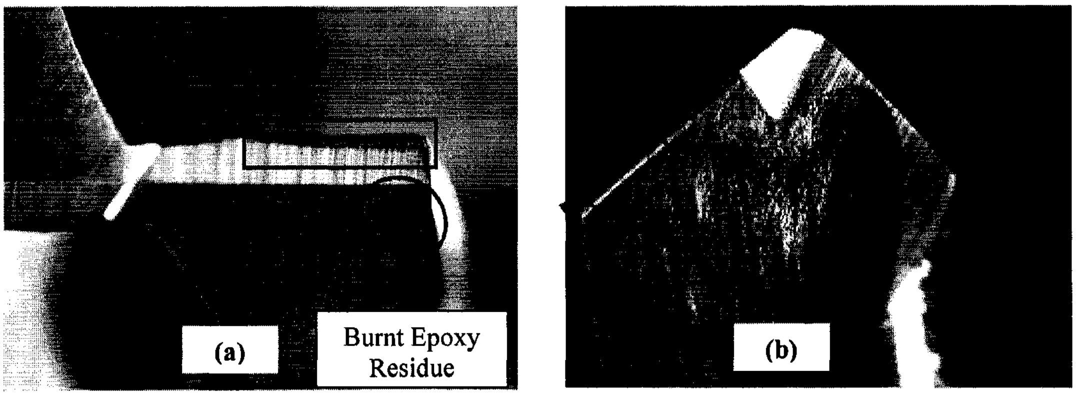

Figure 5.2: Abrasive Wear Mechanism of the Drill along the Flank and Rake Face of the Drill during High Speed Drilling (12,000-15,000 rpm) and Low Feed Rate of 100 μm/rev. (a) Flank Wear and Burnt Epoxy Residue after Drilling of 650 holes at Spindle Speed of 12,000 rpm (b) Rake Face Wear after 544 holes during Drilling at Spindle Speed of 15,000 rpm

5.2.2 Tool Wear Analysis at Spindle Speed of 12,000 rpm (188.5 m/min) & 15,000 rpm (235.6 m/min) and Feed Rate of 100 μm/rev

Flank wear was found to be the dominant tool wear mechanism at high spindle speeds of 12,000 and 15,000 rpm, and low feed rate of 100 μm/rev. It is the most common type of tool wear, and is governed by the abrasive wear mechanism. Since it is unavoidable, in most cases, one has to maintain safe progressive flank wear. The progression, however, is not uniform and has been found to occur in stages. Figure 5.3 shows the three regions of flank wear [5]. These regions are explained as below:

(A) Initial (or preliminary) Wear Region: This region is caused by micro-cracking, surface oxidation and carbon loss at the cutting tool tip. During the start of drilling the new cutting edges having sharp corner radius are subjected to small chip contact area. As a result the cutting edges are under high contact pressure, which result in high wear rate. In the initial wear regime the system behaves as a heavily loaded system, since the real contact is a fraction of the actual contact in this region.

(B) Steady Wear Region: After the initial wear or cutting edge rounding, the micro-roughness gets improved in this region, and the wear size becomes proportional to the cutting time. Here the increase in the area of contact between the tool and workpiece results in lower contact stresses. The system therefore acts as lightly loaded system, resulting in more uniform contact stress, and a constant wear rate.

(C) Severe (or ultimate or catastrophic) Wear Region: When the wear size increases to a critical value, the surface roughness of the machined surface decreases, the cutting force and temperature increases rapidly, and as a result the wear rate increases further. In this region the hardness of the tool is reduced and as a result the system behaves as heavily loaded, and eventually the wear rate increases rapidly.

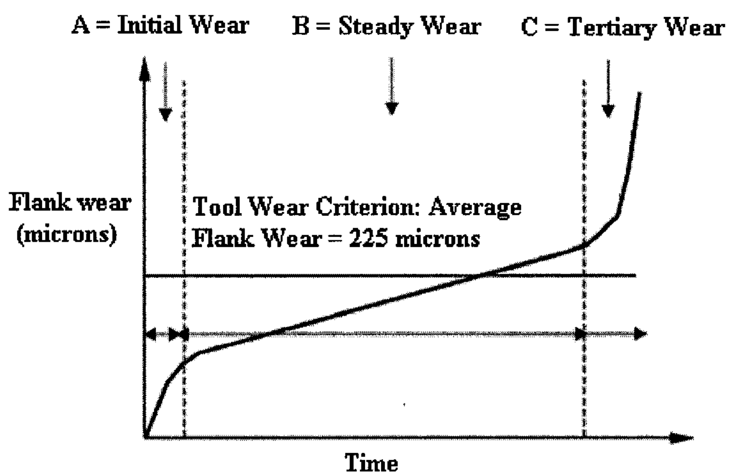

Figure 5.3: Variation of Flank Wear Rate with Cutting Time, Showing the Initial Wear (Heavily Loaded Regime), Steady Wear (Lightly Loaded Regime) and Severe Wear Zone (Heavily Loaded Regime) [62]

The three regions discussed above were evident during the drilling of woven graphite fiber epoxy composites with WC drills. Figures 5.4 and 5.5 illustrate the progression of flank wear "V_b" during high speed drilling at 12,000 and 15,000 rpm, respectively, clearly showing the three distinct regimes. A comparison between the two flank wear progression curves indicates higher wear rate at higher spindle speed of 15,000 rpm as compared to 12,000 rpm. An average flank wear of 300 μm was chosen as the end of tool life criterion, as per ASTM standards for tool wear [56]. However, during the course of experimentation it was observed that high level of delamination and hole geometry errors occurred as the wear progressed to the tertiary zone. So it was decided to stop the experiments, when the average flank wear reached a value of 225 μm.

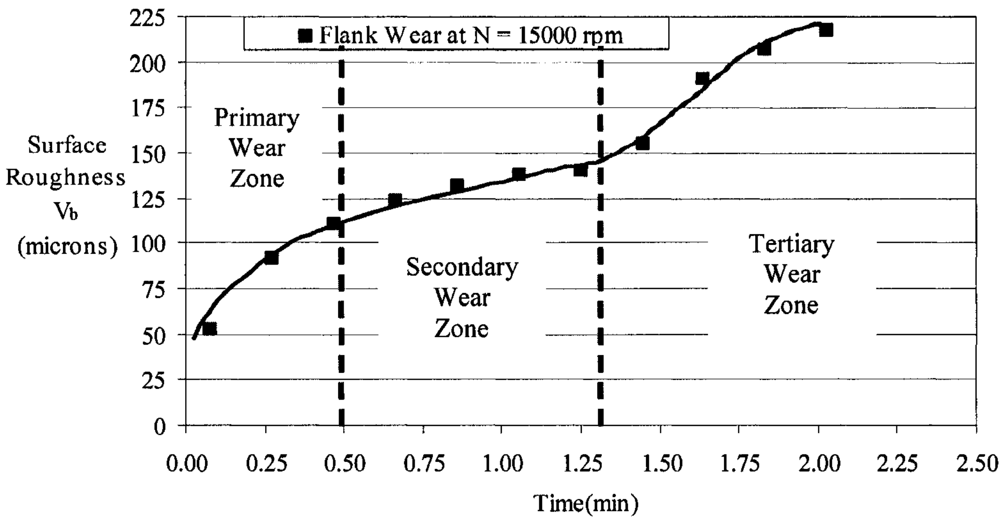

Figure 5.4: Progression of Flank Wear during Drilling at Spindle Speed of 15,000 rpm and Feed Rate of 100 μm/rev

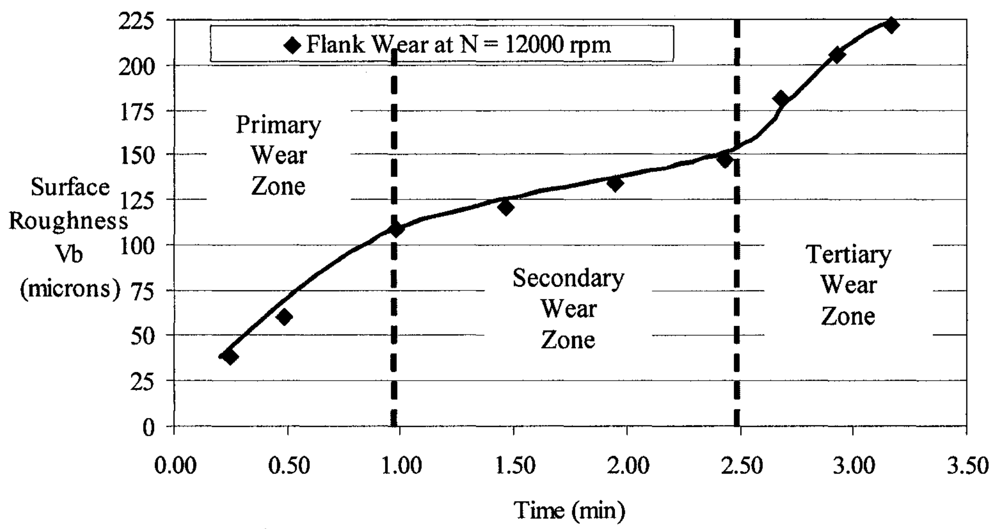

Figure 5.5: Progression of Flank Wear during Drilling at Spindle Speed of 12,000 rpm and Feed Rate of 100 μm/rev

The main findings about the flank wear regimes / zones, at high drilling speeds of 12,000 and 15,000 rpm, are as follows:

i. The primary wear zone at spindle speed N = 15,000 rpm lasted up to 0.5 min, which was equivalent to about 102 holes drilled at 100 μm/rev, with individual hole depth of 5.9 mm. This is equivalent to a total of 0.6 meters of depth of cut. However, at a lower spindle speed of 12,000 rpm the primary wear zone lasted up to 0.98 min, which was equivalent to 200 holes drilled, or in total 1.19 meters of length of cut. Owing to the fact that this wear zone is a heavily loaded system, chipping of the primary cutting edges, secondary cutting edges, and corners were observed in this zone. The various chipping damages observed have already been illustrated in Figure 5.1.

ii. The secondary wear zone at spindle speed of 15,000 rpm lasted up to 1.35 min, which was equivalent to about 275 drilled holes or 1.62 meters of total drilled length. At a lower spindle speed of 12,000 rpm, the secondary wear regime lasted up to 2.5 min, which is equivalent to about 512 drilled holes, or 3.02 meters of total drilled length. In this regime, the tool encountered abrasive wear. An abrasive wear rate of 38.60 x 10^{-6} meter/sec (depth of average flank wear per unit time) was observed at higher speed of 15,000 rpm as compared to 26.30 x 10^{-6} meter/sec observed at spindle speed of 12,000 rpm. The high wear rate observed at higher speed of 15,000 rpm can be seen from the comparison of Figure 5.4 and Figure 5.5.

iii. In the tertiary zone, the wear rate increased as the wear regime moved from lightly loaded, in the secondary wear zone, to heavily loaded wear regime in the tertiary wear zone. This was due to higher surface roughness, and thus aggressive abrasion. The end of tool life at 15,000 rpm occurred at about 2.12 min, which was equivalent to a total of 544 drilled holes or 3.2 meters of total drilled length. At lower spindle speed of 12,000 rpm, end of tool life, i.e, V_B = 225 μm, was reached at about 3.17 min, which was equivalent to about 650 drilled holes or 3.8 meters of total drilled length. The SEM images in Figures 5.6 (a) - (f) illustrate the end of tool life condition after drilling 544 holes at spindle speed of 15,000 rpm. These SEM images show extensive abrasive wear at the chisel edge as shown in Figure 5.6 (a) and (b), primary cutting edge as shown in Figure 5.6 (c) and (d), the corners as shown in Figure 5.6 (e) and the secondary cutting edge as shown in Figure 5.6 (f)

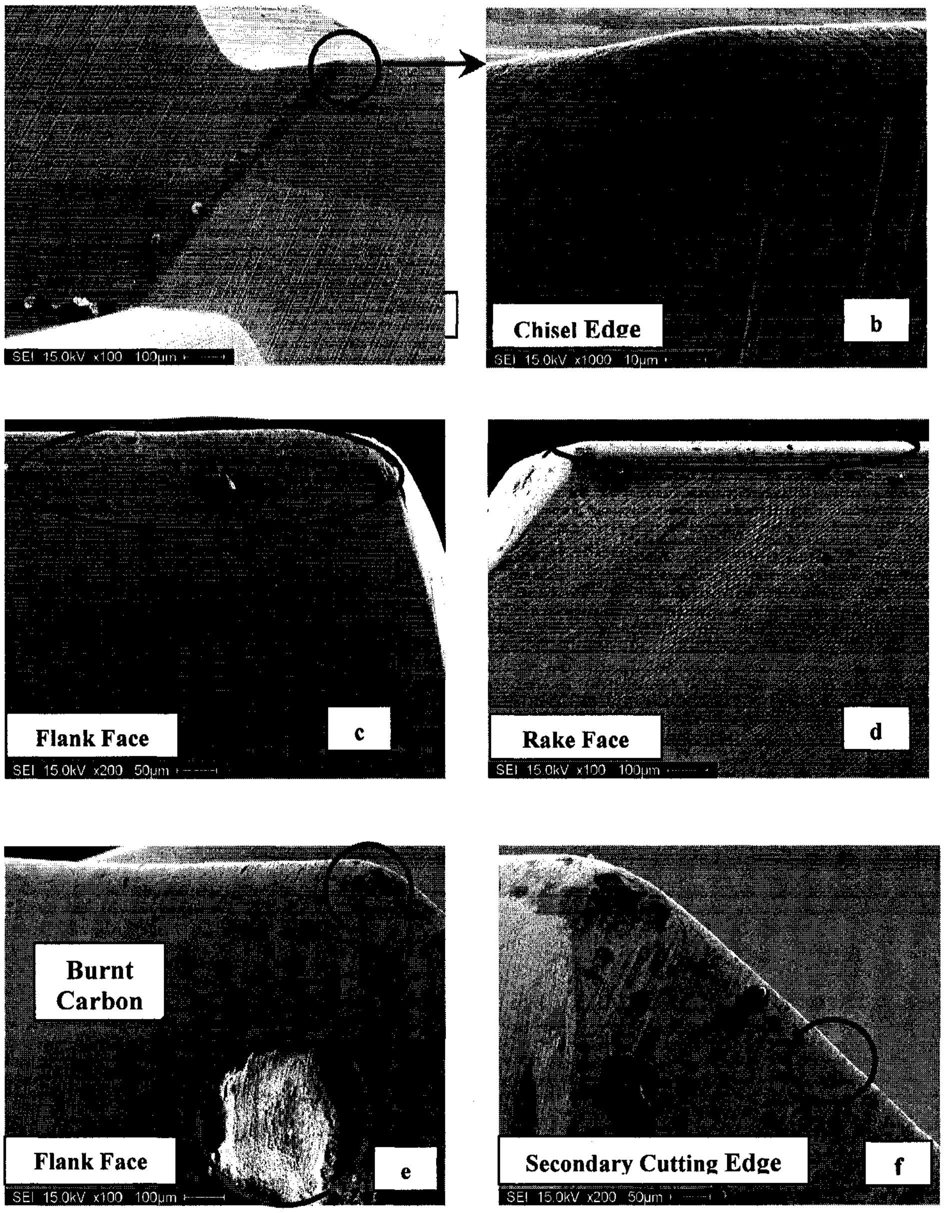

Figure 5.6: SEM Images of Wear Mechanism Observed during Drilling at Spindle Speed of 15,000 rpm and Feed Rate of 100 µm/rev. (a) Chisel Edge Wear, (b) Rounding of Chisel Edge Corner, (c) Flank Wear on the Primary Cutting Edge, (d) Rake Face Wear, (e) Carbon Deposition on the Rake Face and Corner and (f) Wear at the Secondary Cutting edge. The Encircled Areas Represent the Worn Sections in each Image

iv. Owing to higher spindle speed of 15,000 rpm, the abrasive action of graphite fibers on WC drill was more aggressive, and thus resulted in higher wear rate at 15,000 rpm as compared to 12,000 rpm. Also, large quantity of carbon deposits was found on the flank face of the primary cutting edge and the secondary cutting edge. Figure 5.6 (e) illustrates the adherence of carbon i.e. burnt epoxy on the flank face and corner of drill during the continuous drilling process. The chemical analysis performed at the flank face confirmed the adhesion of carbon, as shown in Figure 5.7. In this tool wear study, the high cutting temperature obtained at higher spindle speed of 15,000 rpm coupled with high flank wear was responsible for burning of epoxy.

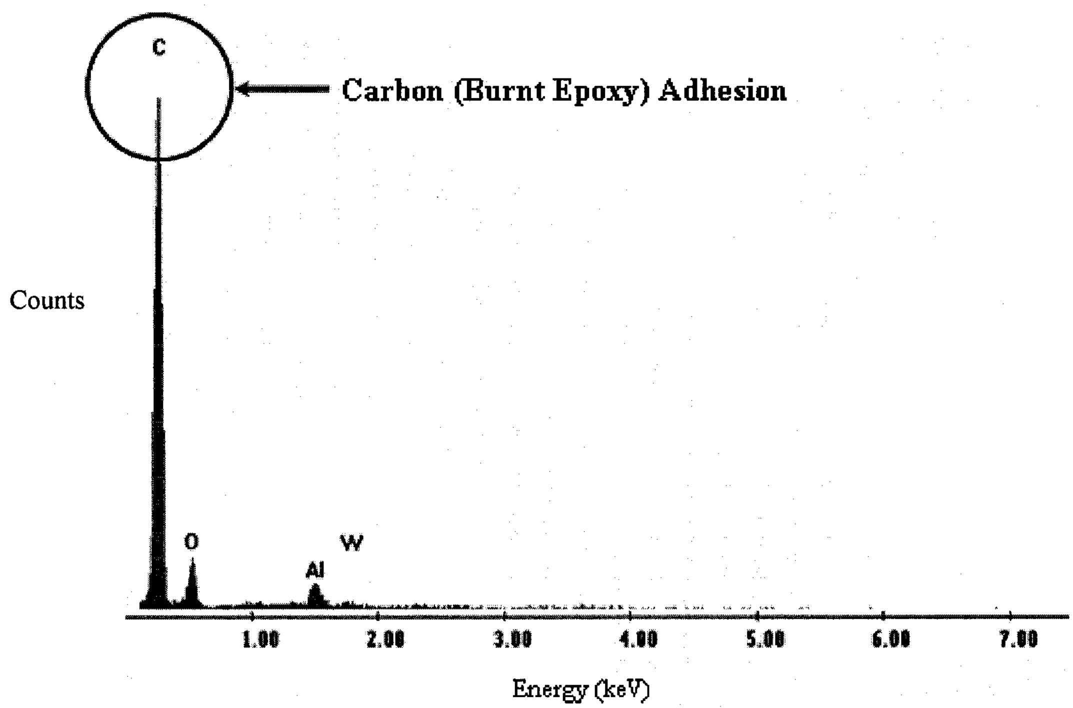

Figure 5.7: Chemical Analysis of Tool Rake Face (shown in Figure 5.61 (e)) of the Drill used at Spindle Speed of 15,000 rpm and Feed Rate of 100 μm/rev, by Using Energy Dispersive Spectrometer during SEM Imaging

The results of the two tool wear experiments were used to establish the relationship between the cutting velocity "V in meter/minute" and the tool life "T in minutes", as proposed by Taylor [5]. The relationship obtained, for the woven graphite epoxy laminate and WC drill used in this research, is given by equation (5.1).

$$VT^{0.56} = 3.08 \tag{5.1}$$

This relationship shows an inverse relation between the cutting velocity and the tool life as observed in the experiments. Similar inverse relationship was found in [44]. This relationship (equation 5.1) can be used to identify the tool life at different cutting speeds and fixed feed rate of 100 μm/rev.

Having established the various mechanisms of tool wear, and the progression of flank wear with time during continuous drilling process, it was necessary to analyze the effect of tool wear on surface delamination and hole quality attributes, namely, hole circularity, hole diameter error, and surface roughness. The following section explains in detail the analysis done for the two investigated speeds of 12,000 rpm and 15,000 rpm.

5.2.3 Effect of tool wear on delamination of composite laminate

5.2.3.1 Effect of tool wear on Entry Delamination

Delamination at the hole entry and exit, was found to increase with the increase in flank wear. Figures 5.8 and 5.9 show the increase of delamination at entry with the progression in flank wear. It is seen that as the flank wear increases the cutting force (F_c) also increases. As a result, the entry delamination increases progressively, resulting in higher delamination at the hole entry. Figure 5.10 shows the entry delamination at the end of tool life (average V_b = 225 μm) for both spindle speeds. Similar results have been reported in [50]. A comparison between the entry delamination and cutting forces at 15,000 rpm (Figure 5.8) and 12,000 rpm (Figure 5.9) revealed lower delamination and cutting forces at higher spindle speed of 15,000 rpm. The reduction in cutting forces at higher spindle speeds is attributed to thermal softening effect, as discussed in section 4.2.2.

At spindle speed of 12,000 rpm, the progression in cutting force and delamination strongly followed the three wear transition zones as shown in Figure 5.9. The cutting force increased rapidly in the tertiary wear zone, and thus resulted in sharp increase in entry delamination. However, the cutting force and entry delamination were found to lag from the start of tertiary zone in case of higher spindle speed of 15,000 rpm as shown in Figure 5.8. In spite of this lag, there still existed a strong correlation between the thrust force and entry delamination.

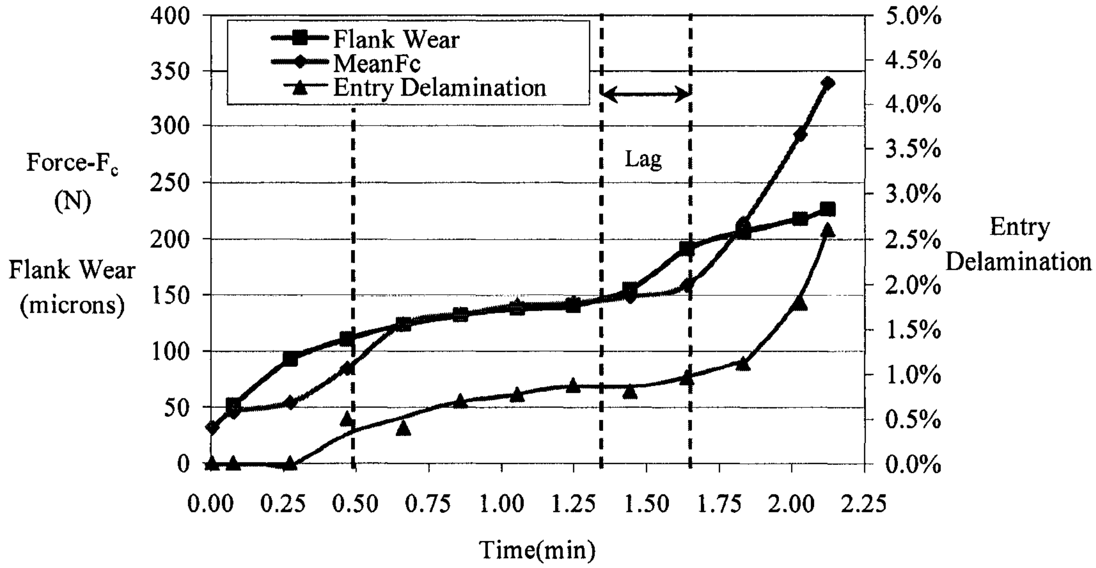

Figure 5.8: Flank Wear and its Effect on Hole Entry Delamination at Spindle Speed of 15,000 rpm and Feed Rate of 100 μm/rev

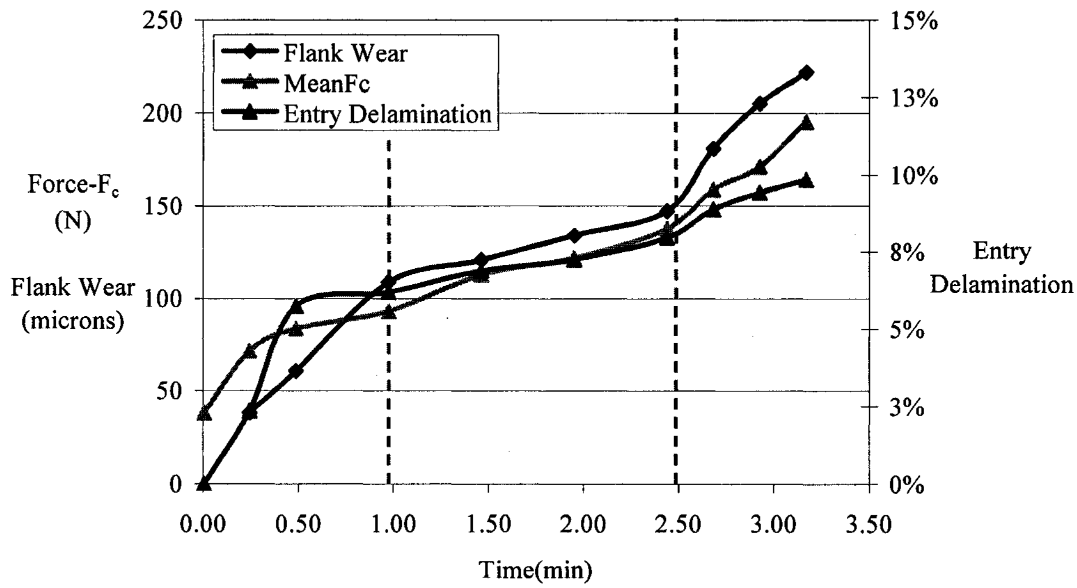

Figure 5.9: Flank Wear and its Effect on Entry Delamination at Spindle Speed of 12,000 rpm and Feed Rate of 100 μm/rev

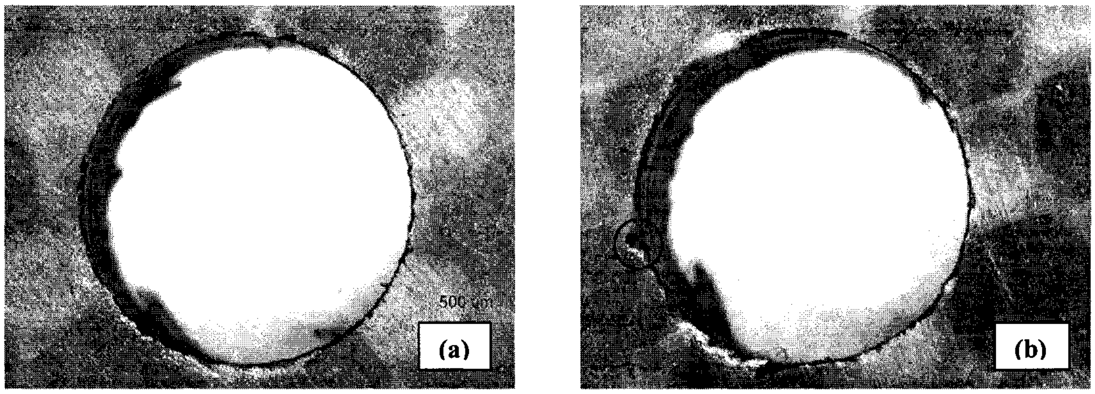

Figure 5.10: Entry Delamination and Hole Circularity at End of Tool Life, i.e., Average Flank Wear = 225 μm for (a) Spindle Speed of 15,000 rpm and Feed Rate of 100 μm/rev (b) Spindle Speed of 12,000 rpm and Feed rate of 100 μm/rev

5.2.3.2 Effect of tool wear on Exit Delamination

Exit or push out delamination showed similar trend as entry delamination. Figures 5.11 and 5.12 show in detail the progression of flank wear, and its effect on thrust force (F_z) and exit delamination at spindle speed of 15,000 and 12,000 rpm, respectively. It is observed that the steady increasing wear rate in the primary and the tertiary wear zone strongly influenced the thrust force, which in turn caused higher delamination. At spindle speed of 12,000 rpm, the thrust force and resulting delamination were found to follow the wear transition zones, as shown in Figure 5.12. Both the forces and delamination increased steadily with rapid increase in flank wear in the primary and the tertiary wear zones. Finally, an exit delamination of about 27% was obtained at the end of tool life. At spindle speed of 15,000 rpm, no delamination was found to occur up to a critical thrust force of 70 N, which was found to be close to the critical thrust force of 62 N obtained in section 4.2.5.2. Beyond 70 N, the delamination increased rapidly in the primary wear zone. The rate of delamination was found to be steady, and followed the flank wear rate in the secondary wear zone. Further, in the tertiary wear zone the delamination increased rapidly reaching a maximum of 30% at the end of tool life. Figure 5.13 (a) and (b) show the exit delamination observed at the end of tool life in the two cases, i.e., at spindle speeds of 15,000 and 12,000 rpm, respectively. Exit delamination of about 30% and 27% were found to occur due to thrust forces of 200 N and 250 N, respectively. Owing to abrasive wear of drill these exit delaminations were, however, more as compared to the delamination obtained for a sharp drill for same magnitude of thrust force, as shown in Figure 4.29. This highlights the importance of monitoring tool wear as it was found to change the delamination characteristics for the same magnitude of thrust force.

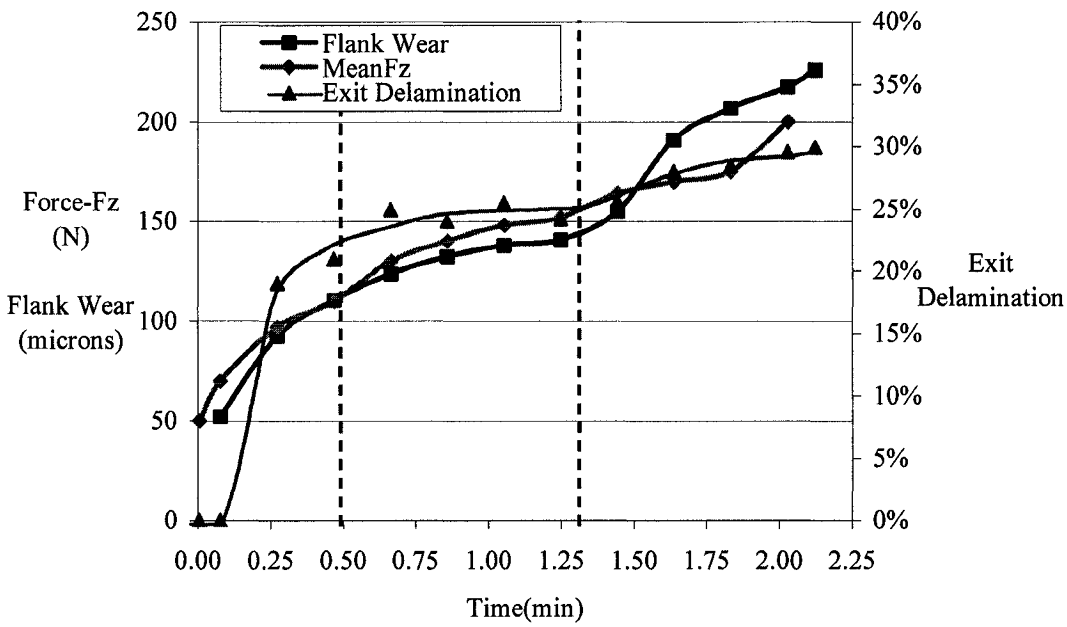

Figure 5.11: Flank Wear and its Effect on Hole Exit Delamination at Spindle Speed of 15,000 rpm and Feed Rate of 100 μm/rev

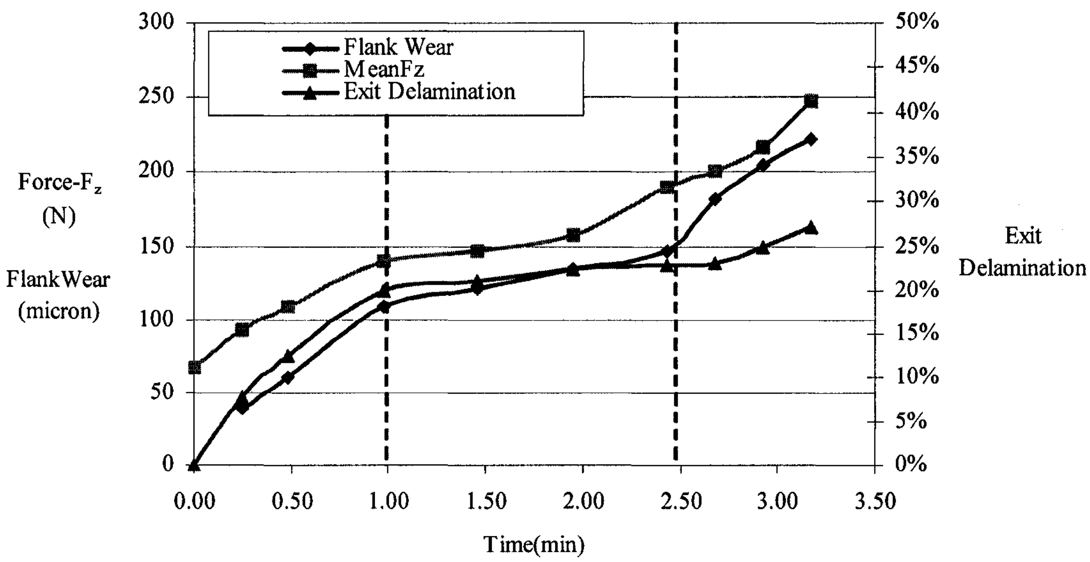

Figure 5.12: Flank Wear and its Effect on Exit Delamination at Spindle Speed of 12,000 rpm and Feed Rate of 100 μm/rev

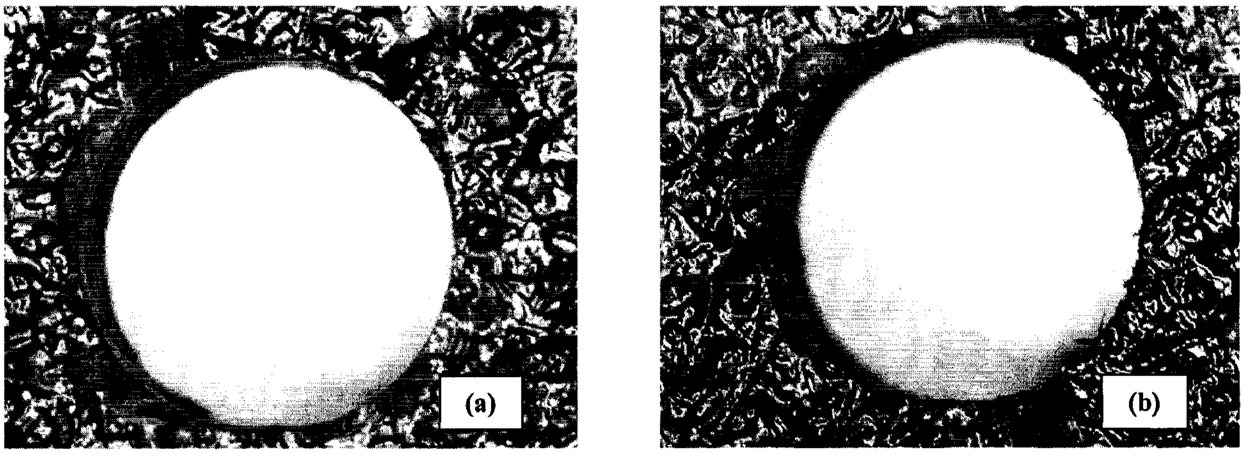

Figure 5.13: Exit delamination at End of Tool Life i.e. Average Flank Wear = 225 μm at (a) Spindle Speed of 15,000 rpm and (b) Spindle Speed of 12,000 rpm and common Feed Rate of 100 μm/rev

5.2.4 Effect of Tool Wear on Hole Circularity Error

Hole circularity error was found to increase with the increase in flank wear at both the investigated spindle speeds of 12,000 and 15,000 rpm. Figures 5.14 and 5.15 illustrate the effect of increasing flank wear on hole entrance circularity. It is evident from the figures that the hole circularity deteriorated progressively with increase in wear rate. The increase in hole circularity error was associated with the increase in thrust force due to the increase in flank wear as shown in Figures 5.14 and 5.15. At spindle speed of 15,000 rpm, a hole circularity error of 0.17% was obtained, while at spindle speed of 12,000 rpm an error of 0.19% was found to occur at the end of tool life. A comparison between the two spindle speeds revealed poor hole circularity of similar magnitude in both cases. However, the rate of increase of thrust force was higher in the case of higher spindle speed of 15,000 rpm, primarily due to higher wear rate. Figures 5.10 (a) and (b) show the evidence of poor hole circularity at the end of tool life for spindle speeds of 15,000 and 12,000 rpm, respectively.

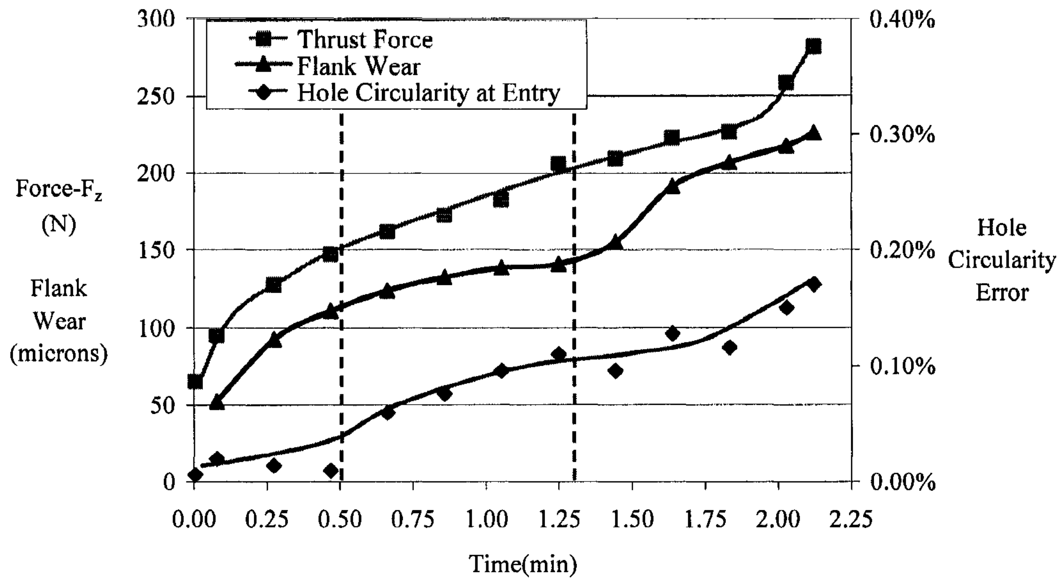

Figure 5.14: Flank Wear and its Effect on Hole Entry Circularity Error at Entry at Spindle Speed of 15,000 rpm and Feed Rate of 100 μm/rev

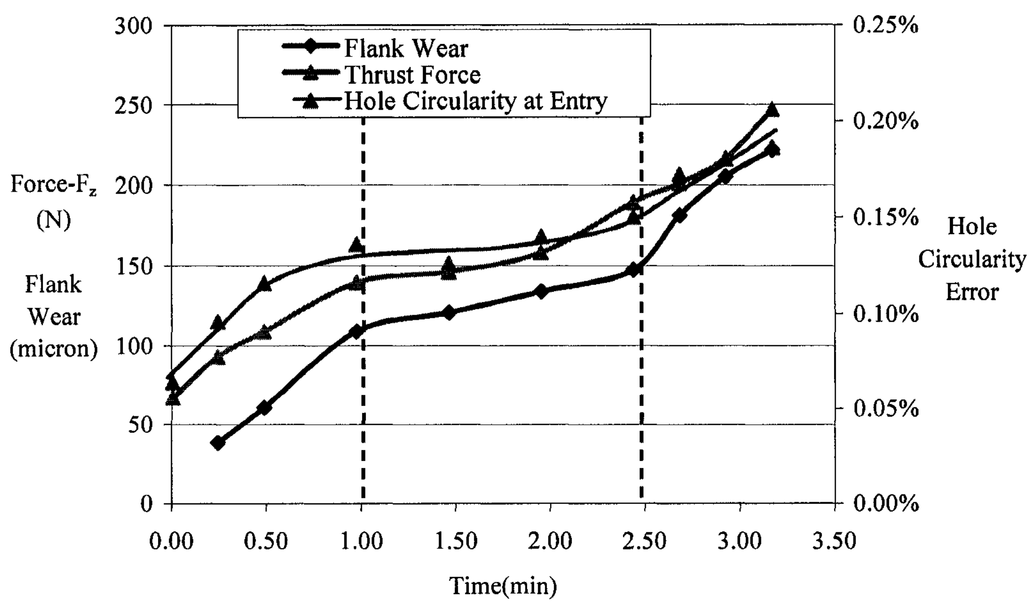

Figure 5.15: Flank Wear and its Effect on Hole Entry Circularity Error at Spindle Speed of 12,000 rpm and Feed Rate of 100 μm/rev

5.2.5 Effect of Tool Wear on Hole Diameter Error at Entrance

During the continuous drilling process, tool flank wear was found to occur at a faster rate in the primary and the tertiary wear zone, while in the secondary wear zone a steady wear rate was observed as shown in Figure 5.16. This flank wear was found to strongly influence the hole diameter at entry. At the start of drilling when the tool is sharp, the holes produced were oversized in the range of 0.08 - 0.12%, similar to the oversize effect observed for spindle speed of 15,000 rpm during machinability assessment in section 4.2.7 and illustrated in Figure 4.43. However, the magnitude of the hole oversize decreased with progression in flank wear in the primary wear zone. Beyond the primary wear zone, only undersized holes were produced due to increasing flank wear. Similar response was reported in [47, 49, 50], wherein during the assessment of coated HSS and tungsten carbide drills, out of tolerance holes were produced with the increase in flank wear. Figures 5.16 and 5.17 illustrate the decrease in hole diameter with the increase in flank wear for spindle speeds of 15,000 and 12,000 rpm, respectively. In both cases it is observed that the decrease in hole diameter closely followed the progression of flank wear with the hole undersize increasing rapidly to about 0.20% at the end of tool life in the tertiary wear zone.

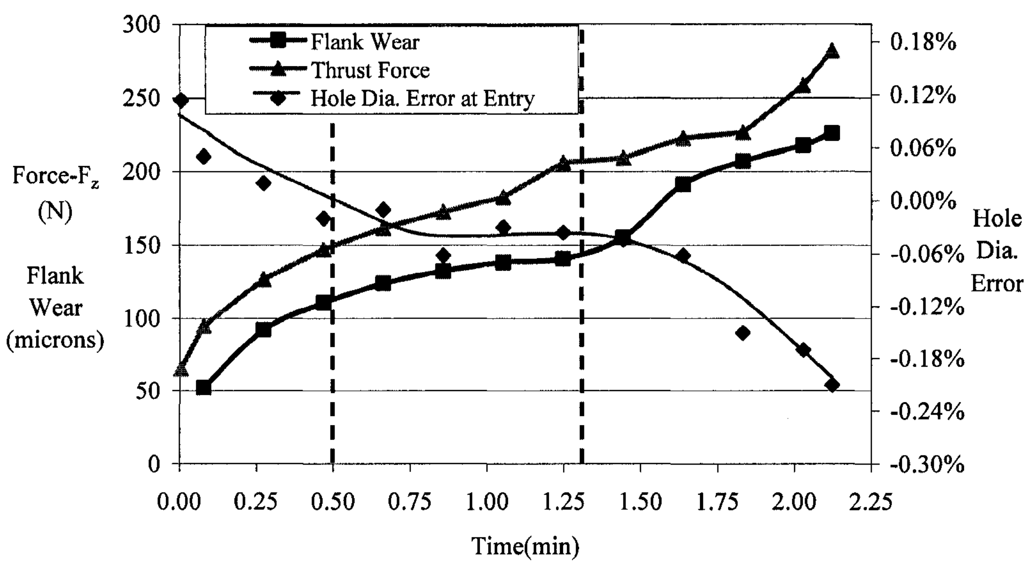

Figure 5.16: Flank Wear and its Effect on Hole Diameter Error at Entry at Spindle Speed of 15,000 rpm and Feed Rate of 100 μm/rev

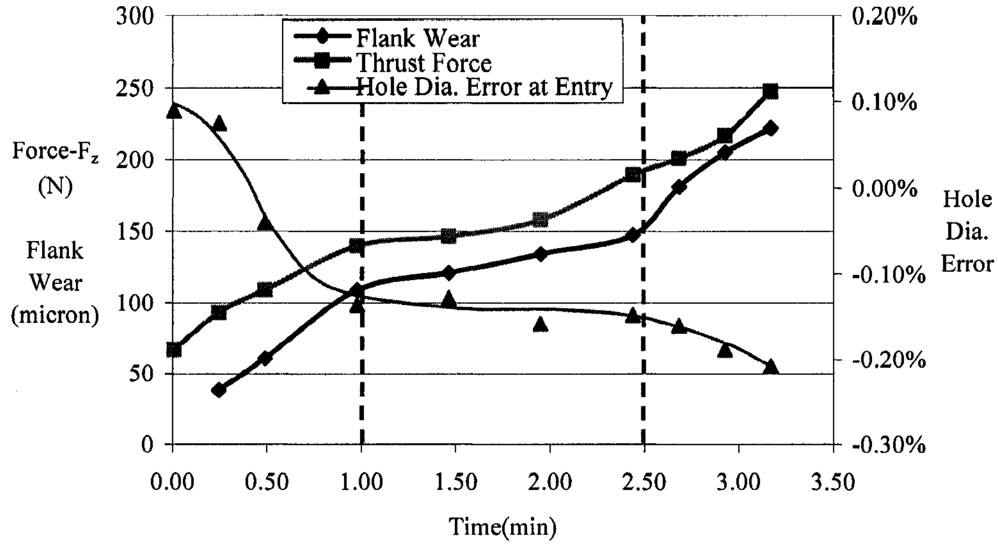

Figure 5.17: Flank Wear and its Effect on Hole diameter Error at Entry at Spindle Speed of 12,000 rpm and Feed Rate of 100 μm/rev

5.2.6 Effect of Tool Wear on Hole Surface Roughness

Hole surface roughness (R_a) was found to increase with the increase in number of drilled holes. This was found to be in agreement with [29]. As indicated earlier in section 5.1.1, at the start of drilling, primary cutting edges, secondary cutting edges and chisel edge of the WC drill experienced chipping at the sharp corners. The initial chipping combined with increasing flank wear resulted in increase in both the thrust and the cutting force. The increasing thrust force resulted in micro-cracks at the ply interfaces, while the increasing cutting force resulted in extensive fiber full out, thus deteriorating the surface finish. Figure 5.18 illustrates the increase in forces with increase in flank wear, which in turn increased the hole surface roughness. The surface roughness deteriorated from about 1.14 μm to 2.0 μm in the primary wear zone (flank wear "V_b" = 111 μm at about 0.5 min), to about 5.0 μm at the end of secondary wear zone (flank wear "V_b" = 141 μm at about 1.3 min) and finally to about 8.00 μm at the end of tool life (flank wear "V_b" = 226 μm at about 2.12 min). The deterioration of surface roughness showed a strong correlation with the progression of flank wear and the three friction regimes.

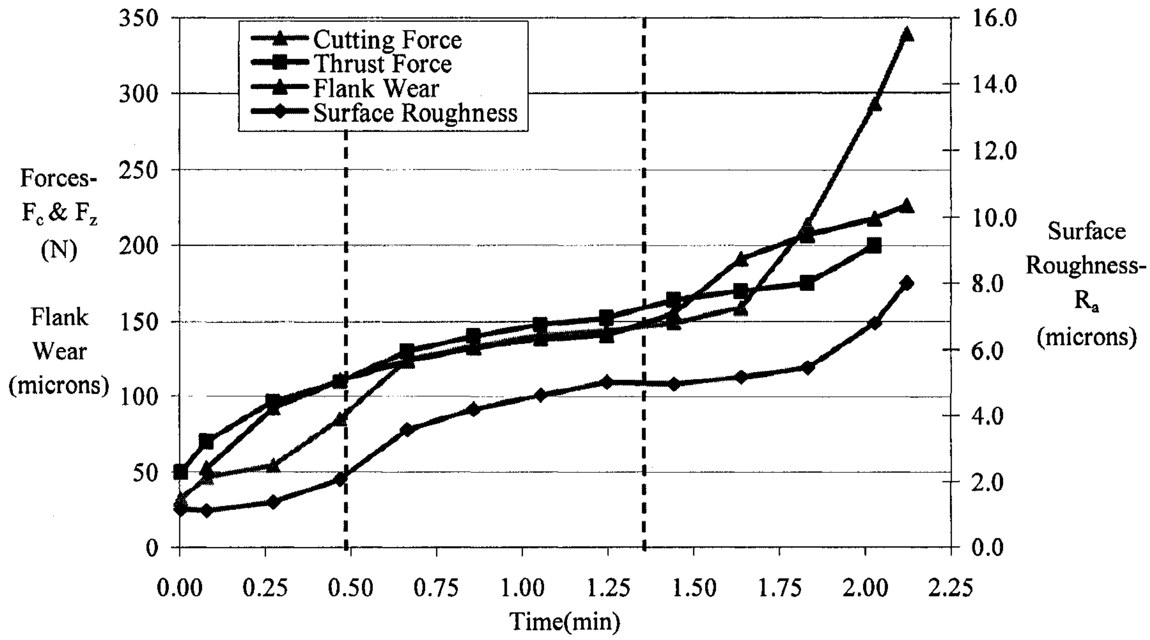

Figure 5.18: Flank Wear and its Effect on Hole Surface Finish and Forces at Spindle Speed of 15,000 rpm and Feed Rate of 100 μm/rev

Figures 5.19 (a), (b) and (c) illustrate the effect of increasing flank wear on surface integrity at spindle speed of 15,000 rpm. The valley void volume of the surface (S_v), which was explained in detail in section 1.10.1.3, has been evaluated using 3-D surface profile measurement. It is evident from these 3-D surface scans that a progressive increase in the value of valley void volume of the surface, i.e., "S_v" occurred with increase in flank wear. Valley void volume of the surface, which is representative of the void content, was found to increase from an initial value of 94 μm at the start of drilling to 197 μm at the end of tool life (i.e. average flank wear V_b = 225 μm). Thus the increase in "S_v" value corroborates the deteriorating effect of increasing forces in causing high density micro cracks and fiber pull outs, and thus deteriorating the hole surface roughness with increase in flank wear during continuous high speed drilling.

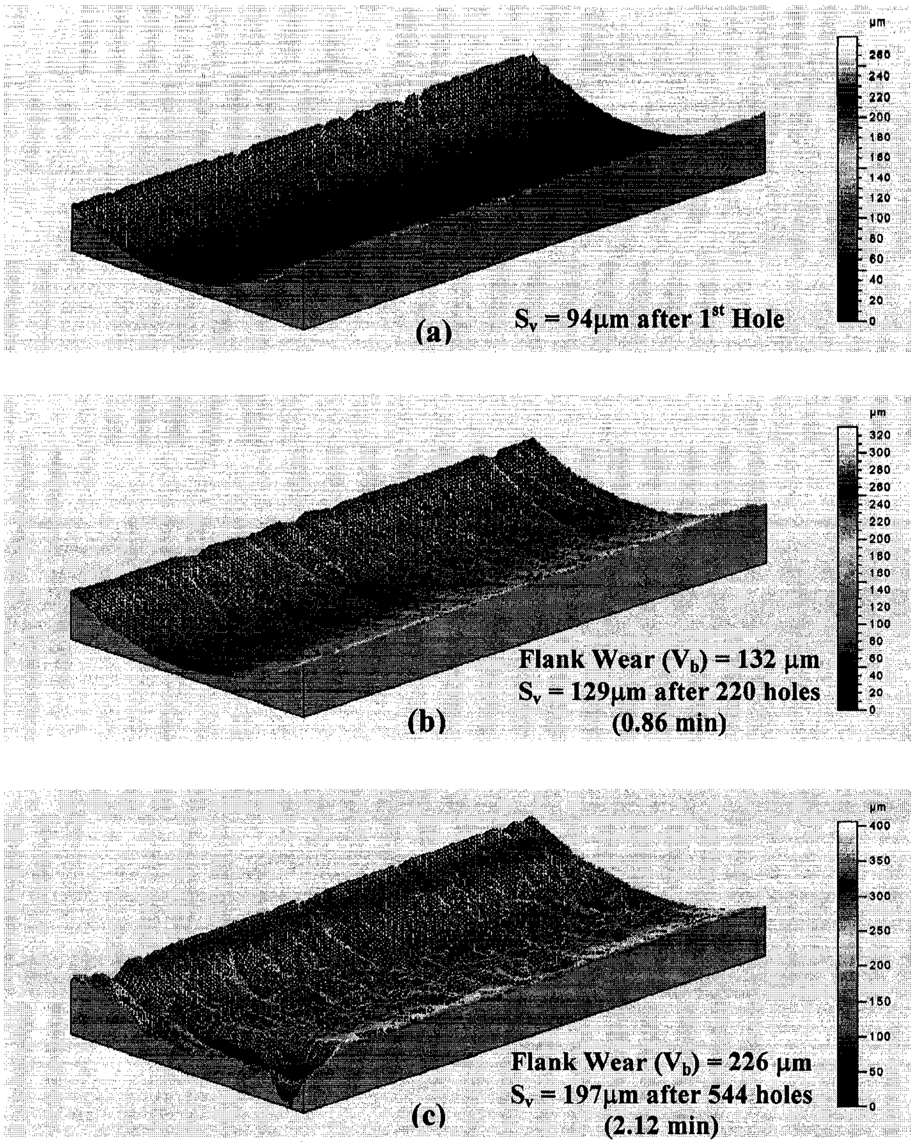

Figure 5.19: Effect of Flank Wear on Valley Void Volume of the Surface, i.e., "Sv" at Spindle Speed of 15,000 rpm and Feed Rate of 100 µm/rev

5.3 Conclusions

This chapter presented in detail the results of the experimental work done for the assessment of tool wear during high speed (12,000 rpm and 15,000 rpm) and low feed (100 µm/rev) drilling. Tool wear mechanisms and the effect of tool wear on hole quality has been analyzed in depth.

Chapter 6

Conclusions and Recommendations for Future Work

6.1 Conclusions

The machinability of woven graphite epoxy composite laminates during conventional drilling with standard point tungsten carbide drills has been evaluated. The high speed machining approach, which was not addressed in the literature, has been investigated and analyzed in detail in this work. The study was carried out to cover a wide range of spindle speeds (1,500 -15,000 rpm) and feed rates (20-800 μm/rev) and assess their effect on the composite laminate. Key damage mechanisms such as hole entry and exit delamination, fiber pull out, matrix burnout, interlaminar delamination at ply interfaces and geometrical errors in hole circularity and diameter, have been identified and characterized for the different cutting conditions.

The composite drilling process has been described using a physics-based approach of measuring the process influencing intermediate variables i.e. the forces, cutting temperature and tool wear for a range of drilling parameters, and analyzing their effect on hole quality attributes. During the machinability assessment, it was established that the forces and cutting temperature generated during drilling have strong effect on quality of the drilled hole. Having established the significance of these intermediate process variables with desired hole quality attributes, namely, surface delamination, hole circularity error, hole diameter error and surface roughness, the process can be controlled by monitoring the intermediate process variables and thus changing the input parameters to achieve predefined hole quality. Figure 6.1 illustrates this approach in detail.

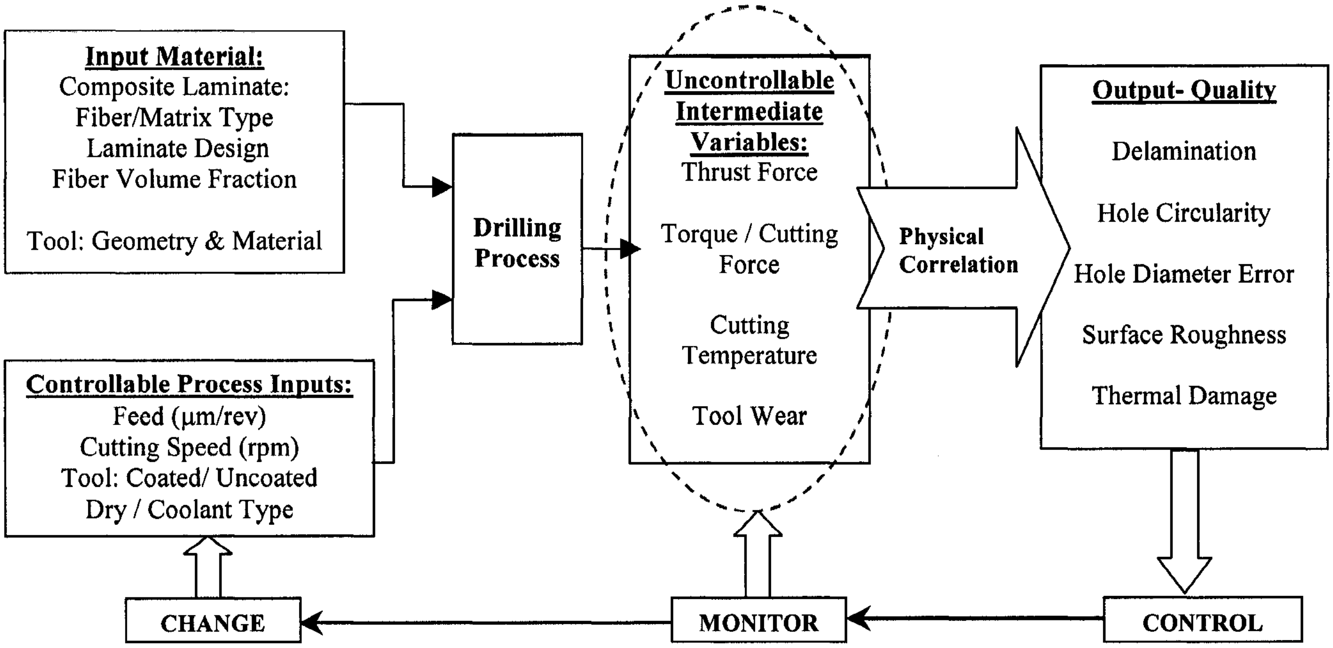

Figure 6.1: An Approach for Damage Control during Drilling of Woven Composites

In high speed drilling regime contrasting results were obtained. The spindle speed of 15,000 rpm was found to reduce delamination damage and improve surface roughness but increase the hole circularity and diameter errors. Finally, it was concluded that the process productivity could be increased and delamination be minimized in the range of 0-25% by increasing the spindle speed up to 15,000 rpm, controlling the feed rate in the range of 60-100 μm/rev and compromising the tolerances of hole quality attributes as illustrated below:

0 % < Hole circularity error < 0.20 %

0 % < Hole diameter error < 0.25 %

0 % < Hole surface roughness < 2.0 μm

The analysis of cutting temperature during the machinability assessment established strong physical correlation between the spindle speed and cutting temperature on the drill flank face. Figures 4.5 – 4.11 illustrate the effect of increasing spindle speed and feed rate in generating higher cutting temperatures. Higher spindle speeds resulted in thermal softening, which reduced the thrust and cutting forces and eventually minimized delamination damage, as shown in machinability map for delamination (Figure 5.51). However, it was also established that at very low feed of 20 μm/rev and high spindle speed of 15,000 rpm, the cutting temperature generated was in the range of glass transition temperature of epoxy and thus resulted in thermal damage, as shown in Figure 4.13. So it was concluded that to realize the benefits of high speed drilling, the feed rate has to be optimized to minimize or eliminate the occurrence of thermal induced damage.

Using the knowledge gained from the machinability assessment and the physics-based approach as illustrated in Figure 6.1, machinability maps were designed. Figures 4.51 - 4.54 describe in detail the effect of changing input parameters, namely spindle speed and feed rate, on hole quality attributes in the form of delamination, hole circularity, hole diameter error and surface roughness machinability maps. These individual machinability maps can be superimposed to produce a combined map as shown in Figure 5.55 and thus find optimum cutting parameters achieving the process design constraints.

The tool wear study established that chipping at the start of drilling and subsequent abrasion are the two dominant wear mechanisms observed during drilling of woven graphite epoxy composites. Abrasive wear on the flank face of the primary cutting edge of the drill was found to be more dominant than the wear on the rake face. It was established that an average flank wear criterion of 225 μm could be reached after drilling of 544 holes of 5.9 mm hole depth at spindle speed of 15,000 rpm and feed rate of 100 μm/rev, while 650 hole could be drilled at spindle speed of 12,000 rpm for the same feed rate.

Flank wear on the primary cutting edges of the WC drill was found to have good agreement with the three friction regimes. Also the transition from primary to secondary and finally to the tertiary wear zones was found to govern the change in intermediate parameters (i.e. cutting forces and temperature) and affect the hole quality parameters i.e. delamination, hole circularity, hole diameter error and surface roughness, as illustrated in

Figures 5.8 – 5.18. Hence, it is concluded that desirable quality attributes could be maintained within predefined tolerances by controlling the intermediate variables (forces and temperature) and a tool change/replacement strategy could be adopted on the basis of monitoring the intermediate variables rather than tracking the progression of flank wear.

6.2 Recommendations for Future Work

The concept of machinability maps established in this work could be used for on-line process control by making use of a variable feed rate strategy during drilling. In future research the knowledge of machinability maps can be used to develop and test an adaptive feed rate control system to avoid delamination by controlling the thrust force below a critical force level and thus produce holes without delamination.

Extensive work is needed to be done to simulate the drilling process using finite element techniques and thus optimize the process performance in terms of cutting forces, surface delamination and tool life. However, the key to this future work is the development of constitutive laws for non-homogeneous and anisotropic laminated composites based on fracture mechanics approach and defining the layered type of material model within a finite element environment

Another task that has immense potential is the area of on-line non-destructive testing of delamination for better damage control. This approach could be integrated with the machine tool control system and a feed back about the damage can be used to adjust the cutting parameters and reduce further damage. An initial assessment of the effectiveness of Ultrasonic C-scan, a non destructive testing technique, was done to prove its benefits in damage assessment. Figure 6.2 shows an Ultrasonic C-scan of the woven graphite epoxy laminate used in this research work. The scan distinctly highlights the hole without any delamination and the ones with varying delamination. It is also evident that the difference between a delamination and no delamination remains a qualitative assessment. This approach also doesn't distinguish between the internal and the surface damages and hence needs to be further investigated and evaluated critically for its effectiveness.

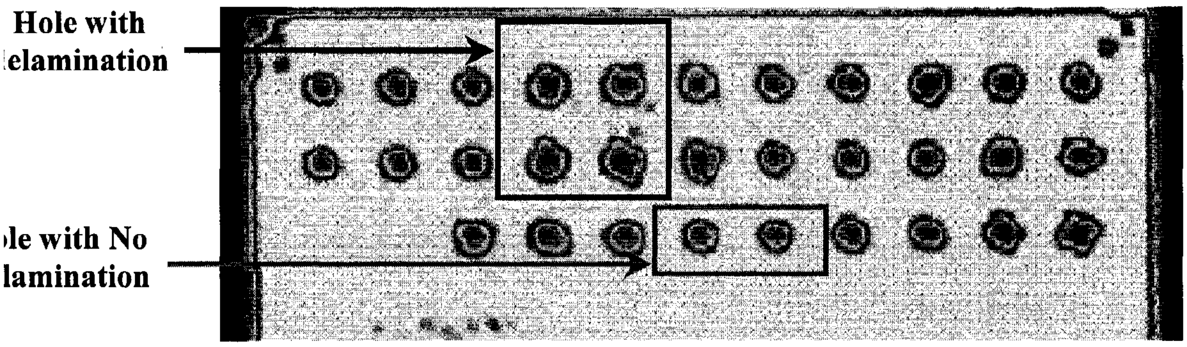

Figure 6.2: Ultrasonic C-Scan of Woven Graphite Epoxy Laminate showing its Delamination Damage Identification Capability

Future research could focus on hybrid machining technologies like vibration assisted drilling, rather than just the conventional technique used in this research work. The vibration assisted drilling involves superposition of low frequency and low amplitude vibration on the workpiece or tool during the conventional drilling process. This technique has been found very useful in minimization of burr and damage during aluminium machining and hence can be investigated for composites, especially with the objective of reducing thermal damage to the laminate by using interrupted cutting approach in vibration assisted drilling.

References

[1] Lessard, L. "MECH 530: Mechanics of Composite Materials". Course Notes – McGill University, 2003.

[2] Komanduri, R. "Machining Fibre-reinforced Composites". Mechanical Engineering, 115, No.4, pp.58-64, 1993.

[3] Schwartz, M.M. "Machining of Composites". SAMPE Journal, 32, No.2, pp. 18-25, 04/1996.

[4] Hubert, P. "MECH 501: Processing of Composite Materials". Course Notes – McGill University, 2004.

[5] Shaw, M.C., Metal Cutting Principles. Oxford Press, 1998.

[6] Koplev, A., Lystrup, Aa., Vorm, T. "The Cutting Process, Chips And Cutting Forces in Machining CFRP". Composites, 14, No. 4, pp. 371-376, 1983.

[7] Teti, R. "Machining of Composites Materials". Annals of CIRP, Vol. 51, pp. 611 – 634, 2002.

[8] Tandon, S., Jain, V.K., Kumar, P., Rajukar, K.P. "Investigations into Machining of Composites". Precision Engineering, 12, No. 4, pp. 227-237, 1990.

[9] Gordon, S., Hillery, M.T. "A Review of the Cutting of Composite Materials". Proceedings of Institution of Mechanical Engineers, Vol. 217, Part L: J. Materials: Design and Application, pp. 35-45, 2003.

[10] Jahanmir, S., Ramulu, M., Koshy, P. Machining of Ceramics and Composites. Marcel Dekker, 1999.

[11] Li, G.S., Lau, W.S., Zhang, Y.Z. "In-process Drill Wear and Breakage Monitoring for a Machining Centre Based on Cutting Force Parameters". International Journal of Machine Tools and Manufacture, Vol. 32, No. 6, pp. 855-867,1992

[12] Ho-Cheng Hong. "An Analysis of Drilling Of Composite Materials". Phd Dissertation, Mechanical Engineering, University of California Berkley, 1988.

[13] Khashaba, U.A. "Delamination in Drilling GFR- Thermoset Composites". Composite Structures, Vol. 63, pp. 313-327, 2003

[14] Oxford, C. J. "On the Drilling of Metals -1 Basic Mechanics of the Process". Transaction of ASME, Vol. 77, pp. 103-114, 1955.

[15] Shaw, M.C., Oxford, C.J. "On the Drilling of Metals - 2 The Torque and Thrust in Drilling". Transaction of ASME, Vol. 77, pp. 139-148, 1955.

[16] Tsai, S.W. Introduction to Composite Materials. CRC Press, 1980.

[17] Horn, G.P., Mackin, T.J., Kurath, P. "Composite Machining Damage Quantification Using Thermoelastic Stress Analysis". Polymer Composites, Vol. 23, No. 2, pp. 193-200, 2002.

[18] Ho-Cheng, H., Dharan, C.K.H. "Delamination during Drilling in Composite Laminates". Transactions of ASME, Vol. 112, pp. 236-239, 1990.

[19] Shuaib, A.N., Al-Sulaiman, F.A., Hamid, F. "Machinability of Kevlar 49 Composite Laminates While Using Standard TiN Coated HSS". Machining Science and Technology, Vol. 8, No. 3, pp. 449-467, 2004.

[20] Caprino, G., Tagliaferri, V. "Damage Development in Drilling Glass Fiber Reinforced Plastics". International Journal of Machine Tools and Manufacture, Vol. 35, No. 6, pp. 817-829, 1995.

[21] ISO 4288:1196 Geometrical Product Specifications – Surface Texture. 2nd Edition. 1996.

[22] Jain, S., Yang, D.C.H. "Effect of Feed Rate and Chisel Edge on Delamination in Composite Drilling". Transactions of ASME, Vol. 115, pp. 398-405, 1993.

[23] Tsao, C.C., Chen, W.C. "Prediction of the Location of Delamination in the Drilling of Composite Laminates". Journal of Material Processing Technology, Vol. 70, pp. 185-189, 1997.

[24] Zhang, L.B., Wang, L.J., Liu, X.Y. "A Mechanical Model for Predicting Critical Thrust Force in Drilling Composite Laminates". Proceedings of Institution of Mechanical Engineers, Vol. 215, Part B, pp.135-146, 2001.

[25] Lachaud, F., Piquet, R., Collombet, F., Surcin, L. "Drilling of Composite Structures". Composite Structure, Vol. 52, pp. 511-516, 2001.

[26] Dharan, C.K.H. "Fracture Mechanics of Composite Materials". ASME Journal of Engineering Material & Technology, Vol. 100, pp. 233, 1978.

[27] Konig, W., Wulf, Ch., Crass, P. and Willerscheid, H. "Machining of Fibre Reinforced Plastics". Annals of the CIRP, Vol. 34, No. 2, pp. 537-548.

[28] Wong, T.L., Wu, S.M. and Croy, G.M. "An Analysis of Delamination in Drilling Composite Materials". Proceedings of 14th SAMPE Technical Conference, pp. 471-483, 1982.

[29] Malhotra, S.K. "Some Studies on Drilling of Fibrous Composites". Journal of Materials Processing Technology, Vol. 24, pp. 291-300, 1990

[30] Kapoor, S.G, Chandrasekharan, V., DeVor, R.E. "A Mechanistic Approach to Predicting the Cutting Forces in Drilling: With Application to CFRP". Transactions of ASME, pp. 559-570, Nov 1995.

[31] Ho-Cheng, H., Tsao, C.C. "The Effect of Chisel Length and Associated Pilot Hole on Delamination When Drilling Composite Materials". International Journal of Machine Tools and Manufacture, Vol. 43, pp.1087-1092, 2003.

[32] Ho-Cheng, H and Puw, H.Y. "On Drilling Characteristics of FR Thermosets and Thermoplastics". International Journal of Machine Tools and Manufacture, Vol. 32, pp. 583-592, 1992.

[33] Tsao, C.C., Ho-Cheng, H. "Computerized Tomography and C-Scan for Measuring Delamination in the Drilling of Composite Materials Using Various Drills". International Journal of Machine Tools and Manufacture, Vol. 45, pp. 1282-1287, 2005.

[34] Lin, S.C. and Chen, I.K. "Drilling Carbon Fiber–Reinforced Composite Material at High Speed". Wear, Vol. 194, 156-162, 1996.

[35] Sonbaty, El., Khashaba, U.A., Machaly, T. "Factors affecting the Machinability of GFRP/Epoxy Composites". Composite Structures, Vol. 63, 329-338, 2004.

[36] Dharan, C.K.H., Saghizadeh, H. "Delamination Fracture Toughness of Graphite and Aramid Epoxy Composites". Transactions of ASME, Vol.108, pp. 290-295, 1986.

[37] Tagliaferri, V., Caprino, G., Diterlizzi, A. "Effect of Drilling Parameters on the Finish and Mechanical Properties of GFRP Composites". International Journal of Machine Tools and Manufacture, Vol. 30, No. 1, pp. 77-84, 1990.

[38] Di Paola, G., Kapoor, S.G., Devor, R.E. "An Experimental Investigation of the Crack Growth Phenomenon for Drilling of FRP Composites". ASME Journal of Engineering Industry, Vol. 118, pp. 104-110, 1996.

[39] Enemuoh, E. U., El-Gizawy, A.S., Okafor, A.C. "An Approach for Development of Damage Free Drilling of Carbon Fiber Reinforced Thermosets". International Journal of Machine Tools and Manufacture, Vol. 41, pp. 1795-1814, 2001.

[40] Enemuoh, E. U., El-Gizawy, A.S., Okafor, A.C., "Machinability Characterization in Drilling Graphite Fiber Reinforced Composites". Transactions of NAMRI/SME, Vol. XXVI, pp. 45-50, 1998.

[41] Davim, J.P and Pedro, R. "Study of Delamination in Drilling CFRP Using Design Experiments". Composite Structures, Vol. 59, 481-487, 2003.

[42] Kim, D., Ramulu, M., Doan, X. "Influence of Consolidation Process on the Drilling Performance and Machinability of PIXA-M and PEEK Thermoplastic Composites". Journal of Thermoplastic Composite Materials, Vol. 18, pp. 195-217, 2005.

[43] Tsao, C.C., Ho-Cheng, H. "Taguchi Analysis of Delamination Associated With Various Drill Bits in Drilling Of Composite Material". International Journal of Machine Tools and Manufacture, Vol. 44, pp. 1085-1090, 2004.

[44] Kim, D., Ramulu, M. "Drilling Process Optimization for Graphite/ Bismaleimide-Titanium Alloy Stacks". Composite Structures, Vol. 63, pp. 101-114, 2004.

[45] Konig, W., Graβ,.P. "Quality Definition and Assessment in Drilling of Fiber Reinforced Thermosets". CIRP Annals, Vol. 38, pp. 119-124, 1989.

[46] Bhattacharyya, D., Horrigan, D.P.W. "A Study of Hole Drilling in Kevlar Composites". Composites Science and Technology, Vol. 58, pp. 267-283, 1998.

[47] Ramkumar, J., Malhotra, S.K., Krishnamurthy, R. "Studies on Drilling of Glass/Epoxy Laminates Using Coated High Speed Steel Drills". Materials and Manufacturing Processes, Vol. 15(2), pp. 213-222, 2002.

[48] Brinksmeier, E., Janssen, R. "Session on Cutting (C) –C/10 Drilling of Multi-Layer Composite Materials Consisting of Carbon Fiber Reinforced Plastics, Titanium and Aluminium Alloys". CIRP Annals, Vol. 51, No. 1, pp. 87-90, 2002.

[49] Murphy, C., Byrne, G., Gilchrist, M.D. "The Performance of Coated Tungsten Carbide Drills When Machining Carbon Fiber-Reinforced Epoxy Composite

Materials". Proceedings of Institution of Mechanical Engineers, Vol. 216, pp. 143-152, 2002.

[50] Inoue, H., Aoyama, E., Hirogaski, T., Ogawa, K., Matushita, H., Kitahara, Y., Katayama, T. "Influence of Tool Wear on Internal Damage in Small Diameter Drilling in GFRP". Composite Structures, Vol. 39(1), pp. 55-62, 1997.

[51] Velayudham, A., Krishnamurthy, R., Soundarapandian, T. "Evaluation of Drilling Characteristics of High Volume Fraction Fibre Glass Reinforced Polymeric Composite". International Journal of Machine Tools and Manufacture, Vol. 45, pp. 399-406, 2005.

[52] Weinert, K., Kempmann, C. "Cutting Temperatures and Their Effects on the Machining Behaviour in Drilling Reinforced Plastic Composites". Advanced Engineering Materials, Vol. 6(8), pp. 684-689, 2004.

[53] Nagao,T., Hatamura, Y. "Investigation into Drilling Laminated Printed Circuit Board using a Torque-Thrust-Temperature Sensor". Annals of CIRP, Vol. 37(1), pp. 79-82, 1988.

[54] Bhatnagar, N., Ramakrishnan, N., Naik, N.K. "Experimental Investigation on Tool Tip Temperature during Drilling of FRP Composites". Materials and Manufacturing Processes, Vol. 64 (2), pp. 19-25, 1994.

[55] Chen, W.C. "Some Experimental Investigations in the Drilling of CFRP Composite Laminates". International Journal of Machine Tools and Manufacture, Vol. 45, pp. 399-406, 2005.

[56] ISO 8688: Tool Life Testing in Milling –Part 1: Face Milling. 1st Edition, 1989.

[57] http://www.makino.com/machines/product_information.aspx?id=5

[58] http://www.dandrea.com/ing/home.html

[59] http://www.kennametalipg.com/pdf/MR05015C.pdf

[60] Kennametal Holemaking Tooling Catalog 3070

[61] http://www.taylor-hobson.com/talysurfpgi.htm

[62] http://www.mame.mu.oz.au/manuf-sci3/436413/tool_wear.htm

Appendices

Appendix 1: Estimation of Steady State Temperature at N = 8,500 rpm and f = 200 μm/rev

The methodology used for the estimation of steady state temperature (θ_s) and time constant (τ) using MS Excel Solver tool is as below:

1) The experimental data of cutting temperature with time is obtained using the instrumented tool at spindle speed of 8,500 rpm and feed rate of 200 μm/rev.
2) The initial values of estimated steady state temperature (θ_s) and estimated time constant (τ) are assumed, while the initial room temperature (θ_i) is taken from the measured data as shown in Table A1.1.
3) The value of normalized temperature based on the time constant and the steady state temperature, as described by equation 5.2, are calculated in column 4 and 5 of Table A1.2 , respectively.
4) The error/difference between the calculated normalised temperature based on time constant and the steady state temperature is evaluated in column 6 and the square of this error in computed in column 7.
5) The optimization is done with least sum of the square of error as the objective subjected to constraints of "θ_s" and "τ".
6) The optimized values, i.e., θ_s = 294.8 °C and τ = 0.7 sec are used to compute the predicted cutting temperature as per equation (5.1) and shown in column 8 of Table A1.2.
7) The measured cutting temperature and predicted steady state are plotted against time as shown in Figure A1.1.
8) The estimated value of time constant i.e. 0.7 sec agrees well with the value calculated by using the definition of time constant i.e. the time necessary for the thermocouple to reach 63.22 % (1 - 1/e) of the maximum possible temperature change i.e. ($\theta_s - \theta_i$) as shown in Figure A1.2.

Table A1.1: Evaluation of Steady State Temperature and Time Constant for Cutting Conditions at Spindle Speed of 8,500 rpm and Feed Rate of 200 μm/rev

Initial Room Temperature	θ_i	28.12	deg C
Estimated Steady State Temperature	θ_s	294.80	deg C
Estimated Time Constant from Optimization	τ	0.70	sec
Data Sampling Time Interval	δt	0.0002	sec

Table A1.2: Optimization of Steady State Temperature and Time Constant for Cutting Conditions Using the Least Square Error Method for Spindle Speed of 8,500 rpm and Feed Rate of 200 μm/rev

Experimental Data		**Estimated Temperature by Optimization using MS Excel Solver Tool**					
1	**2**	**3**	**4**	**5**	**6**	**7**	**8**
t (sec)	**Measured Temp. (deg. C)**	**t/τ**	**$(1-e^{-t/\tau})$**	**$(\theta-\theta_i)/(\theta-\theta_s)$**	**Error = (4 - 5)**	**Error^2**	**Predicted Temp. (deg. C)**
0.10	54.94	0.14	0.13	0.10	0.0327	0.00107	64
0.20	90.90	0.29	0.25	0.24	0.0131	0.00017	94
0.30	119.76	0.43	0.35	0.34	0.0050	0.00002	121
0.40	144.26	0.57	0.44	0.44	0.0001	0.00000	144
0.50	161.46	0.71	0.51	0.50	0.0105	0.00011	164
0.60	177.04	0.86	0.58	0.56	0.0173	0.00030	182
0.70	189.00	1.00	0.63	0.60	0.0288	0.00083	197
0.80	202.68	1.14	0.68	0.65	0.0266	0.00071	210
0.86	211.44	1.23	0.71	0.69	0.0199	0.00040	217
1.26	Temperature could not be measured from 1 – 7 seconds. Temperature has been predicted by considering the system as 1st Order Linear and using the estimated steady state temperature and time constant						250
2.06							281
3.06							291
4.06							294
5.06							295
6.06							295
7.06							295
Optimized Time Constant (sec)							0.70
Optimized Steady State Temperature (deg. C)							294.8

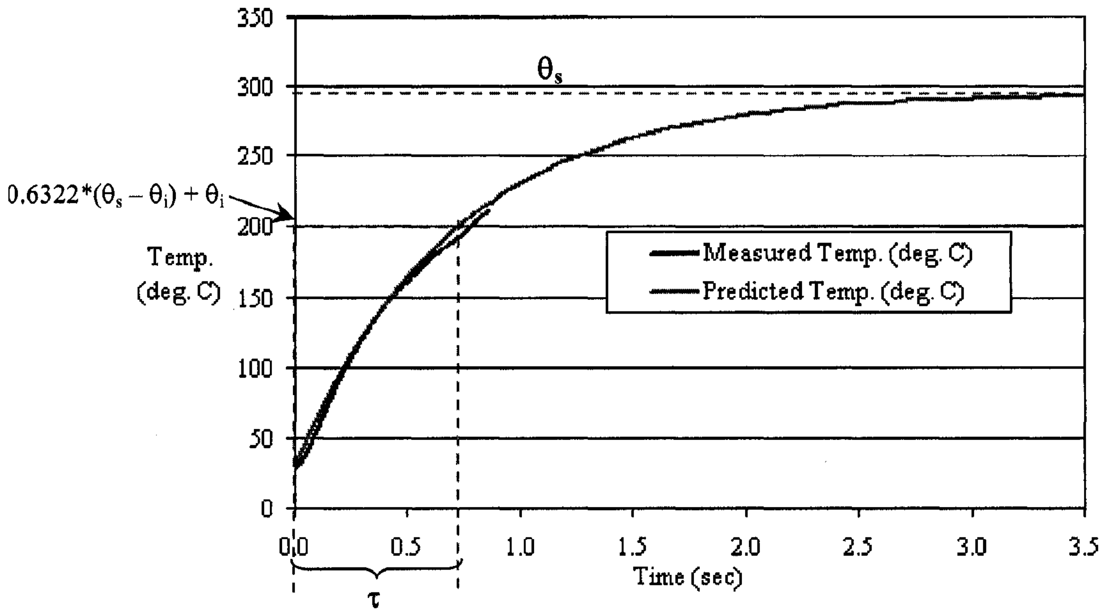

Figure A1.1: Temperature Time Curve of the Measured Temperature during Experimental Test and the Predicted Temperature using Theory of First Order Linear System at Spindle Speed of 8,500 rpm and Feed Rate of 200 μm/rev

Appendix 2: Critical Thrust Force and Cutting Force Calculation based on Ho-Cheng and Dharan Model [12, 18]

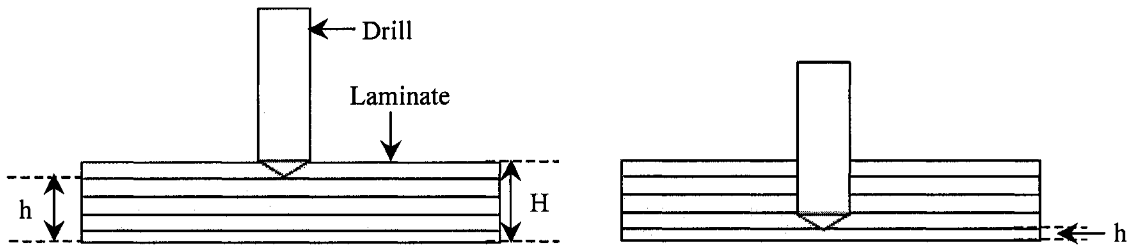

Figure A2.1: Peel Up and Push Out of Top most and Bottom most Ply of the Laminate

Table A2.1: Evaluation of Critical Thrust and Cutting Force at Push Out/Exit Delamination and Peel Up/ Entry Delamination

Calculation for Critical Thrust Force during Push Out				
Parameter	**Symbol**	**Value**	**Units**	**Notes**
Critical Crack Propagation Energy in Mode I	G_{IC}	266	J/m2	Refer Table 3.1
Modulus of Elasticity	E	58	Gpa	Refer Table 3.1
Laminate Thickness	H	5.9	mm	
No of Plies	m	28		
Uncut depth under the tool i.e ply thickness of top most ply	h	0.21	mm	
Poisson's ratio	ν	0.3	m/m	Refer Table 1.1
Fiber Volume Fraction	ν_f	0.6		Refer Table 3.1
$8 \times G_{IC} \times E \times h^3$		1154.73	N	Refer Equation (2.1)
$3 \times (1-\nu^2)$		2.73	m/m	Refer Equation (2.1)
F_z^*		65	N	Refer Equation (2.1)
Calculation for Critical Cutting Force during Peel Up				
Uncut depth under the tool i.e ply thickness of bottom most ply	H-h	0.21	mm	
$8 \times G_{IC} \times E \times (H-h)^3$		1154.73	N	Refer Equation (2.2)
$3 \times (1-\nu^2)$		2.73	m/m	Refer Equation (2.2)
Peel Up Factor "k_p" for Graphite/Epoxy and Standard Twist Drill		0.68		Refer [12]
F_c^*		44	N	Refer Equation (2.2)

Appendix 3: Optical Images of the Graphite/Epoxy Chips Produced at Different Cutting Conditions

Table A3.1: Cutting Conditions i.e. Spindle Speeds and Feeds for the Optical Images of Collected Chips

Image No	Spindle Speed (rpm)	Feed Rate (μm/rev)	Comments on type of chips
(a)	**1,500**	**20**	**Flaky Chips**
(b)	**1,500**	**800**	**Thick Chips**
(c)	**15,000**	**20**	**Powdery Chips**
(d)	**15,000**	**800**	**Thin Chips**

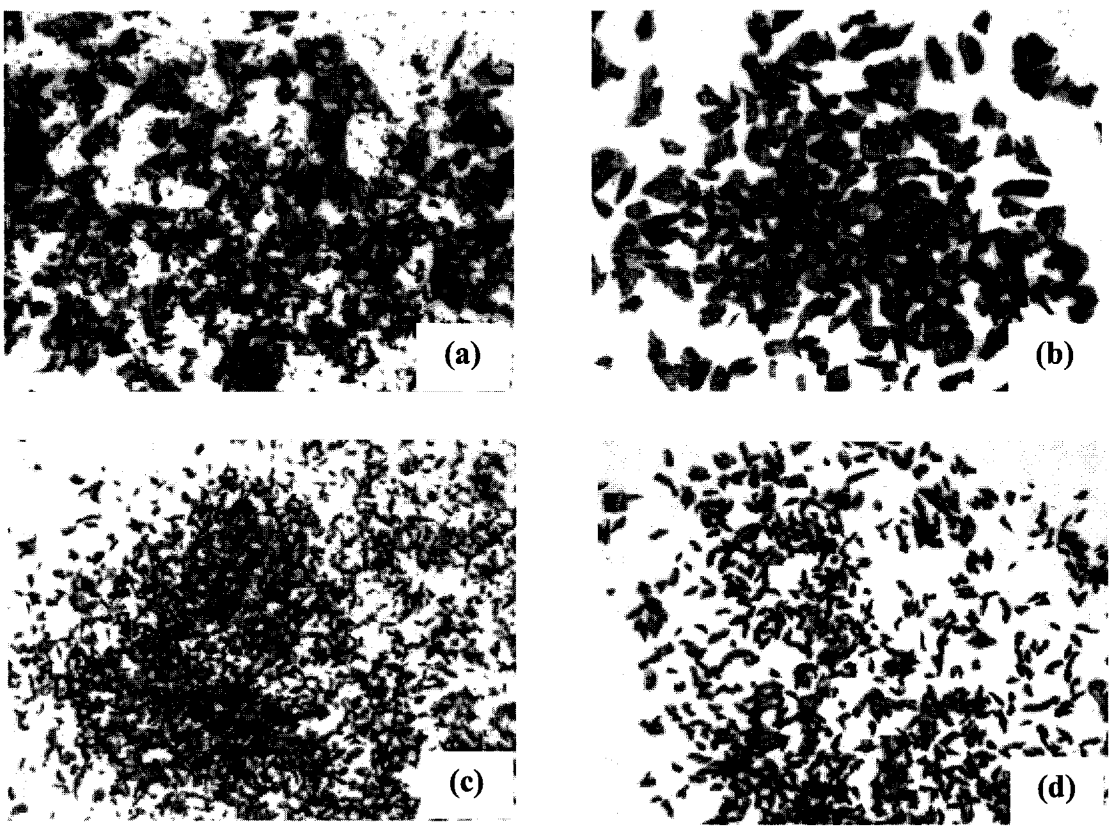

Figure A3.1: Optical Images of Collected Chips of Woven Graphite Fiber Epoxy Composite. Image (a) Shows Flaky Chips Obtained at Low Spindle Speed of 1,500 rpm and Low Feed Rate of 20 μm/rev. Image (b) Shows Thick Chips Obtained at Low Spindle Speed of 1,500 rpm and High Feed Rate of 800 μm/rev. Image (c) Shows Powdery Chips Obtained at High Spindle Speed of 15,000 rpm and Low Feed Rate of 20 μm/rev. Image (d) Shows Thin Chips Obtained at High Spindle Speed of 15,000 rpm and High Feed Rate of 800 μm/rev